



City Research Online

City, University of London Institutional Repository

Citation: Ansari, A. (1992). Thermally driven tall cavity flows in porous media.
(Unpublished Doctoral thesis, City, University of London)

This is the accepted version of the paper.

This version of the publication may differ from the final published version.

Permanent repository link: <https://openaccess.city.ac.uk/id/eprint/29032/>

Link to published version:

Copyright: City Research Online aims to make research outputs of City, University of London available to a wider audience. Copyright and Moral Rights remain with the author(s) and/or copyright holders. URLs from City Research Online may be freely distributed and linked to.

Reuse: Copies of full items can be used for personal research or study, educational, or not-for-profit purposes without prior permission or charge. Provided that the authors, title and full bibliographic details are credited, a hyperlink and/or URL is given for the original metadata page and the content is not changed in any way.

Thermally Driven Tall Cavity Flows in Porous Media

Ali Ansari

A thesis submitted for the degree of

Doctor of Philosophy

Department of Mathematics

City University

London

September 1992

Acknowledgement

My sincerest gratitude to my supervisor Professor
P.G.Daniels for his guidance and encouragement during
the preparation of this thesis

Abstract

Thermally driven flows in a two-dimensional rectangular cavity filled with a fluid-saturated porous medium are considered when the applied temperature difference is perpendicular to the gravity vector. The flow depends on two non-dimensional parameters, the Darcy-Rayleigh number A and the cavity aspect ratio h (height/length). The motion is generated by maintaining the vertical sidewalls of the cavity at different constant temperatures and attention is focussed on the limit of large aspect ratio, $h \rightarrow \infty$. Use of asymptotic and numerical methods leads to an excellent correlation with existing results for the heat transfer across the cavity, and a prediction of the conditions needed to minimize the heat transfer.

The basic problem for $h \gg 1$ and finite Darcy-Rayleigh numbers, A , is formulated in Chapter 2, leading to a nonlinear end-zone problem which is studied in detail in Chapters 3-5. Asymptotic methods are used to solve the problem analytically for small A in Chapter 3 and for large A in Chapter 4. Numerical solutions for finite values of A are obtained in Chapter 5. Convective effects become important throughout the slot when A is of order h and solutions for the main core flow in this regime are considered in Chapter 6. A position of minimum heat transfer is identified. Properties of the flow near the ends of the slot are considered in Chapter 7 and the results are related in the limit as $A/h \rightarrow \infty$ to existing theories for high Darcy-Rayleigh number flow in finite aspect-ratio cavities.

Contents

Chapter 1	Introduction
	1.1 Background and mathematical model
	1.2 Previous work
	1.3 Present work
Chapter 2	Convection in a vertical slot filled with a porous medium
	2.1 Introduction
	2.2 Formulation
	2.3 Solution for large aspect ratio , $h \gg 1$
	2.4 End region
	2.5 End-region solution, $z \rightarrow \infty$.
Chapter 3	Solution of the end-zone problem for small Darcy-Rayleigh numbers, $A \ll 1$
	3.1 Introduction
	3.2 Inner expansion, $z = O(1)$
	3.3 Outer expansion, $z = O(A^{-1})$
Chapter 4	Solution of the end-zone problem for large Darcy-Rayleigh numbers, $A \gg 1$
	4.1 Introduction
	4.2 Outer zone, $z = O(A)$
	4.3 Inner regions, $z = O(1)$
	4.4 Inner horizontal layer, $z = O(A^{-1/4})$
	4.5 Corner regions

Chapter 5	Numerical solution of the end-zone problem
	5.1 Introduction
	5.2 Numerical method
	5.3 Numerical results
Chapter 6	Convection in a vertical slot filled with a porous medium for Darcy-Rayleigh numbers $A=O(h)$
	6.1 Introduction
	6.2 Formulation
	6.3 Core solution
	6.4 Numerical method
	6.5 Numerical results
	6.6 Heat transfer
Chapter 7	Solution of the end-zone problems for Darcy-Rayleigh numbers $A=O(h)$
	7.1 Introduction
	7.2 Core structure, $Z \rightarrow 0$
	7.3 End-zone solution
	7.4 Inner horizontal layer
	7.5 The limiting structure for $A/h \rightarrow \infty$.
	7.6 Discussion

Chapter 1 Introduction

1.1 Background and mathematical model

The term porous medium is used for solid fissured rocks, ceramics, fibrous aggregates, filter paper, sand and for other solids which contain holes. The holes may be filled with a gas or a liquid. Thus in general a porous medium consists of a portion of space occupied by heterogeneous or multiphase matter (Bear, 1968). The solid phase is usually called the solid matrix and that space within the porous domain which is not part of the solid matrix is referred to as the void space (or pore space). The solid phase should be distributed through the porous medium in such a way that it is present inside any representative elementary volume. Essential characteristics of a porous medium are that the specific surface of the solid matrix is relatively high and that the various openings comprising the void space are relatively small. The specific surface, S , of a porous material is defined as the total interstitial surface area of the pores, S , per unit bulk volume, V , of the porous medium, $S = S/V$. For example, the specific surface of a porous material made of identical spheres of radius R in a cubical packing is $S = 4\pi R^2 / (2R)^3 = \pi/2R$. It thus becomes obvious that fine materials will exhibit a much greater specific surface than will coarse materials.

At least some of the pores comprising the void space should be interconnected, and the interconnected pore space is sometimes termed the effective pore space. As far

as flow through porous media is concerned, unconnected pores may be considered as part of the solid matrix. Certain portions of the interconnected pore space may, in fact, also be ineffective as far as flow through the medium is concerned. For example, pores may be 'dead-end' pores (or 'blind' pores), i.e. pores or channels with only a narrow single connection to the interconnected pore space, so that almost no flow occurs through them. A suitable definition of the effective pore space is that any two points within the space may be connected by a curve that lies completely within it. Moreover, except for special cases, any two such points may be connected by many curves with an arbitrary maximal distance between any two of them. For a finite porous medium this maximal distance is limited by the dimensions of the domain.

In the present work it will be assumed that the motion of the liquid or gas through the porous medium conforms to Darcy's law (Lapwood 1948) which states that a fluid flow with velocity \underline{u}^* through a porous medium experiences a resistance force equal to $g\underline{u}^*/K$ per unit mass, where K is a constant with the dimensions of velocity and g is the acceleration due to gravity. Incorporating this resistance force in Newton's law of motion gives the momentum equation

$$\rho \frac{D\underline{u}^*}{Dt^*} = - \underline{\nabla}^* p^* - \frac{\rho g \underline{u}^*}{K} + \rho \underline{F}^* , \quad (1.1.1)$$

where p^* is the pressure, ρ is the fluid density and \underline{F}^* is any external force per unit mass. Also $\underline{\nabla}^*$ is the gradient operator and $D/Dt^* = \partial/\partial t^* + \underline{u}^* \cdot \underline{\nabla}^*$ denotes

differentiation following the motion, where t^* is the time. In the absence of any sources, the mass of fluid is conserved, leading to the continuity or 'mass-conservation' equation

$$\frac{\partial \rho}{\partial t} + \nabla \cdot (\rho \underline{u}) = 0 . \quad (1.1.2)$$

In addition, the thermal energy equation is assumed to take the form

$$\frac{DT}{Dt} = \kappa \nabla^2 T , \quad (1.1.3)$$

where T is the temperature of the fluid and κ is the thermal diffusivity. Finally, the density of the fluid will be assumed to be linearly dependent on its temperature, so that the equation of state may be written in the form

$$\rho = \rho_0 [1 - \alpha (T - T_0)] , \quad (1.1.4)$$

where α is the coefficient of thermal expansion and ρ_0 is the density of the fluid at temperature T_0 .

The present work is concerned with buoyancy-driven flows where the external force is due to gravity. The z^* axis of Cartesian coordinates (x^*, y^*, z^*) is taken vertically upwards so that $\underline{F} = (0, 0, -g)$ and the governing equations can then be taken as

$$\frac{\partial u}{\partial x} + \frac{\partial v}{\partial y} + \frac{\partial w}{\partial z} = 0 , \quad (1.1.5)$$

$$\rho_0 \left(\frac{\partial u}{\partial t} + u \frac{\partial u}{\partial x} + v \frac{\partial u}{\partial y} + w \frac{\partial u}{\partial z} \right) = - \frac{\partial p}{\partial x} - \rho_0 \frac{\nu}{k} u , \quad (1.1.6)$$

$$\rho_0 \left(\frac{\partial v^*}{\partial t^*} + u^* \frac{\partial v^*}{\partial x^*} + v^* \frac{\partial v^*}{\partial y^*} + w^* \frac{\partial v^*}{\partial z^*} \right) = - \frac{\partial p^*}{\partial y^*} - \rho_0 \frac{\nu}{k} v^*, \quad (1.1.7)$$

$$\rho_0 \left(\frac{\partial w^*}{\partial t^*} + u^* \frac{\partial w^*}{\partial x^*} + v^* \frac{\partial w^*}{\partial y^*} + w^* \frac{\partial w^*}{\partial z^*} \right) = - \frac{\partial p^*}{\partial z^*} - \rho_0 \frac{\nu}{k} w^* - \rho_0 g (1 - \alpha (T^* - T_0^*)), \quad (1.1.8)$$

$$\frac{\partial T^*}{\partial t^*} + u^* \frac{\partial T^*}{\partial x^*} + v^* \frac{\partial T^*}{\partial y^*} + w^* \frac{\partial T^*}{\partial z^*} = \kappa \nabla^{*2} T^*. \quad (1.1.9)$$

where $\underline{u}^* = (u^*, v^*, w^*)$. Here the Oberbeck-Boussinesq approximation has been assumed, in which changes in the density are neglected except where coupled with the gravitational acceleration term. Also the constant K has been replaced by the permeability, defined as $k = K\nu/g$ where ν is the kinematic viscosity. The system (1.1.5-9) may be non-dimensionalised by setting

$$\left. \begin{aligned} (u^*, v^*, w^*) &= \frac{\kappa}{\ell^*} (\bar{u}, \bar{v}, \bar{w}), \\ (x^*, y^*, z^*) &= \ell^* (x, y, z), \\ t^* &= \frac{\ell^{*2}}{\kappa} t \end{aligned} \right\} \quad (1.1.10)$$

where ℓ^* is a typical length scale of the system, and by defining

$$\left. \begin{aligned} T^* &= T_0^* + \Delta T^* \bar{T}, \\ p^* &= p_0^* - \rho_0 g z^* + \left(\frac{\rho_0 \nu \kappa}{k} \right) \bar{p} \end{aligned} \right\} \quad (1.1.11)$$

where ΔT^* is a typical temperature difference and p_0^* is an arbitrary constant. This gives

$$\frac{\partial \bar{u}}{\partial x} + \frac{\partial \bar{v}}{\partial y} + \frac{\partial \bar{w}}{\partial z} = 0 \quad , \quad (1.1.12)$$

$$\epsilon \left(\frac{\partial \bar{u}}{\partial t} + \bar{u} \frac{\partial \bar{u}}{\partial x} + \bar{v} \frac{\partial \bar{u}}{\partial y} + \bar{w} \frac{\partial \bar{u}}{\partial z} \right) = - \frac{\partial \bar{p}}{\partial x} - \bar{u} \quad , \quad (1.1.13)$$

$$\epsilon \left(\frac{\partial \bar{v}}{\partial t} + \bar{u} \frac{\partial \bar{v}}{\partial x} + \bar{v} \frac{\partial \bar{v}}{\partial y} + \bar{w} \frac{\partial \bar{v}}{\partial z} \right) = - \frac{\partial \bar{p}}{\partial y} - \bar{v} \quad , \quad (1.1.14)$$

$$\epsilon \left(\frac{\partial \bar{w}}{\partial t} + \bar{u} \frac{\partial \bar{w}}{\partial x} + \bar{v} \frac{\partial \bar{w}}{\partial y} + \bar{w} \frac{\partial \bar{w}}{\partial z} \right) = - \frac{\partial \bar{p}}{\partial z} - \bar{w} + A\bar{T} \quad , \quad (1.1.15)$$

$$\frac{\partial \bar{T}}{\partial t} + \bar{u} \frac{\partial \bar{T}}{\partial x} + \bar{v} \frac{\partial \bar{T}}{\partial y} + \bar{w} \frac{\partial \bar{T}}{\partial z} = \nabla^2 \bar{T} \quad , \quad (1.1.16)$$

where $\nabla^2 = \partial^2/\partial x^2 + \partial^2/\partial y^2 + \partial^2/\partial z^2$,

$$A = \frac{\alpha g \Delta T^* k l^*}{\kappa \nu} \quad (1.1.17)$$

is the Darcy-Rayleigh number and $\epsilon = k \kappa / \nu l^{*2}$ is a non-dimensional parameter which for many porous-media flows can be assumed to be small. In the limit as $\epsilon \rightarrow 0$ the governing equations for three-dimensional flow become

$$\frac{\partial \bar{u}}{\partial x} + \frac{\partial \bar{v}}{\partial y} + \frac{\partial \bar{w}}{\partial z} = 0 \quad , \quad (1.1.18)$$

$$\frac{\partial \bar{p}}{\partial x} + \bar{u} = 0 \quad , \quad (1.1.19)$$

$$\frac{\partial \bar{p}}{\partial y} + \bar{v} = 0 \quad , \quad (1.1.20)$$

$$\frac{\partial \bar{p}}{\partial z} + \bar{w} - A\bar{T} = 0 \quad , \quad (1.1.21)$$

$$\frac{\partial \bar{T}}{\partial t} + \bar{u} \frac{\partial \bar{T}}{\partial x} + \bar{v} \frac{\partial \bar{T}}{\partial y} + \bar{w} \frac{\partial \bar{T}}{\partial z} = \nabla^2 \bar{T} \quad , \quad (1.1.22)$$

(Lapwood 1948). For steady, two-dimensional flow, independent of y , the system may be further reduced to the form

$$\nabla^2 \bar{\psi} = -A \frac{\partial \bar{T}}{\partial x} \quad , \quad (1.1.23)$$

$$\nabla^2 \bar{T} = \frac{\partial (\bar{T}, \bar{\psi})}{\partial (x, z)} \quad , \quad (1.1.24)$$

where $\nabla^2 = \partial^2 / \partial x^2 + \partial^2 / \partial z^2$, $\bar{\psi}$ is the non-dimensional stream function defined by

$$\bar{u} = \frac{\partial \bar{\psi}}{\partial z} \quad , \quad \bar{w} = - \frac{\partial \bar{\psi}}{\partial x} \quad , \quad (1.1.25)$$

and the pressure has been eliminated .

The present study is concerned chiefly with solutions of (1.1.23,24) in rectangular geometries. There are applications in a wide variety of areas. Convective heat transfer in a confined rectangular cavity packed with a porous medium is of practical importance, for example, in the nuclear power industry where porous insulating materials are used in multishield structures surrounding the core of a nuclear reactor, and in regenerative heat exchangers (Seki, Fukusako and Inaba 1978). There are also applications in high performance building insulation, solar power collectors, energy-efficient drying processes, the cooling of nuclear fuel in shipping flasks and water-filled storage bays, thermal energy storage tanks and chemical catalytic reactors. On a wider scale, porous media flows are of interest in relation to the underground spread of pollutants, geothermal energy systems and convection in the Earth's crust (Prasad and Kulacki 1984,1984a). For many, but not all, of these applications the simplest realistic mathematical model consists of two-dimensional flow in a rectangular cavity filled with a porous medium

and heated from the side. The horizontal thermal gradient generates motion via the buoyancy term in (1.1.23) and it is the nature of this motion, and of the corresponding heat transfer properties of the system which are generally of interest.

The geometrical configuration to be studied here consists of a two-dimensional cavity defined by the region $0 \leq x^* \leq l^*$, $0 \leq z^* \leq h^*$, with vertical side walls at $x^* = 0$ and $x^* = l^*$ maintained at constant temperatures T_0^* and $T_0^* + \Delta T^*$ respectively, equivalent to

$$\bar{T} = 0 \quad (x = 0) \quad , \quad \bar{T} = 1 \quad (x = 1) \quad . \quad (1.1.26)$$

If the horizontal walls are thermally insulating the boundary conditions for the temperature are

$$\frac{\partial \bar{T}}{\partial z} = 0 \quad (z = 0 \quad , \quad z = h) \quad , \quad (1.1.27)$$

while if they are conducting

$$\bar{T} = x \quad (z = 0 \quad , \quad z = h) \quad , \quad (1.1.28)$$

where $h = h^*/l^*$ is the aspect ratio of the cavity. The cavity walls are also impermeable, in which case

$$\bar{\psi} = 0 \quad (x = 0 \quad , \quad 1) \quad , \quad (z = 0 \quad , \quad h) \quad . \quad (1.1.29)$$

An important property of the flow is the amount of heat which passes through each vertical wall of the cavity. This is measured typically by the Nusselt number for the cold wall, defined by

$$Nu^* = \int_0^{h^*} \left. \frac{\partial T^*}{\partial x^*} \right|_{x^* = 0} dz^* \quad , \quad (1.1.30)$$

or, in non-dimensional form

$$\frac{Nu}{\Delta T} = Nu = \int_0^h \frac{\partial \bar{T}}{\partial X} \Big|_{x=0} dz. \quad (1.1.31)$$

1.2 Previous work

There has been a considerable amount of previous work on thermally-driven cavity flows in porous media. Studies concerned with the motion generated by maintaining the vertical walls of a rectangular cavity at different constant temperatures can be divided roughly into those concerned with finite aspect ratios and those for which the aspect ratio h is either small or large. Both analytical and numerical methods have been used to obtain solutions and to make predictions of the heat transfer across the cavity.

For cavities of finite aspect ratio, much of the theoretical work has concentrated on describing the boundary-layer structure of the flow in the limit of large Darcy-Rayleigh number, $A \rightarrow \infty$. Weber(1975) identified the main features of this structure, which consists of a core region flanked by vertical boundary layers of thickness $A^{-1/2}$ near each vertical wall. This type of structure was first identified in the case of a Newtonian fluid by Gill (1966). The core region is vertically stratified and contains a horizontal two-way flow which is entrained and detrained by the vertical boundary layers, which transport the fluid up near the hot wall and down near the cold wall, completing the main single-cell circulation in the cavity. Weber (1975) used an Oseen method to solve the vertical

boundary-layer equations and this led to a prediction of the Nusselt number of the form

$$\text{Nu} \sim (\text{Ah}/3)^{1/2}, \quad A \longrightarrow \infty \quad (1.2.1)$$

Walker and Homsy (1978) discussed the finite aspect ratio case and used a semi-numerical approach to obtain series expansions for the solution in powers of A at fixed values of h. They also considered the boundary-layer limit and used a finite-difference method to solve the vertical boundary-layer equations, giving

$$\text{Nu} \sim 0.51(\text{Ah})^{1/2}, \quad A \longrightarrow \infty \quad (1.2.2)$$

and improving upon the Oseen result obtained by Weber. Simpkins and Blythe (1980) further investigated the solution of the vertical boundary-layer system using an integral method and found results in excellent agreement with (1.2.2) for three types of boundary-layer velocity profile

$$\left. \begin{aligned} \text{Nu} &\sim 0.521 (\text{Ah})^{1/2} && \text{(polynomial-exponential)} \\ \text{Nu} &\sim 0.508 (\text{Ah})^{1/2} && \text{(exponential)} \\ \text{Nu} &\sim 0.510 (\text{Ah})^{1/2} && \text{(inner-outer)} \end{aligned} \right\} \quad (1.2.3)$$

They also extended this work to include the effect of a temperature-dependent viscosity (Blythe and Simpkins 1981).

All of the work on the high Darcy-Rayleigh number limit to this point had been based on the assumption of a 'mass-flux hypothesis'. This assumes that the vertical boundary layers empty into the core, so that horizontal boundary layers near the top and bottom walls of the cavity

carry a negligible amount of mass flux in comparison with that conveyed across the core . The first steps towards confirming the validity of this assumption were taken by Blythe , Daniels and Simpkins (1982) who considered in detail the asymptotic structure of the solution near each end of the vertical boundary layer. They found that the solution for the stream function behaves as the square root of the vertical co-ordinate, correcting a previous assumption made by Walker and Homsy (1978). This result, consistent with the mass-flux hypothesis, led to a description of the structure of the solution near the horizontal walls of the cavity for the case where these walls are thermally insulated (Daniels, Blythe and Simpkins 1982). The horizontal boundary-layer structure consists of two layers , an outer layer of thickness order $A^{-1/4}$, which is dominated by convection, and an inner layer of thickness order $A^{-5/16}$, in which conduction is important. Corner regions where the horizontal and vertical boundary layers meet were also considered, leading to a self-consistent leading order solution for the high Darcy-Rayleigh number flow throughout the cavity. The asymptotic properties identified by Blythe, Daniels and Simpkins (1982) also allowed an accurate numerical solution of the vertical boundary-layer system to be undertaken (Daniels 1983) and this led to a prediction of the Nusselt number of the form

$$\text{Nu} \sim 0.52 (Ah)^{1/2}, \quad A \longrightarrow \infty . \quad (1.2.4)$$

There have been a number of theoretical studies concerned with thermally-driven flows in shallow cavities,

where $h \ll 1$. Walker and Homsy (1978) found solutions for values of the Darcy-Rayleigh number, $A \ll h^{-2}$, using the approach adopted by Cormack, Leal and Imberger (1974) for the equivalent Newtonian problem. For finite values of Ah^2 the solution throughout most of the cavity is a two-way flow parallel to the horizontal boundaries driven by lateral conduction. The flow is turned in end regions of roughly square cross-section near each vertical wall where the full nonlinear equations apply. Approximate solutions for this region were obtained by Bejan and Tien (1978) and a more detailed study, which included numerical solutions of the end-zone problem, was undertaken by Daniels, Blythe and Simpkins (1986). The Nusselt number for this 'intermediate' regime is

$$Nu \sim h \left(1 + \frac{1}{120} A^2 h^4 \right), \quad h \longrightarrow 0. \quad (1.2.5)$$

As the Darcy-Rayleigh number increases, the end regions spread across the cavity, leading to a new non-parallel core-flow when A is of order h^{-3} . In this so-called 'merged-layer' regime studied by Daniels, Simpkins and Blythe (1989) the core region is governed by the horizontal boundary-layer equations and the motion is no longer uni-cellular, with inner circulatory motions in each half of the cavity completed via vertical boundary layers along the sidewalls. The merged-layer regime is particularly important as it covers a wide range of parameter space, $25 \leq Ah^3 \leq 10^4$. The Nusselt number in this regime has the form

$$Nu \sim h^{-1} \hat{Nu}(Ah^3), \quad h \longrightarrow 0, \quad (1.2.6)$$

where \hat{Nu} is a function only of the variable Ah^3 . As

$$Ah^3 \longrightarrow 0 ,$$

$$\hat{Nu} \sim \frac{1}{120} (Ah^3)^2 , \quad (1.2.7)$$

consistent with the intermediate result (1.2.5) while as

$$Ah^3 \longrightarrow \infty ,$$

$$\hat{Nu} \sim 0.52 (Ah^3)^{1/2} , \quad (1.2.8)$$

consistent with the boundary-layer regime for a cavity of finite aspect ratio , where (1.2.4) applies . This latter regime is recovered by a limiting process in which the regions governed by the horizontal boundary-layer equations become progressively thinner and are restricted to the neighbourhood of the horizontal boundaries, leaving a vertically stratified horizontal motion in the core. A full discussion of the various flow regimes for shallow cavities is given by Blythe, Simpkins and Daniels (1983).

In contrast , there is comparatively little previous analytical work on thermally-driven porous media flows in tall cavities , where $h \gg 1$. Gill (1969) showed that such flows are stable in the conductive regime while Riley (1988) has considered the effect of spatially periodic boundary imperfections in the form of surface undulations of the sidewalls. The core flow was assumed to lie in the conductive regime and it was shown that out-of-phase imperfections can significantly enhance the heat transfer across the cavity. Other work on tall cavity flows has been carried out mainly by numerical or experimental methods. Chan, Ivey and Barry (1970), Bankvall (1974) and Lauriat and Prasad (1987) have reported numerical results for aspect ratios in the range $1 \leq h \leq 50$ while Prasad and Kulacki

(1984b) have considered the extended range $1/20 \leq h \leq 100$. Burns, Chow and Tien(1977) have studied the effect of mass injection in tall cavities , in connection with cavity wall leakage, while Prasad and Kulacki (1984a) have considered how the flow is affected by constant heat-flux boundary conditions for aspect ratios in the range $1 \leq h \leq 5$. Experimental results for tall cavities have been obtained by Klarsfeld (1970) and Seki, Fukusako and Inaba (1978), and for lower aspect ratios both experimental and numerical work has been carried out by Holst and Aziz (1972) and Haadjizadeh and Tien(1983). Hickox and Gartling (1981) have also obtained numerical results for shallow cavity flows with $1/10 < h < 1/2$ while for tall cavities Prasad and Kulacki (1984) have considered the effect of an annular geometry .

1.3 Present work

This thesis is concerned with thermally-driven cavity flows in porous media where the aspect ratio of the cavity is large , i.e . the height of the cavity is large compared with the width. The flow is driven by maintaining the vertical walls of the cavity at different constant temperatures and attention is focussed on the case for which the horizontal end walls are thermally insulated . As shown earlier , for Darcy flow in the Boussinesq approximation there are two non-dimensional parameters which determine the flow, the Darcy-Rayleigh number A and the aspect ratio h . Chapters 2,3,4 and 5 are concerned with the solution for order-one Darcy-Rayleigh numbers A , such that $A \ll h$ where $h \gg 1$. Chapter 2 is concerned with the

basic formulation of the problem and the identification of the important end regions near the horizontal walls where nonlinear effects come into play and accommodate the turning motion of the main single-cell circulation. Solutions of the end-zone problem, which determine a first correction to the conductive heat transfer across the cavity, are found by both asymptotic and numerical methods. In Chapters 3 and 4 the method of matched asymptotic expansions is used to obtain solutions for small and large values of the Darcy-Rayleigh number, respectively. Numerical solutions for intermediate values of A are found in Chapter 5.

The remainder of the thesis is concerned with the break-down of the conduction-dominated flow when the Darcy-Rayleigh number, A , is comparable with the aspect ratio h , and $h \gg 1$. Heat transfer across the cavity is no longer dominated by conduction and the main core flow throughout the cavity can be found using a vertical boundary-layer approximation. The core solution is determined in Chapter 6 for a range of values of A/h and this leads to one of the major results of the present work - a prediction of the cavity width for which the heat transfer of the high Darcy-Rayleigh number flow is a minimum. Chapter 7 contains a discussion of the relevant end-zone structure for $A/h = O(1)$ and provides an overall picture of the flow which, as $A/h \rightarrow \infty$, is consistent with the high Darcy-Rayleigh number flow in a cavity of finite aspect ratio ($A \gg 1, h = O(1)$).

Chapter 2 Convection in a vertical slot filled with a
porous medium

2.1 Introduction

In this chapter, the basic problem of convection in a rectangular cavity filled with a porous medium is formulated. The structure of the motion generated by maintaining the vertical walls at different constant temperatures is considered in the tall-cavity limit, $h \rightarrow \infty$. The governing equations and boundary conditions are stated in Section 2.2 using the non-dimensional formulation outlined in Chapter 1, based on Darcy's law and the Oberbeck-Boussinesq approximation. The steady-state flow is dependent on two non-dimensional parameters, the Darcy-Rayleigh number, A , and the aspect ratio, h . In Section 2.3 the solution is considered in the limit when h is large and A is finite, and it is shown that the flow domain divides into a main core region where $0 < z < h$ and end-zones at the top and bottom of the cavity, where $h-z=O(1)$ and $z=O(1)$ respectively. In the core region the flow is conduction-dominated and parallel to the vertical walls while in the end regions, where the flow is turned, there is a more complicated motion. Symmetry properties of the flow imply that it is only necessary to consider one of the end zones, and at the base of the cavity where $z=O(1)$ it is found that the leading approximations to the stream function and temperature satisfy the full nonlinear

equations of motion, together with boundary conditions needed to ensure that the solution matches with that in the core as $z \rightarrow \infty$. The end-region problem contains only one parameter, A and in general requires a numerical solution (which is undertaken in Chapter 5). Asymptotic solutions for small and large values of A are considered in Chapters 3 and 4. The end-region problem is stated in Section 2.4 and in Section 2.5 some of its general properties are considered with particular reference to the manner in which the parallel-flow core solution is recovered as $z \rightarrow \infty$. This leads to a fourth-order ordinary differential eigenvalue problem which determines the exponential decay-rate associated with the solution and thus a measure of the vertical extent of the end region. The eigenvalue problem is solved using both analytical and numerical techniques.

2.2 Formulation

Consider steady, two-dimensional motion in a rectangular cavity $0 \leq x^* \leq \ell^*$, $0 \leq z^* \leq h^*$ filled with a porous medium. The motion is driven by maintaining the two vertical walls $x^* = 0$ and $x^* = \ell^*$ at different constant temperatures $T^* = T_0^*$ and $T^* = T_0^* + \Delta T^*$ and the horizontal walls are thermally insulating. Then, as outlined in Chapter 1, the Darcy equations governing motion in the Oberbeck-Boussinesq approximation may be written in the non-dimensional form

$$\nabla^2 \bar{\psi} = -A \frac{\partial \bar{T}}{\partial x}, \quad (2.2.1)$$

$$\nabla^2 \bar{T} = \frac{\partial \bar{\psi}}{\partial z} \frac{\partial \bar{T}}{\partial x} - \frac{\partial \bar{\psi}}{\partial x} \frac{\partial \bar{T}}{\partial z}, \quad (2.2.2)$$

where $(x^*, z^*) = \ell^*(x, z)$, $T^* = T_0^* + \Delta T^* \bar{T}$, the stream function $\bar{\psi}$ has been made non-dimensional with respect to κ , and A is the Darcy-Rayleigh number defined by

$$A = \frac{\alpha g \Delta T^* k \ell^*}{\kappa \nu} \quad , \quad (2.2.3)$$

where α is the coefficient of thermal expansion, k is the permeability, g is the acceleration due to gravity, κ is the thermal diffusivity and ν is the kinematic viscosity.

Appropriate boundary conditions on the impermeable walls of the cavity are :

$$\bar{\psi} = \bar{T} = 0 \quad \text{on} \quad x = 0 \quad , \quad (2.2.4)$$

$$\bar{\psi} = 0 \quad , \quad \bar{T} = 1 \quad \text{on} \quad x = 1 \quad , \quad (2.2.5)$$

$$\bar{\psi} = \frac{\partial \bar{T}}{\partial z} = 0 \quad \text{on} \quad z = 0 \quad \text{and} \quad z = h, \quad (2.2.6)$$

where

$$h = h^* / \ell^* \quad (2.2.7)$$

is the cavity aspect ratio .

2.3 Solution for large aspect ratio , $h \gg 1$

In applications to thermal wall insulation and other related problems the solution for large values of h is of primary interest and consideration of the limit $h \rightarrow \infty$ also allows analytical progress to be made. The domain divides into a core region $0 < z < h$ and end regions

near the horizontal walls. In the core region, the vertical gradients may be neglected to a first approximation, leading to solutions for \bar{T} and $\bar{\psi}$ which may be expanded as

$$\bar{T} = T_c(x) + \dots, \quad \bar{\psi} = A \psi_c(x) + \dots, \quad (h \rightarrow \infty). \quad (2.3.1)$$

Substitution into (2.2.2) gives $d^2 T_c / dx^2 = 0$ and with $T_c = 0$ on $x = 0$ and $T_c = 1$ on $x = 1$, the required solution is

$$T_c = x. \quad (2.3.2)$$

It now follows from (2.2.1) that $d^2 \psi_c / dx^2 = -1$ and with $\psi_c = 0$ on $x = 0$ and $x = 1$, the required solution is

$$\psi_c = x(1-x) / 2. \quad (2.3.3)$$

This conductive solution consists of a vertical two-way flow driven by buoyancy, with fluid rising near the hot wall and descending near the cold wall. The solution (2.3.3) does not however satisfy the boundary conditions (2.2.6) on $\bar{\psi}$ at $z=0$ and $z=h$ and end regions are needed to accommodate the necessary turning motion. Since the full governing equations (2.2.1,2) and boundary conditions (2.2.4-6) possess the centro-symmetry properties

$$\left. \begin{aligned} \bar{\psi}(x,z) &= \bar{\psi}(1-x, h-z) \\ \bar{T}(x,z) &= 1 - \bar{T}(1-x, h-z) \end{aligned} \right\} \quad (2.3.4)$$

only the region near the bottom wall need be considered.

2.4 End region

In the end-region at the base of the cavity the solution is expanded in the form

$$\bar{T} = T(x, z) + \dots, \quad \bar{\psi} = \psi(x, z) + \dots, \quad (h \rightarrow \infty), \quad (2.4.1)$$

and from (2.2.1,2) the leading approximations ψ and T satisfy the full nonlinear system

$$\nabla^2 \psi = -A \frac{\partial T}{\partial x}, \quad (2.4.2)$$

$$\nabla^2 T = \frac{\partial \psi}{\partial z} \frac{\partial T}{\partial x} - \frac{\partial \psi}{\partial x} \frac{\partial T}{\partial z}, \quad (2.4.3)$$

with boundary conditions

$$\psi = T = 0 \quad \text{on} \quad x = 0, \quad (2.4.4)$$

$$\psi = 0, \quad T = 1 \quad \text{on} \quad x = 1, \quad (2.4.5)$$

$$\psi = \frac{\partial T}{\partial z} = 0 \quad \text{on} \quad z = 0, \quad (2.4.6)$$

and

$$\psi \rightarrow A\psi_c(x), \quad T \rightarrow T_c(x) \quad \text{as} \quad z \rightarrow \infty. \quad (2.4.7)$$

This system requires numerical solution for general values of the parameter A although some progress can be made analytically if A is either small or large by using asymptotic methods. These various approaches are considered in detail in Chapters 3-5 below. Here some

important properties of the solution are obtained through an investigation of the structure of the solution at large values of z , in particular giving confidence that the parallel-flow limit (2.4.7) can be achieved as $z \rightarrow \infty$ and giving an estimate of the vertical extent of the end region as a function of the Darcy-Rayleigh number, A .

2.5 End-region solution, $z \rightarrow \infty$.

As $z \rightarrow \infty$ it is assumed that ψ and T approach their limiting forms (2.4.7) with an exponential decay, so that

$$\left. \begin{aligned} \psi &\sim A\psi_c + \phi(x)e^{-\alpha z}, \\ T &\sim x + \theta(x)e^{-\alpha z}, \end{aligned} \right\} \quad (z \rightarrow \infty) \quad (2.5.1)$$

where the decay rate α and the functions $\phi(x)$ and $\theta(x)$ are to be determined. Substitution of (2.5.1) into (2.4.2,3) gives

$$\phi'' + \alpha^2 \phi = -A\theta' \quad (2.5.2)$$

$$\theta'' + \alpha^2 \theta - \theta\alpha A\psi_c' + \alpha\phi = 0 \quad (2.5.3)$$

and from (2.4.4,5) the boundary conditions are

$$\phi = \theta = 0 \quad \text{at} \quad x = 0 \quad \text{and} \quad x = 1. \quad (2.5.4)$$

It is easily shown that if α , $\theta(x)$, $\phi(x)$ are solutions of (2.5.2-4), so also are $-\alpha$, $-\theta(1-x)$, $\phi(1-x)$. Furthermore if α is complex then α^* , $\theta^*(x)$, $\phi^*(x)$ are also solutions where $*$ denotes complex conjugate. Thus

in considering the system, attention may be restricted to the first quadrant of the complex α plane. The function ϕ can, in fact, be determined from (2.5.2-4) to yield a single fourth-order eigenvalue problem for θ :

$$\theta^{IV} + \theta''(2\alpha^2 - A\alpha\psi_c') + A\alpha\theta' + (\alpha^4 - \alpha^3 A\psi_c')\theta = 0 \quad , \quad (2.5.5)$$

$$\theta = \theta' = 0 \quad \text{on } x=0 \quad \text{and} \quad x=1 \quad . \quad (2.5.6)$$

To solve (2.5.5,6) numerically, it is assumed that

$$\theta = \theta_r + i\theta_i \quad , \quad \alpha = \alpha_r + i\alpha_i \quad , \quad (2.5.7)$$

and substitution into (2.5.5) gives a pair of real coupled fourth order equations which may be reduced to first order form

$$y_i' = f_i(x, y_1, y_2, \dots, y_8) \quad , \quad (i=1, 2, \dots, 8) \quad (2.5.8)$$

by introducing the variables

$$\begin{aligned} y_1 &= \theta_r \quad , & y_2 &= \theta_i \quad , \\ y_3 &= \theta_r' = y_1' = f_1 \quad , & y_4 &= \theta_i' = y_2' = f_2 \quad , \\ y_5 &= \theta_r'' = y_3' = f_3 \quad , & y_6 &= \theta_i'' = y_4' = f_4 \quad , \\ y_7 &= \theta_r''' = y_5' = f_5 \quad , & y_8 &= \theta_i''' = y_6' = f_6 \quad , \end{aligned} \quad (2.5.9)$$

with

$$\begin{aligned}
f_7 = & \{A\alpha_r \psi_c' - 2(\alpha_r^2 - \alpha_i^2)\} y_5 + \{4\alpha_r \alpha_i - A\alpha_i \psi_c'\} y_6 - A\alpha_r y_3 + A\alpha_i y_4 \\
& - \{\alpha_r^4 - 6\alpha_r^2 \alpha_i^2 + \alpha_i^4 - (\alpha_r^3 - 3\alpha_r \alpha_i^2) A\psi_c'\} y_1 \\
& + \{4\alpha_r \alpha_i (\alpha_r^2 - \alpha_i^2) + (\alpha_i^3 - 3\alpha_i \alpha_r^2) A\psi_c'\} y_2, \tag{2.5.10}
\end{aligned}$$

$$\begin{aligned}
f_8 = & \{A\alpha_r \psi_c' - 2(\alpha_r^2 - \alpha_i^2)\} y_6 - \{4\alpha_r \alpha_i - A\alpha_i \psi_c'\} y_5 - A\alpha_r y_4 - A\alpha_i y_3 \\
& - \{\alpha_r^4 - 6\alpha_r^2 \alpha_i^2 + \alpha_i^4 - (\alpha_r^3 - 3\alpha_r \alpha_i^2) A\psi_c'\} y_2 \\
& - \{4\alpha_r \alpha_i (\alpha_r^2 - \alpha_i^2) + (\alpha_i^3 - 3\alpha_i \alpha_r^2) A\psi_c'\} y_1. \tag{2.5.11}
\end{aligned}$$

This allows the solution to be obtained numerically by a fourth-order Runge Kutta scheme. The solution vector is written as :

$$\underline{Y} = (Y_1, Y_2, \dots, Y_8) \tag{2.5.12}$$

and a solution constructed in the form

$$\underline{y} = a\underline{y}^{(1)} + b\underline{y}^{(2)}, \tag{2.5.13}$$

where a and b are complex constants, by computing from initial states

$$\underline{y}^{(1)} = (0, 0, 1, 0, 0, 0, 0, 0), \quad \underline{y}^{(2)} = (0, 0, 0, 0, 0, 0, 1, 0), \tag{2.5.14}$$

at $x=0$. Then the boundary conditions $\theta = \theta'' = 0$ at $x=1$, are satisfied provided that

$$d_r + id_i = \begin{bmatrix} Y_1^{(1)} + iy_2^{(1)} & Y_1^{(2)} + iy_2^{(2)} \\ Y_5^{(1)} + iy_6^{(1)} & Y_5^{(2)} + iy_6^{(2)} \end{bmatrix} = 0 \quad (2.5.15)$$

at $x=1$. The real and imaginary parts of this equation determine α_r and α_i . Most calculations of d_r and d_i were carried out with a step size $\Delta x=0.01$ in the Runge-Kutta scheme and the zeros (2.5.15) were located using Newton iteration for a function of two variables as follows. Assuming initial guesses for α_r and α_i the Newton increments q_r, q_i are such that

$$\left. \begin{aligned} d_r(\alpha_r + q_r, \alpha_i + q_i) &= d_r(\alpha_r, \alpha_i) + q_r \frac{\partial d_r}{\partial \alpha_r} + q_i \frac{\partial d_r}{\partial \alpha_i} = 0, \\ d_i(\alpha_r + q_r, \alpha_i + q_i) &= d_i(\alpha_r, \alpha_i) + q_r \frac{\partial d_i}{\partial \alpha_r} + q_i \frac{\partial d_i}{\partial \alpha_i} = 0, \end{aligned} \right\} \quad (2.5.16)$$

and may therefore be calculated from the formulae

$$q_r = (d_i \frac{\partial d_i}{\partial \alpha_i} - d_r \frac{\partial d_r}{\partial \alpha_i}) / J, \quad q_i = (d_i \frac{\partial d_r}{\partial \alpha_r} - d_r \frac{\partial d_i}{\partial \alpha_r}) / J, \quad (2.5.17)$$

where $J = \partial(d_r, d_i) / \partial(\alpha_i, \alpha_r)$. This provides the new approximation $\alpha_r + q_r$ and $\alpha_i + q_i$. The partial derivatives in (2.5.17) are evaluated numerically by calculating d_r and d_i at appropriate neighbouring values of α_r and α_i and the iteration continues until d_r and d_i are zero to within a required tolerance, usually taken as 10^{-7} . Solution branches in the complex α plane were generally located by marching forwards in the direction of A increasing, using the solution for the

previous value of A as an initial guess . In this way the various branches could be found by starting from known solutions $\alpha_r = n\pi$, $\alpha_i = 0$ ($n = 1, 2, \dots$) at $A=0$ (see below) . The results are shown in Figures 2.1 - 2.3. The figures show an interesting behaviour, with extensive regions in which α is complex, corresponding to a damped oscillatory component in the flow. Only the lowest branch appears to remain purely real and this determines the e-folding decay length of the end-region, $z \sim \alpha^{-1}$. Although higher branches contain complex sections, successive bifurcations appear to leave them purely real as $A \rightarrow \infty$. The results suggest that there is always a doubly-infinite family of eigenvalues, α , with positive real part, indicating that the end-region problem (2.4.2-7) is likely to have a consistent solution for all values of A , unlike related problems for Newtonian fluids where the parallel core-flow sometimes gives way to multiple cells (Daniels 1987 , Daniels, Blythe and Simpkins 1987).

Some of the key features of the solution of the eigenvalue problem can be obtained by asymptotic analysis. In particular the solution for small A is obtained by expanding θ and α in powers of A :

$$\left. \begin{aligned} \theta &= \theta_0 + A\theta_1 + A^2\theta_2 + \dots \\ \alpha &= \alpha_0 + A\alpha_1 + A^2\alpha_2 + \dots \end{aligned} \right\} A \rightarrow 0 . \quad (2.5.18)$$

Substitution into (2.5.5,6) then gives at leading order

$$\left. \begin{aligned} \theta_0^{IV} + 2\alpha_0^2 \theta_0'' + \alpha_0^4 \theta_0 &= 0 & ; \\ \theta_0 = \theta_0'' = 0 & \text{ at } x=0, 1 & , \end{aligned} \right\} \quad (2.5.19)$$

with solution

$$\theta_0 = a \sin n\pi x \quad , \quad \alpha_0 = n\pi \quad (n=1, 2, \dots) \quad , \quad (2.5.20)$$

where a is an arbitrary constant. From terms of order A , θ_1 is found to satisfy

$$\left. \begin{aligned} \theta_1^{IV} + 2n^2 \pi^2 \theta_1'' + n^4 \pi^4 \theta_1 &= -a_0 n^2 \pi^2 \cos n\pi x & ; \\ \theta_1 = \theta_1'' = 0 & \text{ at } x=0, 1 & , \end{aligned} \right\} \quad (2.5.21)$$

and although terms involving α_1 do not contribute, this has a consistent solution

$$\theta_1 = \frac{1}{8} a_0 \left\{ x(x-1) \cos n\pi x - \frac{1}{n\pi} \left(x - \frac{1}{2}\right) \sin n\pi x \right\} + a_1 \sin n\pi x \quad (2.5.22)$$

where a_1 is a further arbitrary constant. From terms of order A^2 , θ_2 is found to satisfy

$$\begin{aligned} \theta_2^{IV} + 2\alpha_0^2 \theta_2'' + \alpha_0^4 \theta_2 &= \theta_0' (\alpha_1 \psi_c' - 4\alpha_0 \alpha_2 - 2\alpha_1^2) + \\ &\theta_1'' (\alpha_0 \psi_c' - 4\alpha_0 \alpha_1) - \alpha_0 \theta_1' - \alpha_1 \theta_0' + \theta_0 (3\alpha_0^2 \alpha_1 \psi_c' \\ &- 6\alpha_0^2 \alpha_1^2 - 4\alpha_0^3 \alpha_2) + \theta_1 (\alpha_0^3 \psi_c' - 4\alpha_0^3 \alpha_1) & ; \end{aligned} \quad (2.5.23)$$

$$\theta_2 = \theta_2'' = 0 \quad \text{ at } x=0, 1 .$$

Multiplying the equation for θ_2 by $\sin n\pi x$ and integrating from $x=0$ to $x=1$ gives

$$a_0 \left\{ \frac{1}{32} + n^2 \pi^2 \alpha_1^2 - \frac{n^2 \pi^2}{192} \right\} = 0 \quad , \quad (2.5.24)$$

so that

$$\alpha_1 = \pm \left(\frac{n^2 \pi^2 - 6}{192 n^2 \pi^2} \right)^{1/2} \quad , \quad n=1,2,3,\dots \quad . \quad (2.5.25)$$

This result is consistent with the departure of the eigenvalues α from the neighbourhood of $A=0$, as found in the numerical solution shown in Figure 2.1. From each value $\alpha_0 = n\pi$ at $A=0$ two real branches are generated whose initial slopes correspond to the positive and negative values of α_1 given by (2.5.25) with

$$\alpha \sim n\pi \pm A \left(\frac{n^2 \pi^2 - 6}{192 n^2 \pi^2} \right)^{1/2} + O(A^2) \quad \text{as } A \rightarrow 0. \quad (2.5.26)$$

At higher values of A all but the lowest of these branches appear to follow a bifurcation sequence in which the solution contains one or more complex sections but eventually reverts to real form at large Darcy-Rayleigh numbers.

For large values of A solutions are sought in the form

$$\theta \sim \bar{\theta}(x) \quad , \quad \alpha \sim \bar{\alpha}/A \quad (A \rightarrow \infty) \quad , \quad (2.5.27)$$

and substitution into (2.5.5,6) gives :

$$\left. \begin{aligned} \tilde{\theta}^{IV} - \tilde{\alpha} \psi \tilde{\theta}'' + \tilde{\alpha} \tilde{\theta}' &= 0 ; \\ \tilde{\theta} = \tilde{\theta}' &= 0 \text{ at } x=0,1 . \end{aligned} \right\} \quad (2.5.28)$$

Solutions for the eigenvalue $\tilde{\alpha}$ were obtained using the appropriate simplified form of the Runge Kutta scheme outlined previously. Real eigenvalues were obtained in increasing order of magnitude as follows :

$$\tilde{\alpha} = 83.1 \quad , \quad 548.4 \quad , \quad 1332 \quad , \dots \quad (2.5.29)$$

and correspond to the leading branches of the numerical solution shown in Figure 2.1. Note that as $A \rightarrow \infty$ the end-zone expands on the vertical scale

$$z \sim A \tilde{\alpha}^{-1} \approx 0.012 A \quad , \quad (2.5.30)$$

leading to breakdown of the structure described in Section 2.3 when this becomes comparable with the cavity height, h . A more detailed investigation of the structure of the end-zone solution for large values of A is undertaken in Chapter 4 below .

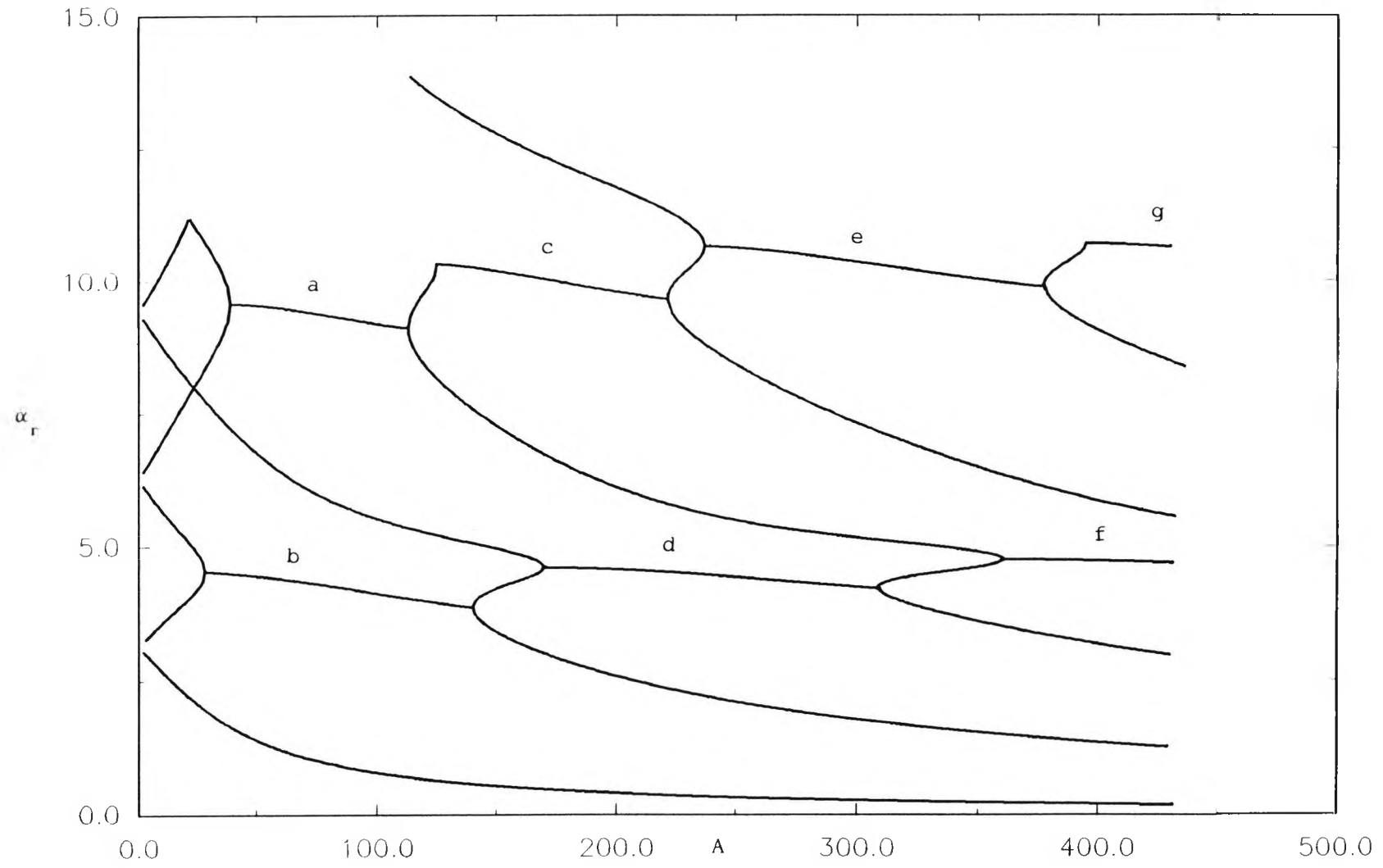


Figure 2.1 : The real parts of eigenvalue α against A

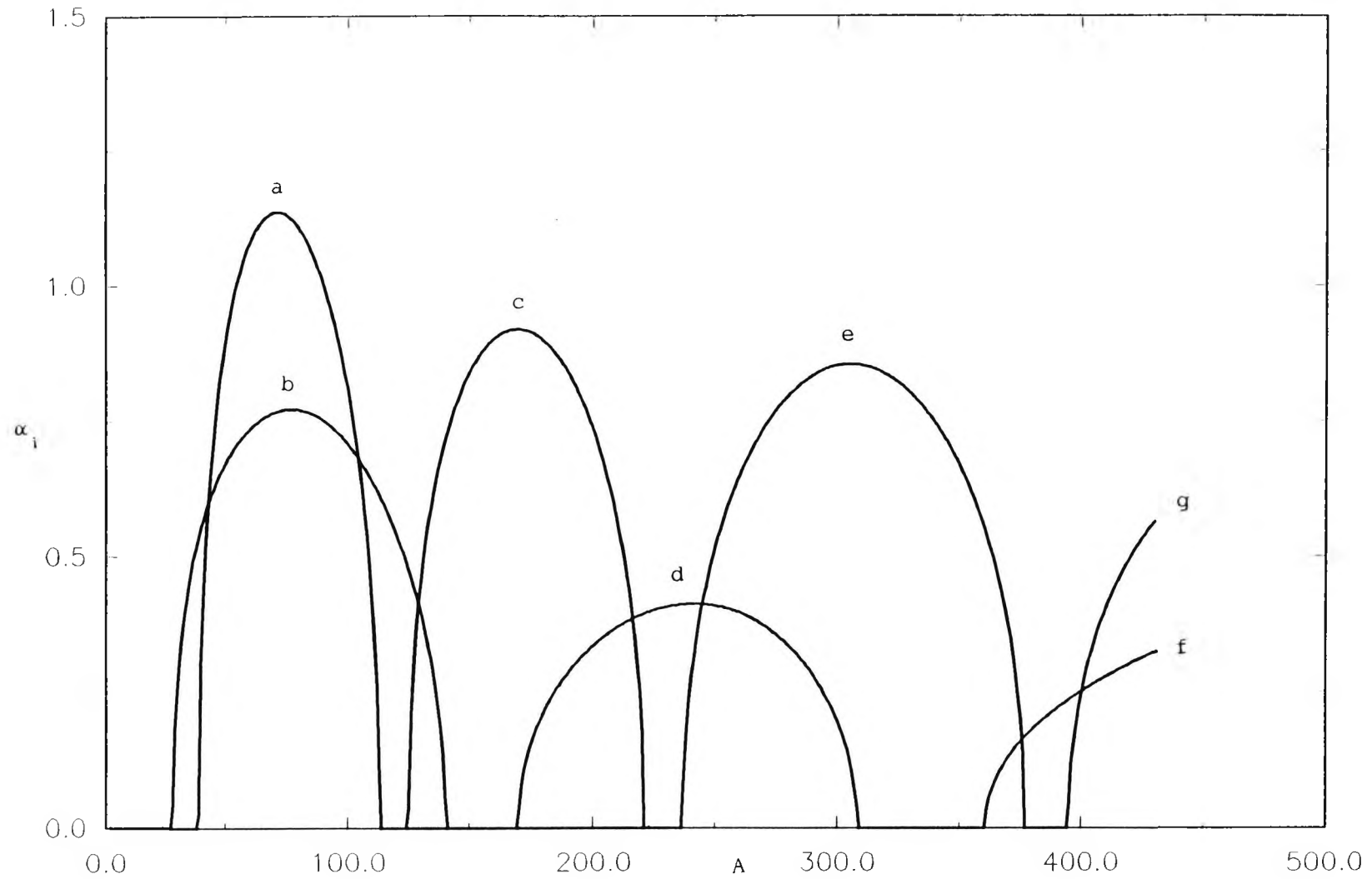


Figure 2.2 : The imaginary parts of eigenvalue α against A

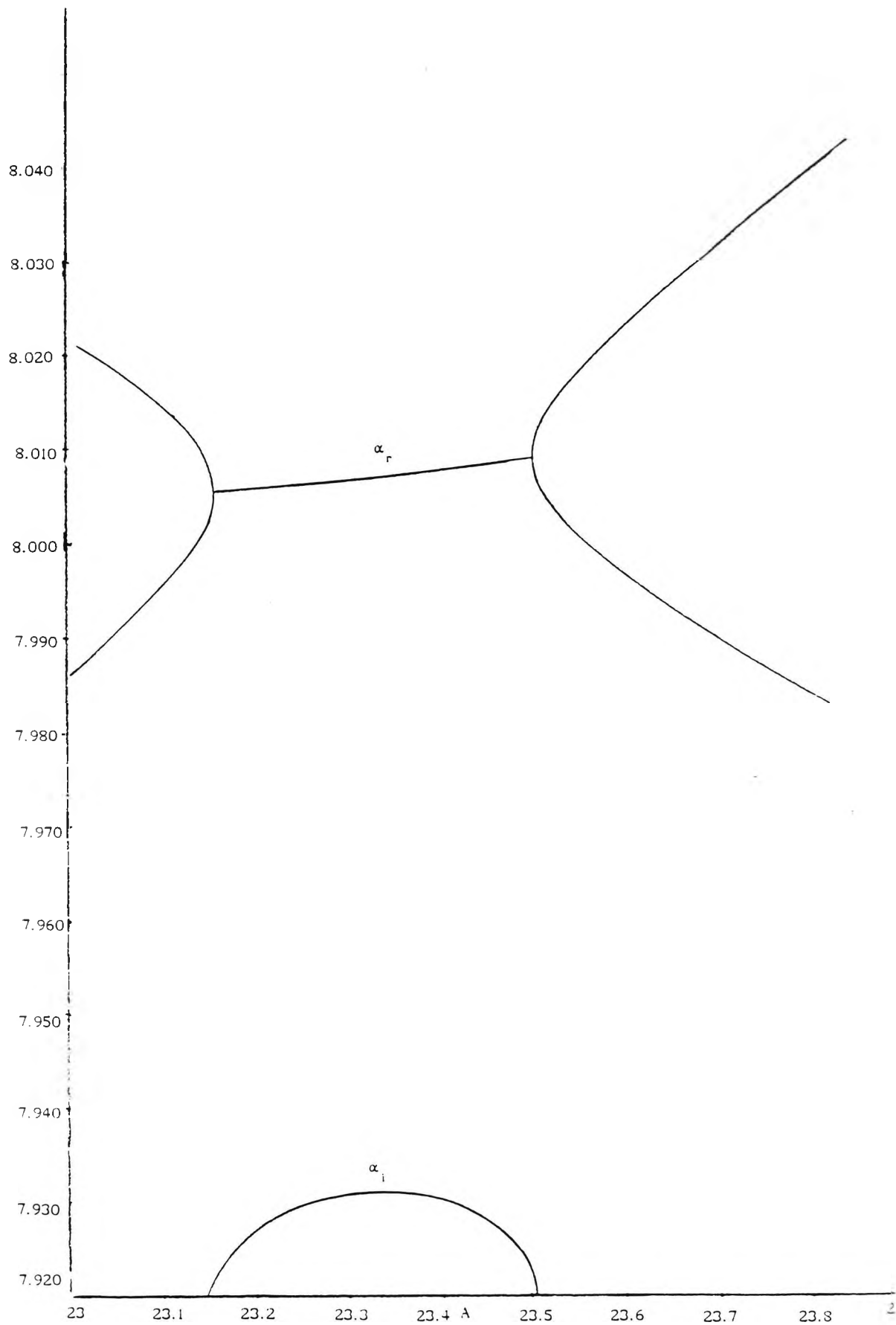


Figure 2.3 : The real and imaginary parts of eigenvalue α against A for $23 \leq A \leq 23.9$

Darcy-Rayleigh numbers, $A \ll 1$

3.1 Introduction

In this Chapter the solution of the end-zone problem is studied for small values of the Darcy-Rayleigh number A . In the limit as $A \rightarrow 0$ it is shown that the domain subdivides into inner and outer regions, with the major variation occurring in the inner region where $z = O(1)$. Here T and ψ are expanded in powers of the small parameter, A , and solutions for the first two terms in each expansion are found in Section 3.2 using Fourier series expansions in x . At large values of z , the exponentially small parts of these expansions break down, leading to the necessity for an outer region where $z = O(A^{-1})$. The outer solution for T and ψ is considered in Section 3.3 where it is shown that the exponential part of the solution adjusts from the outer form of the inner solution to a new form consistent with the structure associated with the eigenvalue problem studied in Section 2.5.

3.2 Inner expansion, $z = O(1)$

In the inner region where $z = O(1)$ the solution for the temperature, T , and stream function, ψ , may be expanded in the form

$$T = T_c(x) + AT_1(x, z) + A^2T_2(x, z) + \dots, \quad (3.2.1)$$

$$\psi = A(\psi_c(x) + \psi_1(x, z)) + A^2\psi_2(x, z) + A^3\psi_3(x, z) + \dots, \quad (3.2.2)$$

as $A \rightarrow 0$. It should be noted that the leading term in the temperature, $T_c = x$, is consistent with all of the boundary conditions (2.4.4-7) and therefore remains uniformly valid throughout the end region as $A \rightarrow 0$. Substitution into equation (2.4.2) now shows, from terms of order A , that

$$\nabla^2 \psi_1 = 0 \quad (3.2.3)$$

with, from (2.4.4-7), boundary conditions

$$\psi_1 = 0 \quad \text{on } x=0, \quad x=1, \quad (3.2.4)$$

$$\psi_1 = -\psi_c \quad \text{on } z=0, \quad (3.2.5)$$

$$\psi_1 \rightarrow 0 \quad \text{as } z \rightarrow \infty. \quad (3.2.6)$$

The solution for ψ_1 can be found by the method of separation of variables. Application of the boundary conditions at $x=0$, $x=1$ and as $z \rightarrow \infty$ yields

$$\psi_1 = \sum_{n=1}^{\infty} a_n e^{-n\pi z} \sin n\pi x \quad (3.2.7)$$

and the coefficients a_n are determined from the final condition on $z=0$, giving

$$a_n = \int_0^1 x(x-1) \sin n\pi x \, dx = \frac{2((-1)^n - 1)}{n^3 \pi^3}. \quad (3.2.8)$$

Thus, writing $n=2m-1$,

$$\psi_1 = -\frac{4}{\pi^3} \sum_{m=1}^{\infty} \frac{e^{-(2m-1)\pi z}}{(2m-1)^3} \sin(2m-1)\pi x. \quad (3.2.9)$$

From terms of order A in (2.4.3), T_1 satisfies

$$\nabla^2 T_1 = \frac{\partial \psi_1}{\partial z} \quad (3.2.10)$$

with, from (2.4.4-7), boundary conditions

$$T_1 = 0 \quad \text{on} \quad x=0, 1, \quad (3.2.11)$$

$$\frac{\partial T_1}{\partial z} = 0 \quad \text{on} \quad z=0, \quad (3.2.12)$$

$$T_1 \longrightarrow 0 \quad \text{as} \quad z \longrightarrow \infty. \quad (3.2.13)$$

The solution can be expressed as the sum of a particular solution which balances the right-hand side of (3.2.10) and satisfies the boundary conditions at $x=0$, $x=1$ and as $z \longrightarrow \infty$, and a complementary solution, which contains the coefficients b_m :

$$T_1 = -\frac{2}{\pi^3} \sum_{m=1}^{\infty} \frac{ze^{-(2m-1)\pi z}}{(2m-1)^3} \sin(2m-1)\pi x + \sum_{m=1}^{\infty} b_m e^{-(2m-1)\pi z} \sin(2m-1)\pi x. \quad (3.2.14)$$

These coefficients are determined by application of the remaining boundary condition, $\partial T_1 / \partial z = 0$ on $z=0$, which gives

$$b_m = \frac{-2}{(2m-1)^4 \pi^4} \quad (m=1, 2, \dots). \quad (3.2.15)$$

Thus

$$T_1 = -\frac{2}{\pi^4} \sum_{m=1}^{\infty} \left\{ \frac{(2m-1)\pi z + 1}{(2m-1)^4} \right\} e^{-(2m-1)\pi z} \sin(2m-1)\pi x. \quad (3.2.16)$$

Note that this contribution to the temperature field is a symmetric function of $(x - \frac{1}{2})$.

From terms of order A^2 in (2.4.2) it is found that ψ_2 satisfies

$$\nabla^2 \psi_2 = -\frac{\partial T_1}{\partial x} \quad (3.2.17)$$

with, from (2.4.4-7), boundary conditions

$$\psi_2 = 0 \quad \text{on } x=0, 1 \quad , \quad (3.2.18)$$

$$\psi_2 \longrightarrow 0 \quad \text{as } z \longrightarrow \infty \quad , \quad (3.2.19)$$

$$\psi_2 = 0 \quad \text{on } z=0 \quad . \quad (3.2.20)$$

To find a particular solution of (3.2.17), ψ_{2p} , which balances the right-hand side, and satisfies the boundary conditions on $x=0$, $x=1$ and as $z \longrightarrow \infty$, it is possible to restrict attention to a function which is antisymmetric about $x=1/2$. Taking into account the form of T_1 , a suitable trial solution is of the form

$$\begin{aligned} \psi_{2p} = \sum_{m=1}^{\infty} \{ (\alpha_m z + \beta_m) e^{-(2m-1)\pi z} (x - \frac{1}{2}) \sin(2m-1)\pi x \\ + \gamma_m e^{-(2m-1)\pi z} x(x-1) \cos(2m-1)\pi x \} \quad (3.2.21) \\ (m=1, 2, \dots) \end{aligned}$$

where α_m , β_m , γ_m are coefficients to be determined. Substitution into (3.2.17) then gives

$$\alpha_m = \frac{1}{(2m-1)^3 \pi^3} \quad , \quad \gamma_m = -\frac{1}{2(2m-1)^3 \pi^3} \quad , \quad \beta_m = \frac{3}{2(2m-1)^4 \pi^4} \quad (m=1, 2, \dots) \quad (3.2.22)$$

and the complete solution for ψ_2 is

$$\psi_2 = \psi_{2p} + \psi_{2c} \quad (3.2.23)$$

where

$$\psi_{2c} = \sum_{n=1}^{\infty} \delta_n e^{-n\pi z} \sin n\pi x \quad , \quad (3.2.24)$$

with the coefficients δ_n chosen to ensure that the final

boundary condition, $\psi_2=0$ on $z=0$, is satisfied. Thus

$$\delta_n = 2 \int_0^1 f(x) \sin n\pi x \, dx \quad (3.2.25)$$

where

$$f(x) = \frac{1}{2\pi^3} \sum_{m=1}^{\infty} \left\{ \frac{x(x-1)}{(2m-1)^3} \cos(2m-1)\pi x - \frac{3(x - \frac{1}{2})}{(2m-1)^4\pi} \sin(2m-1)\pi x \right\}. \quad (3.2.26)$$

It follows that $\delta_n=0$ for odd values of n and after integration by parts

$$\delta_n = \frac{2}{\pi^6} \sum_{m=1}^{\infty} \left\{ \frac{2}{(2m-1)^3} \left[\frac{1}{(2m-1-n)^3} - \frac{1}{(2m-1+n)^3} \right] + \frac{3}{(2m-1)^4} \left[\frac{1}{(2m-1-n)^2} - \frac{1}{(2m-1+n)^2} \right] \right\} \quad (n \text{ even}) \quad (3.2.27)$$

which upon further simplification gives

$$\delta_n = \frac{8n}{\pi^6} \sum_{m=1}^{\infty} \frac{3(2m-1)^2 - n^2}{(2m-1)^3 [(2m-1)^2 - n^2]^3} \quad (n \text{ even}). \quad (3.2.28)$$

Thus finally

$$\psi_2 = \frac{1}{\pi^3} \sum_{m=1}^{\infty} \left\{ \left[\frac{2}{(2m-1)^3} + \frac{3}{2(2m-1)^4\pi} \right] e^{-(2m-1)\pi z} \left(x - \frac{1}{2} \right) \times \right. \\ \left. \sin(2m-1)\pi x - \frac{e^{-(2m-1)\pi z}}{2(2m-1)^3} x(x-1) \cos(2m-1)\pi x \right\} \\ + \frac{16}{\pi^6} \sum_{k=1}^{\infty} \sum_{m=1}^{\infty} \frac{k[4k^2 - 3(2m-1)^2]}{(2m-1)^3 [(2m-1)^2 - 4k^2]^3} e^{-2k\pi z} \sin 2k\pi x. \quad (3.2.29)$$

The solution for ψ_2 is antisymmetric about $x=1/2$ and represents the dominant source of asymmetry in the

end-region flow as A increases from zero.

Summarising, the solution for small A has the form

$$\psi = A \left\{ \frac{x}{2}(1-x) - \frac{4}{\pi^3} \sum_{m=1}^{\infty} \frac{e^{-(2m-1)\pi z}}{(2m-1)^3} \sin(2m-1)\pi x \right\} + A^2 \psi_2 + \dots, \quad (3.2.30)$$

where ψ_2 is given by (3.2.29) and

$$T = x - A \left\{ \frac{2}{\pi^4} \sum_{m=1}^{\infty} \left[\frac{(2m-1)\pi z + 1}{(2m-1)^4} \right] e^{-(2m-1)\pi z} \sin(2m-1)\pi x \right\} + \dots, \quad (3.2.31)$$

in that part of the end-region where x and z are both of order one. It is noticeable, however, that the above expansions break down at large values of z , where $z = O(A^{-1})$. This may be seen by comparing terms of order $Ae^{-\pi z}$ and $A^2 z e^{-\pi z}$ in the form of ψ as $z \rightarrow \infty$. Although the breakdown only affects terms which are exponentially small, it is of interest to identify the correct expansion in the region where $z = O(A^{-1})$, and to resolve the discrepancy between (3.2.30,31) and the expansion for large z outlined in Section 2.5.

3.3 Outer expansion, $z = O(A^{-1})$

Let $\hat{z} = Az$ and then the leading terms in (3.2.30-31) suggest that in the outer region the expansions for T and ψ begin

$$\left. \begin{aligned} \psi &= A\psi_c(x) + Ae^{-\pi\hat{z}/A} \{ \hat{\psi}_1(x, \hat{z}) + A\hat{\psi}_2(x, \hat{z}) + \dots \} + \dots, \\ T &= T_c(x) + e^{-\pi\hat{z}/A} \{ \hat{T}_1(x, \hat{z}) + A\hat{T}_2(x, \hat{z}) + \dots \} + \dots \end{aligned} \right\} \quad (3.3.1)$$

Substitution into (2.4.2,3) then gives, from terms of

order $e^{-\pi\hat{z}/A}$ and $Ae^{-\pi\hat{z}/A}$ respectively,

$$\frac{\partial^2 \hat{T}_1}{\partial x^2} + \pi^2 \hat{T}_1 = 0 \quad , \quad (3.3.2)$$

$$\frac{\partial^2 \hat{\psi}_1}{\partial x^2} + \pi^2 \hat{\psi}_1 = - \frac{\partial \hat{T}_1}{\partial x} \quad , \quad (3.3.3)$$

with boundary conditions $\hat{\psi}_1 = \hat{T}_1 = 0$ at $x=0$ and $x=1$. Thus, from (3.3.2)

$$\hat{T}_1 = A_1(\hat{z}) \sin \pi x \quad , \quad (3.3.4)$$

where A_1 is an arbitrary function of \hat{z} and then, from (3.3.3),

$$\hat{\psi}_1 = B_1(\hat{z}) \sin \pi x - \frac{1}{2} A_1(\hat{z}) (x - \frac{1}{2}) \sin \pi x \quad , \quad (3.3.5)$$

where B_1 is a further arbitrary function of \hat{z} .

From terms of order $Ae^{-\pi\hat{z}/A}$ in (2.4.3),

$$\begin{aligned} \frac{\partial^2 \hat{T}_2}{\partial x^2} + \pi^2 \hat{T}_2 &= 2\pi \frac{\partial \hat{T}_1}{\partial \hat{z}} + \pi \left(\frac{1}{2} - x \right) \hat{T}_1 - \pi \hat{\psi}_1 \\ &= \left\{ \frac{1}{2} \left(\frac{1}{2} - x \right) A_1 - B_1 + 2A_1' \right\} \pi \sin \pi x \quad , \end{aligned} \quad (3.3.6)$$

where $A_1' = dA_1/d\hat{z}$. This has general solution

$$\begin{aligned} \hat{T}_2 &= A_2(\hat{z}) \sin \pi x + C_2(\hat{z}) \cos \pi x + \frac{A_1}{8} \left(x - \frac{1}{2} \right)^2 \cos \pi x \\ &\quad + \frac{1}{2} (B_1 - 2A_1') \left(x - \frac{1}{2} \right) \cos \pi x - \frac{A_1}{8\pi} \left(x - \frac{1}{2} \right) \sin \pi x \end{aligned} \quad (3.3.7)$$

and satisfaction of the boundary conditions $\hat{T}_2 = 0$ at $x=0$

and $x=1$ gives

$$C_2 = -\frac{A_1}{32} \quad \text{and} \quad B_1 = 2A_1' \quad (3.3.8)$$

Thus

$$\hat{T}_2 = \left\{ A_2 - \frac{A_1}{8\pi} \left(x - \frac{1}{2}\right) \right\} \sin \pi x + \frac{A_1}{8} x(x-1) \cos \pi x \quad (3.3.9)$$

where A_2 is an arbitrary function of \hat{z} .

From terms of order $A_1^2 e^{-\pi \hat{z}/A}$ in (2.4.2),

$$\frac{\partial^2 \hat{\psi}_2}{\partial x^2} + \pi^2 \hat{\psi}_2 = -\frac{\partial \hat{T}_2}{\partial x} + 2\pi \frac{\partial \hat{\psi}_1}{\partial \hat{z}}, \quad (3.3.10)$$

which has general solution

$$\begin{aligned} \hat{\psi}_2 = & B_2(\hat{z}) \sin \pi x + D_2(\hat{z}) \cos \pi x - \frac{1}{2} \left(A_2 + \frac{A_1'}{2\pi} \right) \left(x - \frac{1}{2}\right) \sin \pi x \\ & + \left(x - \frac{1}{2}\right) \cos \pi x \left\{ \left(\frac{A_1}{64} - B_1' - \frac{A_1}{16\pi^2}\right) + \frac{A_1'}{4} \left(x - \frac{1}{2}\right) - \frac{A_1}{48} \left(x - \frac{1}{2}\right)^2 \right\} \end{aligned} \quad (3.3.11)$$

and satisfaction of the boundary conditions $\hat{\psi}_2 = 0$ at $x=0$ and $x=1$ gives

$$D_2 = -\frac{A_1'}{16} \quad \text{and} \quad B_1' = \frac{A_1(\pi^2 - 6)}{96\pi^2} \quad (3.3.12)$$

Thus

$$\begin{aligned} \hat{\psi}_2 = & B_2 \sin \pi x - \frac{1}{2} \left(A_2 + \frac{A_1'}{2\pi} \right) \left(x - \frac{1}{2}\right) \sin \pi x \\ & - \cos \pi x \left\{ \frac{A_1}{16} - \frac{A_1}{192} \left(x - \frac{1}{2}\right) - \frac{A_1}{4} \left(x - \frac{1}{2}\right)^2 + \frac{A_1}{48} \left(x - \frac{1}{2}\right)^3 \right\} \end{aligned} \quad (3.3.13)$$

where B_2 is an arbitrary function of \hat{z}

At this stage the solution for $A_1(\hat{z})$ and $B_1(\hat{z})$ can

be completed by solving the coupled equations obtained in

(3.3.8) and (3.3.12):

$$2A_1' = B_1, \quad 96\pi^2 B_1' = (\pi^2 - 6)A_1 \quad (3.3.14)$$

subject to boundary conditions obtained by matching the outer solution to the inner solution found in Section 3.2. The outer limit of the inner solution as $z \rightarrow \infty$ is given by (3.2.30,31) as

$$\psi \sim A(\psi_c - \frac{4}{\pi^3} e^{-\pi z} \sin \pi x + \dots) + \dots, \quad (3.3.15)$$

$$T \sim T_c - \frac{2A}{\pi^4} (\pi z + 1) e^{-\pi z} \sin \pi x + \dots, \quad (3.3.16)$$

which when written in terms of the outer variable \hat{z} becomes

$$\psi \sim A(\psi_c - \frac{4}{\pi^3} e^{-\pi \hat{z}/A} \sin \pi x + \dots) + \dots, \quad (3.3.17)$$

$$T \sim T_c - \frac{2\hat{z}}{\pi^3} e^{-\pi \hat{z}/A} \sin \pi x + \dots. \quad (3.3.18)$$

From (3.3.4) and (3.3.5) the outer solution has the form

$$\psi \sim A\{\psi_c + (B_1 - \frac{1}{2}(x - \frac{1}{2})A_1) e^{-\pi \hat{z}/A} \sin \pi x\} + \dots, \quad (3.3.19)$$

$$T \sim T_c + A_1 e^{-\pi \hat{z}/A} \sin \pi x + \dots \quad (3.3.20)$$

and it follows that matching with (3.3.17,18) requires

$$A_1 \sim -2\hat{z}/\pi^3, \quad B_1 \rightarrow -4/\pi^3 \quad (\hat{z} \rightarrow 0). \quad (3.3.21)$$

Thus the equations (3.3.14) must be solved subject to the conditions

$$A_1 = 0, \quad B_1 = -4/\pi^3 \quad \text{at} \quad \hat{z} = 0, \quad (3.3.22)$$

and it is easily shown that the required solutions are

$$A_1 = -\frac{2}{\omega\pi^3} \sinh \omega \hat{z} \quad (3.3.23)$$

$$B_1 = -\frac{4}{\pi^3} \cosh \omega \hat{z} \quad (3.3.24)$$

where

$$\omega = \left(\frac{\pi^2 - 6}{192\pi^2} \right)^{1/2} \quad (3.3.25)$$

Although these grow exponentially as $\hat{z} \rightarrow \infty$ the corresponding parts of the overall solution still decay, providing a consistent match with the core solution.

In summary, the leading terms in the outer expansions for ψ and T are

$$\psi = A\psi_c(x) - \frac{A}{\pi^3} e^{-\pi\hat{z}/A} \left(4\cosh \omega \hat{z} - \frac{(x-\frac{1}{2})}{\omega} \sinh \omega \hat{z} \right) \sin \pi x + O(A^2 e^{-\pi\hat{z}/A}) \quad (3.3.26)$$

and

$$T = T_c(x) - \frac{2e^{-\pi\hat{z}/A}}{\omega\pi^3} \sinh \omega \hat{z} \sin \pi x + O(Ae^{-\pi\hat{z}/A}) \quad (3.3.27)$$

and these are valid in a region of vertical extent $\hat{z} = O(1)$, equivalent to z of order A^{-1} as $A \rightarrow 0$. At the edge of this region, as $\hat{z} \rightarrow \infty$, the overall exponential decay associated with (3.3.26,27) may be expressed in the form $e^{-\alpha z}$ where

$$\alpha \sim \pi \pm A\omega \quad (A \rightarrow 0) \quad (3.3.28)$$

and with ω given by (3.3.25) this is seen to be consistent with the leading eigenvalue ($n=1$) identified in Section 2.5.

Chapter 4 Solution of the end-zone problem for large

Darcy-Rayleigh numbers $A \gg 1$

4.1 Introduction

In this chapter the structure of the end-zone solution is considered for large values of the Darcy-Rayleigh number. Three main vertical scales emerge in the limit as $A \rightarrow \infty$, giving rise to an outer region of large vertical extent $z=O(A)$, a main inner region of roughly square cross-section where $z=O(1)$ and an inner horizontal layer where $z=O(A^{-1/4})$. The inner regions also subdivide laterally into main sections which span most of the cavity width $0 < x < 1$, and boundary layers on the vertical walls near $x=0$ and $x=1$. A schematic diagram of the overall structure is shown in Figure 4.1.

The outer region is governed by a reduced form of the end-zone equations equivalent to a vertical boundary-layer system and is considered in Section 4.2. One of the key properties of the solution here is its behaviour approaching the base of the cavity, because this determines the nature of the solutions in the inner regions and eventually whether the overall structure is self-consistent. At the base of the outer region the proposed structure consists of three separate regions. Near the hot wall there is a boundary layer region which accommodates the main temperature adjustment from $T=1$ at the wall to $T \approx 0$ in the interior. This drives an upward flow which entrains fluid from the interior region $0 < x < 1$.

Near the cold wall there is a further adjustment but here and throughout the interior region the motion is convectively dominated.

The solution in the outer zone breaks down when the vertical scale becomes comparable with the cavity width, leading to a local structure in which both horizontal and vertical diffusion are significant. The main central zone of this inner region, considered in Section 4.3, consists of descending streamlines which are deflected into the boundary layer on the hot wall where $1-x=O(A^{-1/2})$ and a similarity solution is available. In the central zone, a solution is obtained by use of sine transforms. Because the central zone is convectively dominated, the solution for the temperature field there does not satisfy the thermal boundary condition $\partial T/\partial z=0$ at $z=0$ and as a result a further inner horizontal layer is necessary where $z=O(A^{-1/4})$. Here thermal conduction is significant and a solution of the horizontal thermal boundary-layer equations is required. This is described in Section 4.4, and indicates that the layer is compressed downwards into the bottom corner of the cavity as it approaches the hot wall. Details of the various corner regions are discussed in Section 4.5.

4.2 Outer zone, $z=O(A)$

The eigenvalue calculations of Section 2.5 indicate the existence of an outer region with a long vertical length scale z of order A as $A \rightarrow \infty$. Thus a new variable

$$\tilde{z} = z/A \quad (4.2.1)$$

is introduced and solutions for the temperature and stream function are assumed in the form

$$T = \tilde{T}(x, \tilde{z}) + \dots, \quad \psi = A\tilde{\psi}(x, \tilde{z}) + \dots \quad (4.2.2)$$

Substitution into (2.4.2,3) gives :

$$\frac{\partial^2 \tilde{\psi}}{\partial x^2} = - \frac{\partial \tilde{T}}{\partial x}, \quad (4.2.3)$$

$$\frac{\partial^2 \tilde{T}}{\partial x^2} = \frac{\partial(\tilde{T}, \tilde{\psi})}{\partial(x, \tilde{z})}, \quad (4.2.4)$$

and from (2.4.4,5,7) a solution is required for which

$$\tilde{\psi} = \tilde{T} = 0 \quad \text{at } x=0, \quad (4.2.5)$$

$$\tilde{\psi} = 0, \quad \tilde{T} = 1 \quad \text{at } x=1, \quad (4.2.6)$$

$$\tilde{\psi} \rightarrow \psi_c(x), \quad \tilde{T} \rightarrow T_c(x) \quad \text{as } \tilde{z} \rightarrow \infty, \quad (4.2.7)$$

where $\psi_c = x(1-x)/2$ and $T_c = x$. Although the solution of this system cannot be expected to satisfy the full boundary conditions (2.4.6) at $\tilde{z}=0$, it is shown here that a structure can be found for which

$$\tilde{\psi} \rightarrow 0 \quad \text{as } \tilde{z} \rightarrow 0. \quad (4.2.8)$$

This structure is quite complicated and consists of three separate regions spanning the cavity width $0 \leq x \leq 1$.

Near the hot wall a thermal boundary-layer region where $\eta = (1-x)/\tilde{z}^{1/2} = O(1)$ accommodates the main temperature adjustment from $\tilde{T}=1$ at the wall to $\tilde{T}=0$ in

the interior $0 < x < 1$. Locally,

$$\tilde{\psi} = \tilde{z}^{1/2} F_0(\eta) + \dots, \quad \tilde{T} = G_0(\eta) + \dots \quad (\tilde{z} \rightarrow 0) \quad (4.2.9)$$

and substitution into (4.2.3,4) gives

$$G_0'' = -\frac{1}{2} G_0' F_0, \quad G_0' = F_0'' \quad (4.2.10)$$

Appropriate boundary conditions are

$$G_0 = 1, \quad F_0 = 0 \quad \text{at} \quad \eta = 0 \quad (4.2.11)$$

and

$$G_0 \rightarrow 0, \quad F_0' \rightarrow 0 \quad \text{as} \quad \eta \rightarrow \infty. \quad (4.2.12)$$

Here the temperature must approach its cold-wall value as $\eta \rightarrow \infty$, as a similar temperature adjustment adjacent to the cold wall cannot occur. The system (4.2.10-12) reduces to the following third-order problem for F_0

$$\left. \begin{aligned} F_0'''' + \frac{1}{2} F_0'' F_0 &= 0; \\ F_0 = 0, \quad F_0' = 1 \quad (\eta = 0), \quad F_0' &\rightarrow 0 \quad (\eta \rightarrow \infty) \end{aligned} \right\} \quad (4.2.13)$$

and then the temperature field is given by

$$G_0 = F_0' \quad (4.2.14)$$

A numerical solution of (4.2.13) has been obtained in different contexts by Howarth (1959), Sakiadis (1961) and Singh and Cowling (1963) and shows that $F_0 \rightarrow a_0 = 1.616$ as $\eta \rightarrow \infty$. This behaviour generates a stream function of order $\tilde{z}^{1/2}$ across the interior $0 < x < 1$. A consistent solution near the cold wall requires that \tilde{T} and $\tilde{\psi}$ are of

equal magnitudes there and indeed throughout the region $0 \leq x < 1$ which is convectively-dominated.

Thus for the interior region $0 < x < 1$, it is assumed that

$$\bar{T} = \bar{z}^{1/2} \bar{T}_0(x) + \dots, \quad \bar{\psi} = \bar{z}^{1/2} \bar{\psi}_0(x) + \dots \quad (\bar{z} \rightarrow 0) \quad (4.2.15)$$

and substitution into (4.2.3,4) gives

$$\bar{T}'_0 \bar{\psi}_0 - \bar{\psi}'_0 \bar{T}_0 = 0, \quad \bar{\psi}''_0 = -\bar{T}'_0. \quad (4.2.16)$$

Thus

$$\bar{T}_0 = K \bar{\psi}_0, \quad (4.2.17)$$

where K is an arbitrary constant, and since matching with (4.2.9) requires that $\bar{\psi}_0 \rightarrow a_0$ as $x \rightarrow 1$ the appropriate solution is

$$\bar{\psi}_0 = \frac{a_0}{1-e^{-k}} (1-e^{-kx}), \quad \bar{T}_0 = \frac{a_0 K}{1-e^{-k}} (1-e^{-kx}). \quad (4.2.18)$$

Here it has also been assumed that $\bar{\psi}$ and \bar{T} tend to zero as $x \rightarrow 0$ in order to produce a consistent solution near the cold wall.

Near the cold wall $\bar{\psi}$ and \bar{T} can be expanded in the form

$$\left. \begin{aligned} \bar{\psi} &= \bar{z}^{3/4} f_0(\zeta) + \bar{z}^{11/12} f_{10}(\zeta) + \bar{z} f_1(\zeta) + \dots \\ \bar{T} &= \bar{z}^{3/4} g_0(\zeta) + \bar{z}^{11/12} g_{10}(\zeta) + \bar{z} g_1(\zeta) + \dots \end{aligned} \right\} (\bar{z} \rightarrow 0) \quad (4.2.19)$$

where $\zeta = x/\bar{z}^{1/4}$. Substitution into (4.2.3,4) gives, at leading order

$$f_0'' = 0, \quad g_0'' = \frac{3}{4}f_0'g_0' - \frac{3}{4}g_0'f_0' \quad (4.2.20)$$

and from (4.2.5) it is required that

$$f_0 = g_0 = 0 \quad \text{at} \quad \zeta = 0. \quad (4.2.21)$$

The required solutions which match with (4.2.15) as $\zeta \rightarrow \infty$ are simply the linear limiting forms (4.2.18) as $x \rightarrow 0$, namely

$$f_0 = c_0 \zeta, \quad g_0 = c_0 K \zeta, \quad (4.2.22)$$

where

$$c_0 = \frac{a_0 K}{1 - e^{-K}}. \quad (4.2.23)$$

The terms f_{10}, g_{10} (which will be determined below) are similar linear functions of ζ whose presence is suggested by the analysis of Blythe, Daniels and Simpkins (1982) of a related structure arising at large Darcy-Rayleigh numbers in a cavity of finite aspect ratio. The relation between the present work and that for order one values of h will be discussed in detail in Chapter 7.

The correction terms f_1, g_1 in (4.2.19) satisfy

$$\left. \begin{aligned} g_1'' &= f_1'g_0' - g_1'f_0' + \frac{3}{4}(g_1'f_0' - f_1'g_0') \\ f_1'' &= -g_0' \end{aligned} \right\} \quad (4.2.24)$$

and after substitution of f_0 and g_0 from (4.2.22) it is found that

$$f_1 = -\frac{c_0 K}{2} \zeta^2 + B\zeta, \quad (4.2.25)$$

$$g_1'' - \frac{3}{4}c_0 \zeta g_1' + c_0 g_1 = \frac{1}{4}(c_0^2 K^2 \zeta^2 + c_0 K B \zeta). \quad (4.2.26)$$

Here the wall condition $f_1=0$ at $\zeta=0$ has been applied and at this stage B is an arbitrary constant. The equation for g_1 has general solution

$$g_1 = c_1 \exp\left(\frac{K_1}{4}\zeta^2\right) U\left(-\frac{11}{6}, K_1^{1/2}\zeta\right) + K^2\left(1 - \frac{c_0 \zeta^2}{2}\right) + KB\zeta, \quad (4.2.27)$$

where $U\left(-\frac{11}{6}, K_1^{1/2}\zeta\right)$ is the parabolic cylinder function defined by Abramowitz and Stegun (1965, p.686),

$$K_1 = \frac{3c_0}{4} = \frac{3a_0 K}{4(1-e^{-K})} \quad (4.2.28)$$

and the solution which is exponentially large as $\zeta \rightarrow \infty$ has been excluded. Applying the boundary condition

$g_1=0$ at $\zeta=0$ gives

$$c_1 = 2^{1/3} 3\Gamma(5/6)K^2/\pi^{1/2} = 2.405 K^2 \quad (4.2.29)$$

and since

$$U\left(-\frac{11}{6}, K_1^{1/2}\zeta\right) \sim K_1^{2/3} \zeta^{4/3} \exp\left(-\frac{K_1 \zeta^2}{4}\right) \text{ as } \zeta \rightarrow \infty \quad (4.2.30)$$

it follows that a term of order $\tilde{z}^{2/3}$ in T is generated in the interior $0 < x < 1$.

Thus the interior expansion develops as

$$\left. \begin{aligned} \tilde{\psi} &= \tilde{z}^{1/2} \tilde{\psi}_0(x) + \tilde{z}^{2/3} \tilde{\psi}_1(x) + \dots \\ \tilde{T} &= \tilde{z}^{1/2} \tilde{T}_0(x) + \tilde{z}^{2/3} \tilde{T}_1(x) + \dots \end{aligned} \right\} (\tilde{z} \rightarrow 0) \quad (4.2.31)$$

and correspondingly for the region near the hot wall it is anticipated that

$$\left. \begin{aligned} \tilde{\psi} &= \tilde{z}^{1/2} F_0(\eta) + \tilde{z}^{2/3} F_1(\eta) + \dots \\ \tilde{T} &= G_0(\eta) + \tilde{z}^{1/6} G_1(\eta) + \dots \end{aligned} \right\} (\tilde{z} \rightarrow 0). \quad (4.2.32)$$

Substitution of (4.2.31) into (4.2.3,4) gives

$$\left. \begin{aligned} \frac{2}{3}(\tilde{T}'_0 \tilde{\psi}'_1 - \tilde{T}'_1 \tilde{\psi}'_0) + \frac{1}{2}(\tilde{T}'_1 \tilde{\psi}'_0 - \tilde{T}'_0 \tilde{\psi}'_1) &= 0, \\ \tilde{\psi}'_1{}' &= -\tilde{T}'_1 \end{aligned} \right\} \quad (4.2.33)$$

so that

$$\tilde{T}'_1 = -\tilde{\psi}'_1 + d_1 \quad (4.2.34)$$

where d_1 is a constant and elimination of \tilde{T}'_1 from (4.2.33) gives

$$(1 - e^{-Kx}) \tilde{\psi}'_1{}' + (K - \frac{7}{3}Ke^{-Kx}) \tilde{\psi}'_1 - \frac{4}{3}K^2 e^{-Kx} \tilde{\psi}_1 = -\frac{4}{3}d_1 Ke^{-Kx}. \quad (4.2.35)$$

The general solution is

$$\tilde{\psi}_1 = \frac{d_1}{K} + e^{-Kx} (d_2 + d_3 I_1(x)) \quad (4.2.36)$$

where d_2 and d_3 are further arbitrary constants and

$$I_1(x) = \int_0^{x'=x} e^{Kx'} (1 - e^{-Kx'})^{4/3} dx'. \quad (4.2.37)$$

This integral can be evaluated by means of the substitution $\xi' = (1 - e^{-Kx'})^{1/3}$ so that

$$I_1 = \frac{3}{K} \int_0^{\xi'=\xi} \xi'^6 (1 - \xi'^3)^{-2} d\xi' \quad (4.2.38)$$

where $\xi = (1 - e^{-Kx})^{1/3}$, and after use of integration by parts and partial fractions

$$I_1 = \left\{ \frac{\xi(4-3\xi^3)}{1-\xi^3} + \frac{2}{3} \ln \frac{(1-\xi)^2}{1+\xi+\xi^2} - \frac{4}{\sqrt{3}} \left(\tan^{-1} \frac{1+2\xi}{\sqrt{3}} - \frac{\pi}{6} \right) \right\} / K. \quad (4.2.39)$$

It now follows that

$$\left. \begin{aligned} \tilde{\psi}_1 &= \frac{d_1}{K} + d_2(1 - Kx + \frac{K^2}{2}x^2 + \dots) + \frac{3}{7}d_3K^{4/3}x^{7/3} + \dots, \\ \tilde{T}_1 &= d_1 + d_2K - d_2K^2x - d_3K^{4/3}x^{4/3} + \dots, \end{aligned} \right\} (x \rightarrow 0) \quad (4.2.40)$$

and matching with the wall solution (4.2.19) requires that

$$d_1 = -d_2K, \quad (4.2.41)$$

$$d_3 = \frac{3}{2} \left(\frac{3a_0K^2}{1-e^{-K}} \right)^{2/3} \Gamma(5/6) / \pi^{1/2} \quad (4.2.42)$$

and determines the functions g_{10} and f_{10} as

$$g_{10} = Kf_{10} = -K^2d_2\zeta. \quad (4.2.43)$$

A third condition which finally determines d_1 and d_2 arises from consistency with the solution near the hot wall. The correction terms F_1 and G_1 in (4.2.32) satisfy

$$\left. \begin{aligned} G_1'' &= \frac{1}{6}G_1F_0' - \frac{1}{2}G_1'F_0 - \frac{2}{3}G_0'F_1', & F_1'' &= G_1'; \\ G_1 = F_1 = 0 & \text{ at } \eta = 0, & G_1, F_1' &\rightarrow 0 \quad (\eta \rightarrow \infty). \end{aligned} \right\} \quad (4.2.44)$$

It follows that $G_1 = F_1'$ and hence

$$F_1'''' + \frac{1}{2}F_0F_1'' - \frac{1}{6}F_0'F_1' + \frac{2}{3}F_0''F_1 = 0. \quad (4.2.45)$$

However the solution of this equation subject to the homogeneous boundary conditions

$$F_1 = F_1' = 0 \quad (\eta=0) \quad , \quad F_1' \longrightarrow 0 \quad (\eta \longrightarrow \infty) \quad (4.2.46)$$

is the trivial solution $F_1 = 0$, and thus $G_1 = 0$ also. The interior solution for $\tilde{\psi}_1$ must therefore satisfy

$$\tilde{\psi}_1(1) = 0 \quad , \quad (4.2.47)$$

with the result that

$$d_1 = -d_2 K = \frac{3\Gamma(5/6)}{2\xi_1^3 \pi^{1/2}} \left(\frac{3a_0 K^2}{1-e^{-K}} \right)^{2/3} \left\{ \frac{\xi_1(4-3\xi_1^3)}{1-\xi_1^3} + \frac{2}{3} \ln \frac{(1-\xi_1)^2}{1+\xi_1+\xi_1^2} - \frac{4}{\sqrt{3}} \left(\tan^{-1} \frac{1+2\xi_1}{\sqrt{3}} - \frac{\pi}{6} \right) \right\} \quad (4.2.48)$$

where $\xi_1 = (1-e^{-K})^{1/3}$. The graph of d_1 as a function of K is shown in Figure 4.2 .

In summary ,

$$\tilde{\psi}_1 = \frac{d_1}{K} (1-e^{-Kx}) - \frac{3}{2} \left(\frac{3a_0 K^2}{1-e^{-K}} \right)^{2/3} \frac{\Gamma(5/6)}{\pi^{1/2}} e^{-Kx} I_1(x) \quad (4.2.49)$$

with d_1 given by (4.2.48) and K an arbitrary constant whose value cannot be determined from the local analysis as $\tilde{z} \longrightarrow 0$.

An approximate estimate of K can be deduced from the assumption that convective dominance is maintained all the way down the cold wall. As $\tilde{z} \longrightarrow \infty$ it is known from (4.2.7) that

$$\tilde{\psi} \sim \frac{1}{2} x \quad , \quad \tilde{T} \sim x \quad (4.2.50)$$

near $x=0$, so that the functional relation

$$\tilde{T} = K\tilde{\psi} \quad (4.2.51)$$

applies to a first approximation with $K=2$. This may well provide a good estimate of the actual value of K in the interior solution (4.2.17) as $\tilde{z} \rightarrow 0$ where the isotherms and streamlines descending near the cold wall are turned across the cavity. Graphs of $\tilde{\psi}_0$, \tilde{T}_0 , $\tilde{\psi}_1$ and \tilde{T}_1 for $K=2$ are shown in Figures 4.3 and 4.4.

The structure found above can now be used to predict the behaviour of the flow near the bottom of the end zone where there must be an adjustment to the full adiabatic boundary conditions at $z=0$. Further terms in the interior and wall regions are expected to arise in a similar manner to those described by Blythe, Daniels and Simpkins (1982) for the high Darcy-Rayleigh number limit in a cavity of finite aspect ratio. This leads to a very complicated set of expansions in powers of \tilde{z} as $\tilde{z} \rightarrow 0$, the details of which it will not be necessary to consider here.

4.3 Inner regions, $z=O(1)$

The solution in the outer zone breaks down as $\tilde{z} \rightarrow 0$ because z derivatives in the diffusion term $\nabla^2 \psi$ can no longer be neglected relative to x derivatives. Thus a new structure develops in a central zone where x and z are of order one. The form of the outer solution as $\tilde{z} \rightarrow 0$ suggests that this central zone is flanked by a vertical boundary layer of thickness $x=O(A^{-1/4})$ near the cold wall and a vertical boundary layer of thickness $1-x=O(A^{-1/2})$ near the hot wall (see Figure 4.1). In the layer near the hot wall (region I) it is expected that

$$T = T_1(x_1, z) + \dots, \quad \psi = A^{1/2} \psi_1(x_1, z) + \dots \quad (A \rightarrow \infty), \quad (4.3.1)$$

where $x_1 = A^{1/2}(1-x)$ and substitution into (2.4.2,3) gives the vertical boundary-layer system

$$\frac{\partial^2 T_1}{\partial x_1^2} = \frac{\partial(\psi_1, T_1)}{\partial(x_1, z)}, \quad (4.3.2)$$

$$\frac{\partial^2 \psi_1}{\partial x_1^2} = \frac{\partial T_1}{\partial x_1}. \quad (4.3.3)$$

In the central zone (region II)

$$\psi = A^{1/2} \psi_2(x, z) + \dots, \quad T = A^{-1/2} T_2(x, z) + \dots \quad (A \rightarrow \infty) \quad (4.3.4)$$

and substitution into (2.4.2,3) gives the convection-dominated system

$$\frac{\partial T_2}{\partial x} \frac{\partial \psi_2}{\partial z} - \frac{\partial T_2}{\partial z} \frac{\partial \psi_2}{\partial x} = 0, \quad (4.3.5)$$

$$\nabla^2 \psi_2 = - \frac{\partial T_2}{\partial x}, \quad (4.3.6)$$

while for the layer near the cold wall (region III)

$$\psi = A^{1/4} \psi_3(x_3, z) + \dots, \quad T = A^{3/4} T_3(x_3, z) + \dots \quad (A \rightarrow \infty) \quad (4.3.7)$$

where $x_3 = A^{1/4} x$ and substitution into (2.4.2,3) gives

$$\frac{\partial^2 T_3}{\partial x_3^2} = \frac{\partial(T_3, \psi_3)}{\partial(x_3, z)}, \quad (4.3.8)$$

$$\frac{\partial^2 \psi_3}{\partial x_3^2} = 0. \quad (4.3.9)$$

In region I the solution is generated by the need to adjust the temperature from $T_1=1$ at $x_1=0$ to zero as $x_1 \rightarrow \infty$

and is simply an extension of the similarity form defined in (4.2.9), with

$$T_1 = G_0(\eta) \quad , \quad \psi_1 = z^{1/2} F_0(\eta), \quad (4.3.10)$$

where $\eta = x_1/z^{1/2}$. This implies that the solution in the central zone is generated by the requirement that

$$\psi_2 = a_0 z^{1/2} \quad \text{at} \quad x=1 \quad (4.3.11)$$

and also

$$\psi_2 \sim \frac{a_0(1-e^{-Kx})}{1-e^{-K}} z^{1/2} \quad \text{as} \quad z \rightarrow \infty. \quad (4.3.12)$$

Here the condition (4.3.11) represents matching with the boundary layer solution (4.3.10) in which $F_0(\infty) = a_0$ and (4.3.12) represents matching with the main outer solution (4.2.15) as $z \rightarrow \infty$. Since region II is convection-dominated and from (4.2.17) the temperature field must satisfy $T_2 \sim K\psi_2$ as $z \rightarrow \infty$, it follows that

$$T_2 = K\psi_2 \quad (4.3.13)$$

throughout region II. Thus from (4.3.6) the governing equation for ψ_2 is

$$\nabla^2 \psi_2 = -K \frac{\partial \psi_2}{\partial x} \quad (4.3.14)$$

and this must be solved subject to (4.3.11,12) and the further requirements

$$\psi_2 = 0 \quad \text{at} \quad x=0 \quad , \quad (4.3.15)$$

$$\psi_2 = 0 \quad \text{at} \quad z=0 \quad . \quad (4.3.16)$$

Here (4.3.15) represents matching with the solution in

region III, while (4.3.16) is needed for consistency with the requirement that the stream function vanishes on the lower wall of the cavity .

Note that a consistent solution in region III that satisfies the boundary conditions on the cold wall and matches with the central-zone solution as $x_3 \rightarrow \infty$ is

$$\psi_3 = B(z)x_3, \quad T_3 = KB(z)x_3, \quad (4.3.17)$$

where the function $B(z) = \partial\psi_2/\partial x(0, z)$ and must be determined by solving the problem for ψ_2 .

The main central-zone problem in region II can be solved using a sine transform in z and in order to ensure convergence of the integrals involved it is convenient to consider the slightly modified problem

$$\nabla^2 \psi_2 = -K \frac{\partial \psi_2}{\partial x}, \quad (4.3.18)$$

$$\psi_2 = 0 \quad \text{at} \quad x=0, \quad (4.3.19)$$

$$\psi_2 = 0 \quad \text{at} \quad z=0, \quad (4.3.20)$$

$$\psi_2 = a_0 z^{1/2} e^{-\epsilon z} \quad \text{at} \quad x=1, \quad (4.3.21)$$

$$\psi_2 \sim z^{1/2} e^{-\epsilon z} q(x) \quad \text{as} \quad z \rightarrow \infty. \quad (4.3.22)$$

Here it is readily established that

$$q(x) = a_0 e^{K(1-x)/2} \frac{\sinh[(K^2 - 4\epsilon^2)^{1/2} x/2]}{\sinh[(K^2 - 4\epsilon^2)^{1/2} /2]} \quad (4.3.23)$$

and the desired solution is that obtained in the limit as $\epsilon \rightarrow 0$. The sine transform

$$\bar{\psi}_2(x, \omega) = \int_{z=0}^{z=\infty} \psi_2(x, z) \sin \omega z \, dz, \quad (4.3.24)$$

is introduced and equation (4.3.18) transformed to give

$$\frac{\partial \bar{\psi}_2}{\partial x^2} + K \frac{\partial \bar{\psi}_2}{\partial x} - \omega^2 \bar{\psi}_2 = 0 \quad (4.3.25)$$

having used the boundary conditions (4.3.20,22). From (4.3.19,21) this must be solved subject to

$$\bar{\psi}_2 = 0 \quad \text{on} \quad x=0 \quad (4.3.26)$$

and, from the sine transform of (4.3.21) (Ditkin and Prudnikov 1965, p.269),

$$\bar{\psi}_2 = -\frac{a_0}{2} \left(\frac{\pi}{2}\right)^{1/2} g(\epsilon, \omega) \quad \text{on} \quad x=1 \quad (4.3.27)$$

where

$$g(\epsilon, \omega) = 2 \frac{d}{d\epsilon} \left\{ \frac{[(\epsilon^2 + \omega^2)^{1/2} - \epsilon]^{1/2}}{[\epsilon^2 + \omega^2]^{1/2}} \right\} = \{\epsilon^2 + \omega^2\}^{-3/2} \times \\ \{(\epsilon^2 + \omega^2)^{1/2} - \epsilon\}^{-1/2} \{\epsilon^2 - \omega^2 - \epsilon(\epsilon^2 + \omega^2)^{1/2}\} \quad (4.3.28)$$

It follows that

$$\bar{\psi}_2 = -\frac{a_0}{2} \left(\frac{\pi}{2}\right)^{1/2} \frac{g(\epsilon, \omega) e^{K(1-x)/2}}{\sinh\{(K^2 + 4\omega^2)^{1/2}/2\}} \sinh\{(K^2 + 4\omega^2)^{1/2} x/2\} \quad (4.3.29)$$

and inversion gives

$$\psi_2 = -\frac{a_0}{(2\pi)^{1/2}} e^{K(1-x)/2} \int_{\omega=0}^{\infty} \frac{g(\epsilon, \omega) \sinh\{(K^2 + 4\omega^2)^{1/2} x/2\} \sin\{\omega z\} d\omega}{\sinh\{(K^2 + 4\omega^2)^{1/2}/2\}} \quad (4.3.30)$$

Finally, letting $\epsilon \rightarrow 0$

$$\psi_2 = \frac{a_0}{(2\pi)^{1/2}} e^{K(1-x)/2} \int_0^{\infty} \omega^{-3/2} \sin \omega z \frac{\sinh\{(K^2+4\omega^2)^{1/2}x/2\}}{\sinh\{(K^2+4\omega^2)^{1/2}/2\}} d\omega . \quad (4.3.31)$$

It is easily verified that when $x=1$ the form

$$\psi_2 = \frac{a_0}{(2\pi)^{1/2}} \int_0^{\infty} \omega^{-3/2} \sin \omega z d\omega = a_0 \left(\frac{z}{2\pi}\right)^{1/2} S(0, -1/2) \quad (4.3.32)$$

is consistent with the boundary condition (4.3.11) since the generalized Fresnel integral $S(0, -1/2) = \sqrt{2\pi}$ (Abramowitz and Stegun 1965 ,p.262).

The central zone consists of streamlines descending into the region which are deflected into the vertical boundary layer (region I) near the hot wall. One important feature of the solution is the finite slip velocity generated at the base ($z=0$). From (4.3.31) this is given by

$$U(x) = \frac{\partial \psi_2}{\partial z} (x, 0) = \frac{a_0}{(2\pi)^{1/2}} e^{K(1-x)/2} I(x;K) , \quad (4.3.33)$$

where

$$I(x;K) = \int_{\omega=0}^{\infty} \omega^{-1/2} \frac{\sinh\{(K^2+4\omega^2)^{1/2}x/2\}}{\sinh\{(K^2+4\omega^2)^{1/2}/2\}} d\omega \quad (4.3.34)$$

or, using the substitution $\Omega^2 = K^2 + 4\omega^2$,

$$I(x;K) = \frac{1}{\sqrt{2}} \int_{\Omega=K}^{\infty} \frac{\Omega \sinh(\Omega x/2)}{(\Omega^2 - K^2)^{3/4} \sinh(\Omega/2)} d\Omega . \quad (4.3.35)$$

This integral was evaluated numerically by Simpson's rule

as $I = I_A + I_B$ where

$$I_A = \frac{1}{\sqrt{2}} \int_K^\Delta \frac{\Omega}{(\Omega^2 - K^2)^{3/4}} \left\{ \frac{\sinh(\Omega x/2)}{\sinh(\Omega/2)} - \frac{\sinh(Kx/2)}{\sinh(K/2)} \right\} d\Omega \\ + \sqrt{2} (\Delta^2 - K^2)^{1/4} \frac{\sinh(Kx/2)}{\sinh(K/2)} \quad (4.3.36)$$

$$I_B = \frac{1}{\sqrt{2}} \int_\Delta^\infty \frac{\Omega \sinh(\Omega x/2)}{(\Omega^2 - K^2)^{3/4} \sinh(\Omega/2)} d\Omega, \quad (4.3.37)$$

with the form (4.3.36) in $K < \Omega < \Delta$ chosen to avoid the infinitely singular integrand. Solutions for $U(x)$ with $K=2$, in which the value of Δ was chosen as 3, are shown in Figure 4.5 for various upper limits of integration Ω_∞ . Note that an increasingly large range of integration is required as $x \rightarrow 1$, with the integral I formally divergent at $x=1$.

This divergence reflects the singular form of ψ_2 in the corner $x=1, z=0$ where the solution can be expressed as

$$\tilde{\psi}_2 \sim r^{1/2} f(\theta) \quad (r \rightarrow 0), \quad (4.3.38)$$

where r and θ are cylindrical polar co-ordinates defined by

$$x-1 = r \cos \theta, \quad z = r \sin \theta. \quad (4.3.39)$$

Since the equation (4.3.18) is dominated by the Laplacian operator as $r \rightarrow 0$, f satisfies

$$f'' + \frac{1}{4}f = 0, \quad (4.3.40)$$

giving

$$f = a \cos \frac{\theta}{2} + b \sin \frac{\theta}{2} . \quad (4.3.41)$$

The boundary conditions (4.3.19,20) imply that

$$f=0 \quad (\theta=\pi) \quad , \quad f=a_0 \quad (\theta=\pi/2) \quad , \quad (4.3.42)$$

so that

$$f=\sqrt{2} a_0 \cos \frac{\theta}{2} \quad (4.3.43)$$

and

$$\psi_2 \sim a_0 (2r)^{1/2} \cos \frac{\theta}{2} \quad , \quad r \rightarrow 0 \quad , \quad \pi/2 < \theta < \pi . \quad (4.3.44)$$

This implies that

$$U(x) = \frac{\partial \psi_2}{\partial z}(x, 0) \sim \frac{a_0}{\sqrt{2}(1-x)^{1/2}} \quad , \quad (x \rightarrow 1) \quad (4.3.45)$$

and this asymptotic form agrees well with the numerical integration shown in Figure 4.5.

At the bottom of the central zone the temperature field has the form

$$T_2(x, z) = K\psi_2(x, z) \sim KU(x)z \quad (z \rightarrow 0) . \quad (4.3.46)$$

Thus an inner thermal boundary layer is required in order to reduce the vertical heat transfer to zero at the bottom surface of the cavity. This further inner horizontal layer is considered in the next section. The form of $U(x)$ for various values of K is shown in Figure 4.6.

4.4 Inner horizontal layer , $z=O(A^{-1/4})$

It is readily shown from the governing equations (2.4.2,3) and the limiting form of ψ_2 as $z \rightarrow 0$ in region II that conduction will become significant on a vertical

scale z of order $A^{-1/4}$ near the base of the cavity. From results obtained in the previous section the solution for the temperature and stream function in this inner horizontal layer (region IV) will have the form

$$T = A^{-3/4} T_4(x, z_4) + \dots, \quad \psi = A^{1/4} \psi_4(x, z_4) + \dots \quad (A \rightarrow \infty), \quad (4.4.1)$$

where $z_4 = A^{1/4} z$. Substitution into (2.4.2,3) gives, at leading order,

$$\frac{\partial^2 \psi_4}{\partial z_4^2} = 0, \quad (4.4.2)$$

$$\frac{\partial^2 T_4}{\partial z_4^2} = \frac{\partial T_4}{\partial x} \frac{\partial \psi_4}{\partial z_4} - \frac{\partial T_4}{\partial z_4} \frac{\partial \psi_4}{\partial x} \quad (4.4.3)$$

and the boundary conditions for this horizontal thermal boundary layer are

$$\psi_4 = \frac{\partial T_4}{\partial z_4} = 0 \quad (z_4 = 0), \quad (4.4.4)$$

$$\psi_4 \sim U(x) z_4, \quad T_4 \sim KU(x) z_4 \quad (z_4 \rightarrow \infty), \quad (4.4.5)$$

$$T_4 = 0 \quad (x = 0). \quad (4.4.6)$$

Here (4.4.4) are the conditions at the bottom wall of the cavity, (4.4.5) ensures that the solution matches with that in region II and (4.4.6) is for consistency with the thermal boundary condition on the cold wall.

The solution for ψ_4 is clearly

$$\psi_4 = U(x) z_4 \quad (4.4.7)$$

and substitution of this into equation (4.4.3) gives

$$\frac{\partial^2 T_4}{\partial z_4^2} = U(x) \frac{\partial T_4}{\partial x} - U(x) z_4 \frac{\partial T_4}{\partial z_4} \quad (4.4.8)$$

Using a transformation of the independent variables

$(x, z_4) \longrightarrow (\chi, \psi_4)$ where

$$\chi = \int_0^{x'=x} U(x) dx \quad (4.4.9)$$

it follows that T_4 satisfies

$$\frac{\partial T_4}{\partial \chi} = \frac{\partial^2 T_4}{\partial \psi_4^2} \quad (4.4.10)$$

with boundary conditions

$$\frac{\partial T_4}{\partial \psi_4} = 0 \quad (\psi_4 = 0) \quad (4.4.11)$$

$$T_4 \sim K\psi_4 \quad (\psi_4 \longrightarrow \infty) \quad (4.4.12)$$

$$T_4 = 0 \quad (\chi = 0) \quad (4.4.13)$$

The solution of this system is the similarity form

$$T_4 = \psi_4 V(\Phi) \quad , \quad \Phi = \psi_4 / \chi^{1/2} \quad (4.4.14)$$

where substitution of (4.4.14) into (4.4.10-13) gives

$$V'' + \left(\frac{2}{\Phi} + \frac{\Phi}{2} \right) V' = 0 \quad (4.4.15)$$

with boundary conditions

$$V + \Phi V' \longrightarrow 0 \quad (\Phi \rightarrow 0) \quad , \quad V \longrightarrow K \quad (\Phi \rightarrow \infty) \quad (4.4.16)$$

The required solution is

$$V = K \left\{ \operatorname{erf}(\Phi/2) + \frac{2}{\pi^{1/2} \Phi} \exp(-\Phi^2/4) \right\} \quad (4.4.17)$$

Thus finally, the solution for T_4 is

$$T_4 = K \{ 2(\chi/\pi)^{1/2} \exp(-\psi_4^2/4\chi) + \psi_4 \operatorname{erf}(\psi_4/2\chi^{1/2}) \}. \quad (4.4.18)$$

Here χ is given as a function of x by (4.4.9) and this functional relation is plotted in Figure 4.7 for $K=1, 1.5$ and 2 .

It is now possible to discuss the form of the solution in the inner horizontal layer both as $x \rightarrow 0$ and $x \rightarrow 1$. Approaching the cold wall,

$$U(x) \sim b_0 x \quad (x \rightarrow 0) \quad (4.4.19)$$

and typical values of the constant b_0 are given in Table 4.1. It follows from (4.4.9) that $\chi \sim b_0 x^2/2$ as $x \rightarrow 0$ and so

$$\psi_4 \sim (2b_0)^{1/2} z_4, \quad (4.4.20)$$

indicating that the width of the layer remains finite as $x \rightarrow 0$ and that the stream function and temperature have the forms

$$\psi_4 \sim b_0 x z_4, \quad T_4 \sim b_0 x z_4 V((2b_0)^{1/2} z_4) \quad (x \rightarrow 0). \quad (4.4.21)$$

Approaching the hot wall, it has been shown in Section 4.3 that

$$U(x) \sim \frac{a_0}{\sqrt{2}(1-x)^{1/2}} \quad (x \rightarrow 1) \quad (4.4.22)$$

and χ tends to the finite limiting value χ_0 defined by

$$\chi_0 = \int_0^1 U(x) dx. \quad (4.4.23)$$

Typical values of χ_0 are given in Table 4.1 (see also Figure 4.7). Thus as $x \rightarrow 1$ the stream function and temperature have the forms

$$\psi_4 \sim \frac{a_0 z_4}{\sqrt{2}(1-x)^{1/2}} \quad (4.4.24)$$

$$T_4 \sim \frac{a_0 z_4}{\sqrt{2}(1-x)^{1/2}} V \left(\frac{a_0 z_4}{\sqrt{2\chi_0}(1-x)^{1/2}} \right) \quad (4.4.25)$$

indicating that the inner thermal layer is compressed down to the bottom wall of the cavity as it approaches the hot corner, with $z_4 \sim (1-x)^{1/2}$ as $x \rightarrow 1$.

Finally in this section, it is noted that the results (4.4.7) and (4.4.18) provide predictions of both the slip velocity and the temperature along the bottom wall of the cavity :

$$u(x,0) = \frac{\partial \psi}{\partial z}(x,0) \sim A^{1/2} U(x) \quad , \quad (A \rightarrow \infty) \quad (4.4.26)$$

and

$$T(x,0) \sim A^{-3/4} 2K\chi^{1/2}/\pi^{1/2} \quad , \quad (A \rightarrow \infty) \quad (4.4.27)$$

where χ is given in terms of x by (4.4.9).

4.5 Corner regions

The overall structure of the end-zone solution is completed by considering three corner regions, designated regions V, VI and VII in Figure 4.1. Region V is the square region formed by the continuation of region III on the vertical scale of the inner horizontal layer. Locally the solution is of the form

$$T = A^{-1} T_5(x_3, z_4) + \dots, \quad \psi = \psi_5(x_3, z_4) + \dots \quad (A \rightarrow \infty), \quad (4.5.1)$$

where $x = A^{-1/4} x_3$ and $z = A^{-1/4} z_4$. Substitution into (2.4.2,3) shows that T_5 and ψ_5 satisfy the equations

$$\frac{\partial^2 \psi_5}{\partial x_3^2} + \frac{\partial^2 \psi_5}{\partial z_4^2} = 0, \quad (4.5.2)$$

$$\frac{\partial^2 T_5}{\partial x_3^2} + \frac{\partial^2 T_5}{\partial z_4^2} = \frac{\partial(T_5, \psi_5)}{\partial(x_3, z_4)}. \quad (4.5.3)$$

The solution for ψ_5 which matches with the solution (4.3.17) in region III as $z_4 \rightarrow \infty$, with the solution (4.4.21) in region IV as $x_3 \rightarrow \infty$ and satisfies the wall conditions at $x=0$ and $z_4=0$ is

$$\psi_5 = b_0 x_3 z_4, \quad (4.5.4)$$

where $b_0 = B(0) = U(0)$. Equation (4.5.3) then becomes

$$\frac{\partial^2 T_5}{\partial x_3^2} + \frac{\partial^2 T_5}{\partial z_4^2} = b_0 x_3 \frac{\partial T_5}{\partial x_3} - b_0 z_4 \frac{\partial T_5}{\partial z_4} \quad (4.5.5)$$

and must be solved subject to

$$T_5 = 0 \quad (x_3 = 0), \quad (4.5.6)$$

$$\frac{\partial T_5}{\partial z_4} = 0 \quad (z_4 = 0), \quad (4.5.7)$$

$$T_5 \sim K b_0 x_3 z_4 \quad (z_4 \rightarrow \infty), \quad (4.5.8)$$

$$T_5 \sim b_0 x_3 z_4 V((2b_0)^{1/2} z_4) \quad (x_3 \rightarrow \infty), \quad (4.5.9)$$

where the function V is defined by (4.4.17). The conditions (4.5.6,7) represent the thermal boundary conditions on the wall of the cavity and (4.5.8,9) ensure

consistency with the solutions (4.3.17) and (4.4.21) in regions III and IV respectively.

It is easily established that the required solution for T_5 is

$$T_5 = b_0 x_3 z_4 V((2b_0)^{1/2} z_4) \quad , \quad (4.5.10)$$

the reason being that for this linear function of x_3 , the term $\partial^2 T_5 / \partial x_3^2$ in (4.5.5) is identically zero. The remaining terms are equivalent to those in the equation governing the inner horizontal layer near $x_3=0$ and since the limiting form of the solution there satisfies the wall conditions at $x_3=0$ and $z_4=0$ it remains valid as the leading approximation to the temperature field throughout region V.

Near the hot wall, at the other bottom corner of the cavity, the inner horizontal layer (region IV) and the central zone (region II) merge into a single corner region (region VI) where x and z are both of order $A^{-1/2}$. Here the solution has the form

$$T = A^{-3/4} T_6(x_6, z_6) + \dots \quad , \quad \psi = A^{1/4} \psi_6(x_6, z_6) + \dots \quad , \quad (A \rightarrow \infty) \quad (4.5.11)$$

where $1-x = A^{-1/2} x_6$ and $z = A^{-1/2} z_6$. Substitution into (2.4.2,3) shows that

$$\frac{\partial^2 \psi_6}{\partial x_6^2} + \frac{\partial^2 \psi_6}{\partial z_6^2} = 0 \quad , \quad (4.5.12)$$

$$\frac{\partial(T_6, \psi_6)}{\partial(x_6, z_6)} = 0 \quad . \quad (4.5.13)$$

The functional relation between stream function and temperature implied by (4.5.13) is determined by the isotherms and streamlines entering the region from the inner horizontal layer, requiring, from (4.4.24,25), that

$$T_6 = \psi_6 V(\psi_6 / \chi_0^{1/2}). \quad (4.5.14)$$

The stream function itself is unchanged from the limiting form (4.3.44) identified in the central zone solution, implying that

$$\psi_6 = a_0 (2r_6)^{1/2} \cos \frac{\theta}{2} \quad (4.5.15)$$

where $x_6 = -r_6 \cos \theta$ and $z_6 = r_6 \sin \theta$. This remains the relevant solution of Laplace's equation because the boundary conditions associated with the continuation of the vertical boundary layer adjacent to the hot wall ($\theta = \pi/2$) and the requirement that $\psi_6 = 0$ at $\theta = \pi$ are unchanged. Thus the main feature of the solution in region VI is an adjustment of the temperature field from its linear dependence on stream function in the central zone to the more complex dependence (4.5.14).

As $r_6 \rightarrow 0$, the solution (4.5.15) is finally modified within a corner region where both x and z are of order A^{-1} . Here the solution has the form

$$T = T_7(x_7, z_7) + \dots, \quad \psi = \psi_7(x_7, z_7) + \dots \quad (A \rightarrow \infty), \quad (4.5.16)$$

where $1-x = A^{-1}x_7$ and $z = A^{-1}z_7$. Substitution into (2.4.2,3) shows that T_7 and ψ_7 satisfy the full nonlinear equations

$$\frac{\partial^2 \psi_7}{\partial x_7^2} + \frac{\partial^2 \psi_7}{\partial z_7^2} = \frac{\partial T_7}{\partial x_7} \quad (4.5.17)$$

$$\frac{\partial^2 T_7}{\partial x_7^2} + \frac{\partial^2 T_7}{\partial z_7^2} = \frac{\partial(\psi_7, T_7)}{\partial(x_7, z_7)} \quad (4.5.18)$$

and suitable boundary conditions are

$$\psi_7 = 0, \quad T_7 = 1 \quad (x_7 = 0) \quad (4.5.19)$$

$$\psi_7 = 0, \quad \frac{\partial T_7}{\partial z_7} = 0 \quad (z_7 = 0) \quad (4.5.20)$$

$$\left. \begin{aligned} \psi_7 &\sim a_0 (2r_7)^{1/2} \cos \frac{\theta}{2}, \\ T_7 &\longrightarrow 0 \end{aligned} \right\} (r_7 \longrightarrow \infty, \pi/2 < \theta \leq \pi) \quad (4.5.21)$$

where $x_7 = -r_7 \cos \theta$, $z_7 = r_7 \sin \theta$. Near the hot wall ($\theta = \pi/2$) the vertical boundary layer is initiated as $r \rightarrow \infty$ through the behaviour

$$T_7 \sim G_0(x_7/z_7^{1/2}), \quad \psi_7 \sim z_7^{1/2} F_0(x_7/z_7^{1/2}) \quad (z_7 \rightarrow \infty), \quad (4.5.22)$$

where G_0 and F_0 are the functions first introduced in (4.2.9). A complete solution of (4.5.17-21) would require a numerical approach which is not attempted here, but it is noted that the behaviours (4.5.21,22) indicate an inflow to the corner, with the fluid then being swept upwards to form the vertical boundary layer adjacent to the hot wall.

Overall, the results of this chapter appear to provide a physically realistic and mathematically consistent structure for the end-zone solution in the

high Darcy-Rayleigh number limit. Certain features of the solution, such as the value of the constant K , have not been determined but further discussion will be given in Chapter 5 where a comparison will be made with full numerical solutions of the end-zone problem.

K	b_0	χ_0
1	3.05	1.79
1.5	4.00	1.91
2	4.48	2.00

Table 4.1 : Typical values of $\chi_0 = \int_0^1 U(x) dx$ and b_0 for different values of K

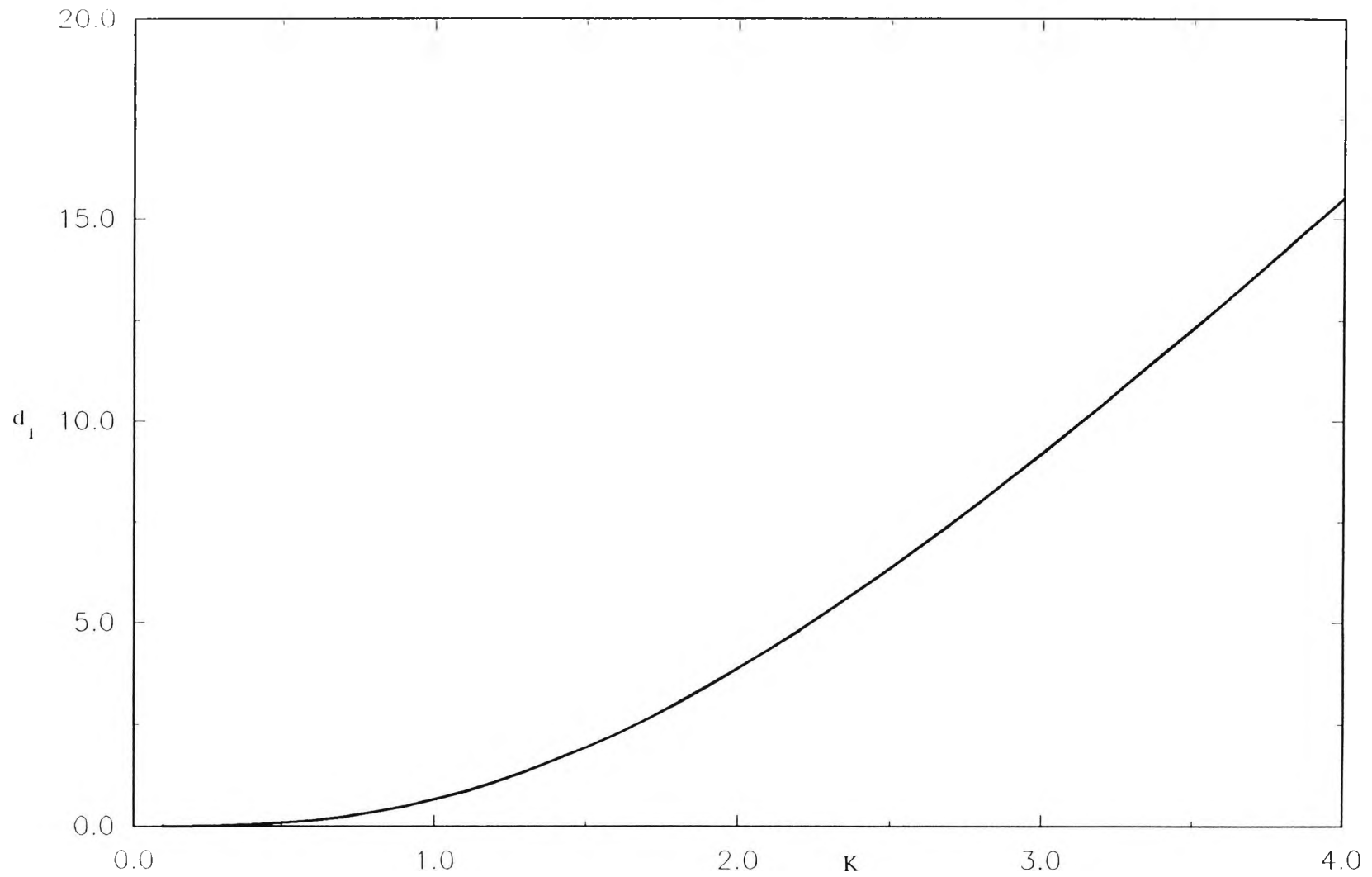


Figure 4.2: The graph of d_1 against κ .

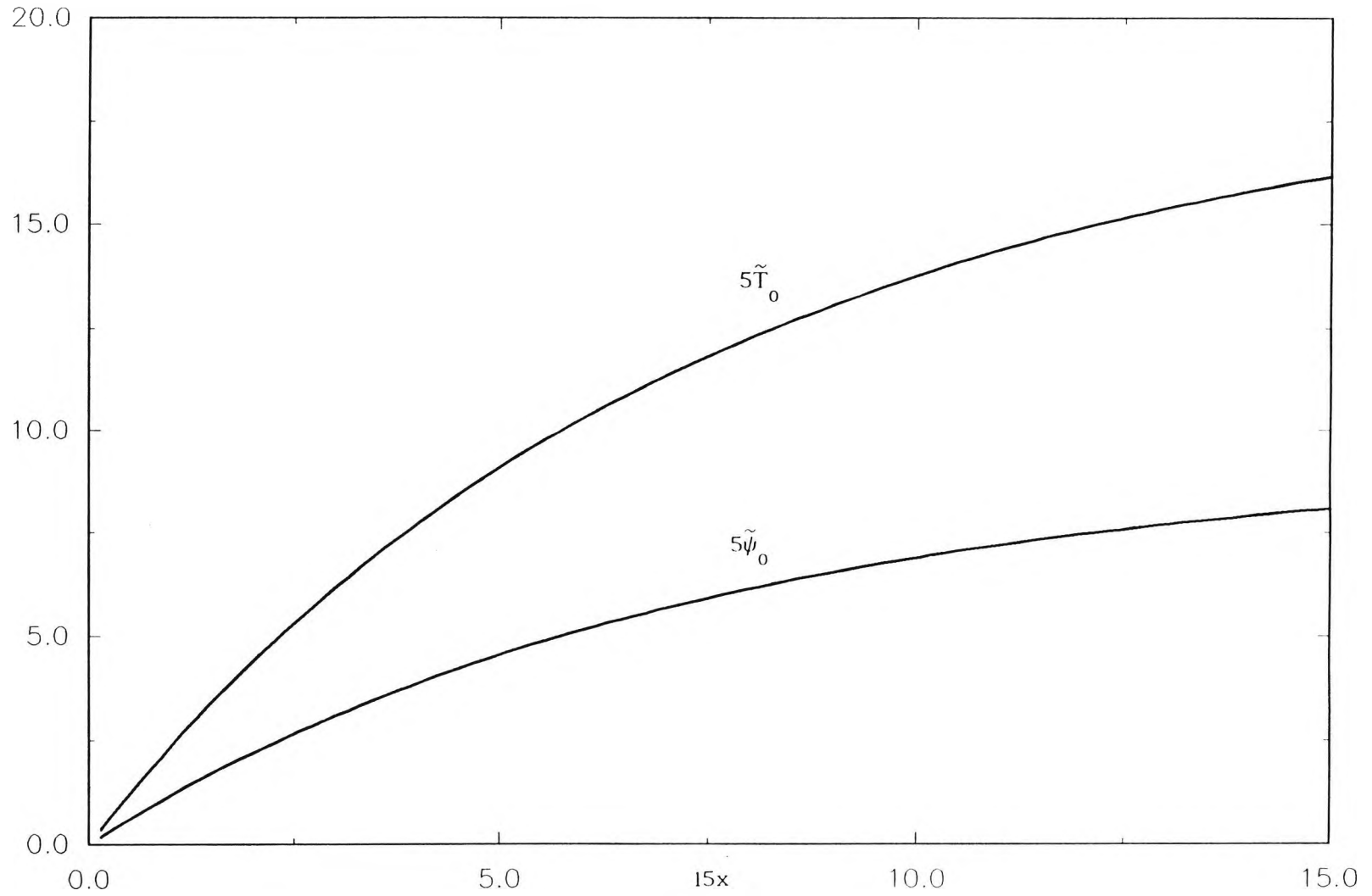


Figure 4.3 : The graphs of $\tilde{\psi}_0$, \tilde{T}_0 against x , for $K=2$.

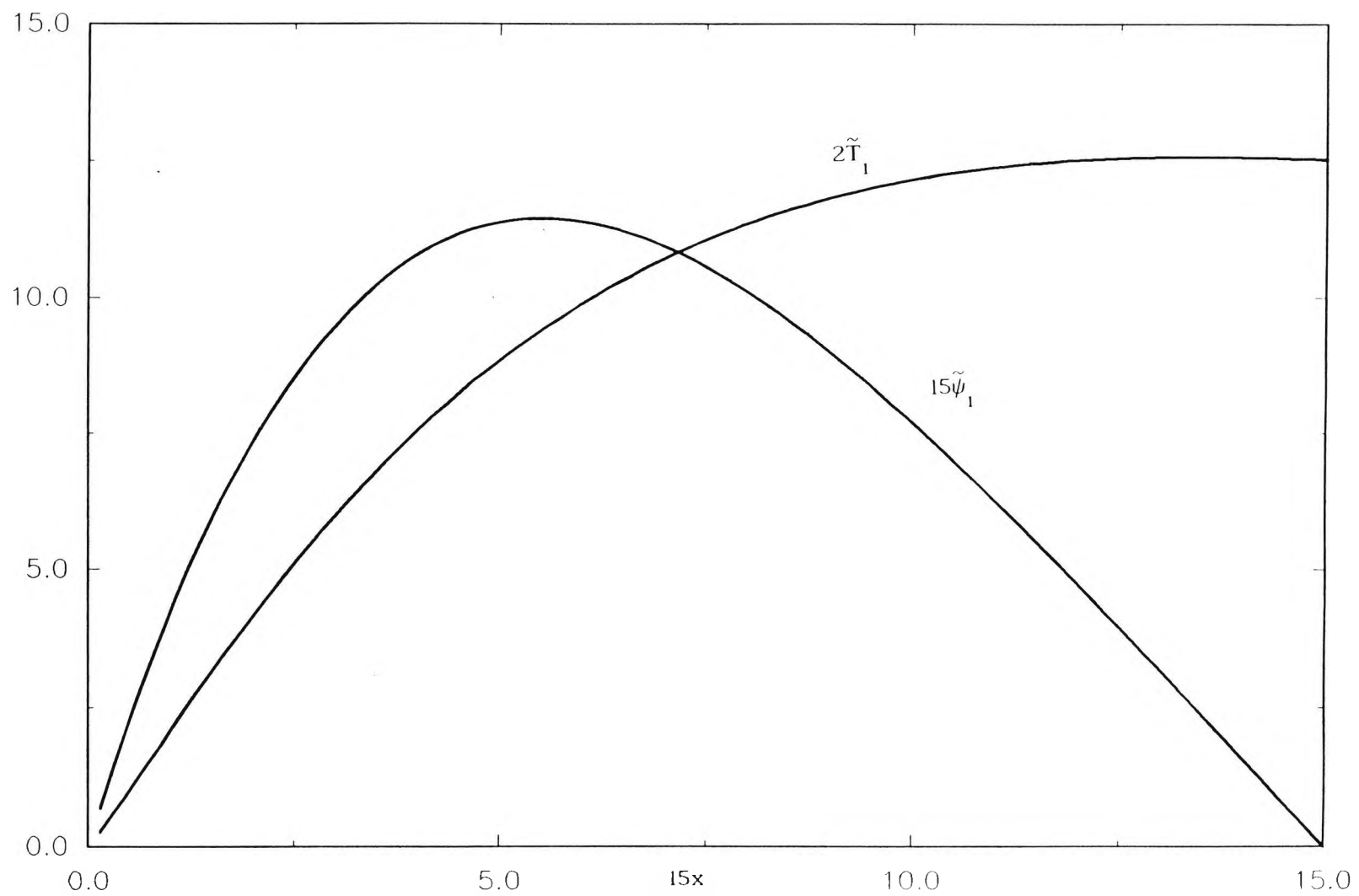


Figure 4.4 : The graphs of $\tilde{\psi}_1$ & \tilde{T}_1 against x , for $K=2$.

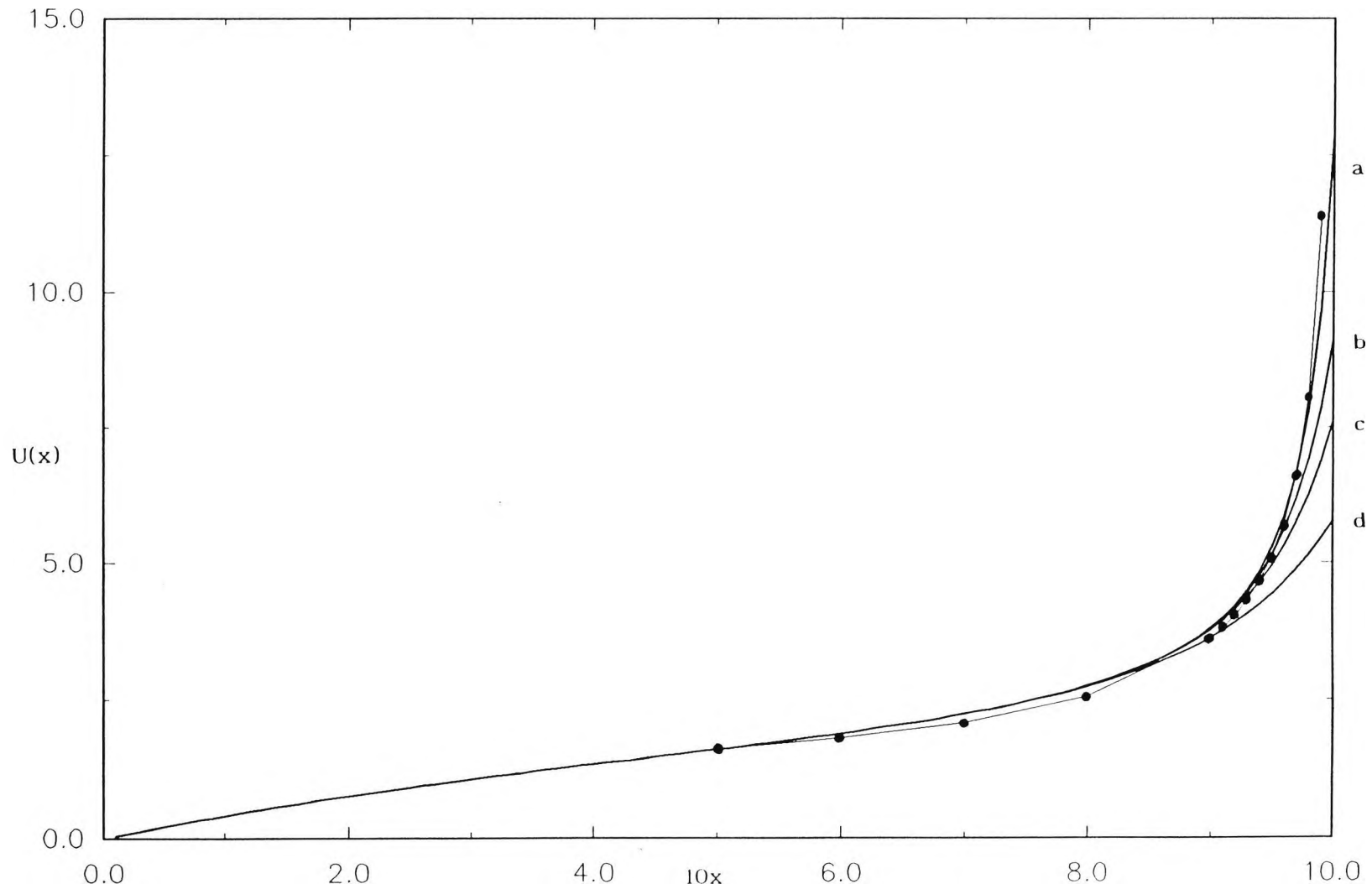


Figure 4.5 : The graph of $U(x) = \frac{\partial \psi^2}{\partial z}(x, 0)$ against x for $K=2$ and for different upper limits of integration, a) $\Omega_\infty=200$, b) $\Omega_\infty=100$, c) $\Omega_\infty=70$, d) $\Omega_\infty=40$. The asymptotic form (4.3.45) is shown by dots.

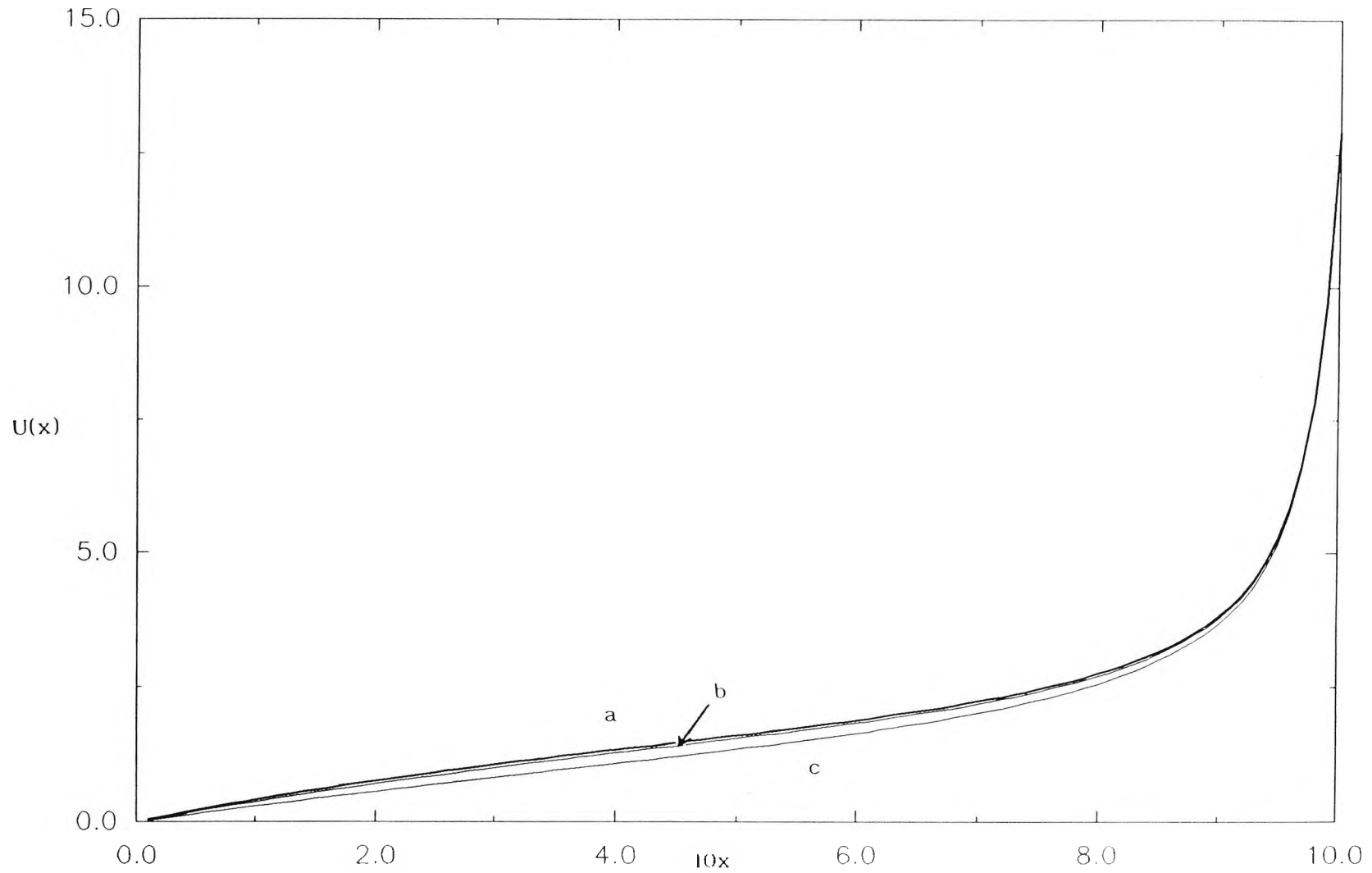


Figure 4.6 : The graph of $U(x)$ against x for different values of K : (a) $K=2$, (b) $K=1.5$, (c) $K=1.0$.

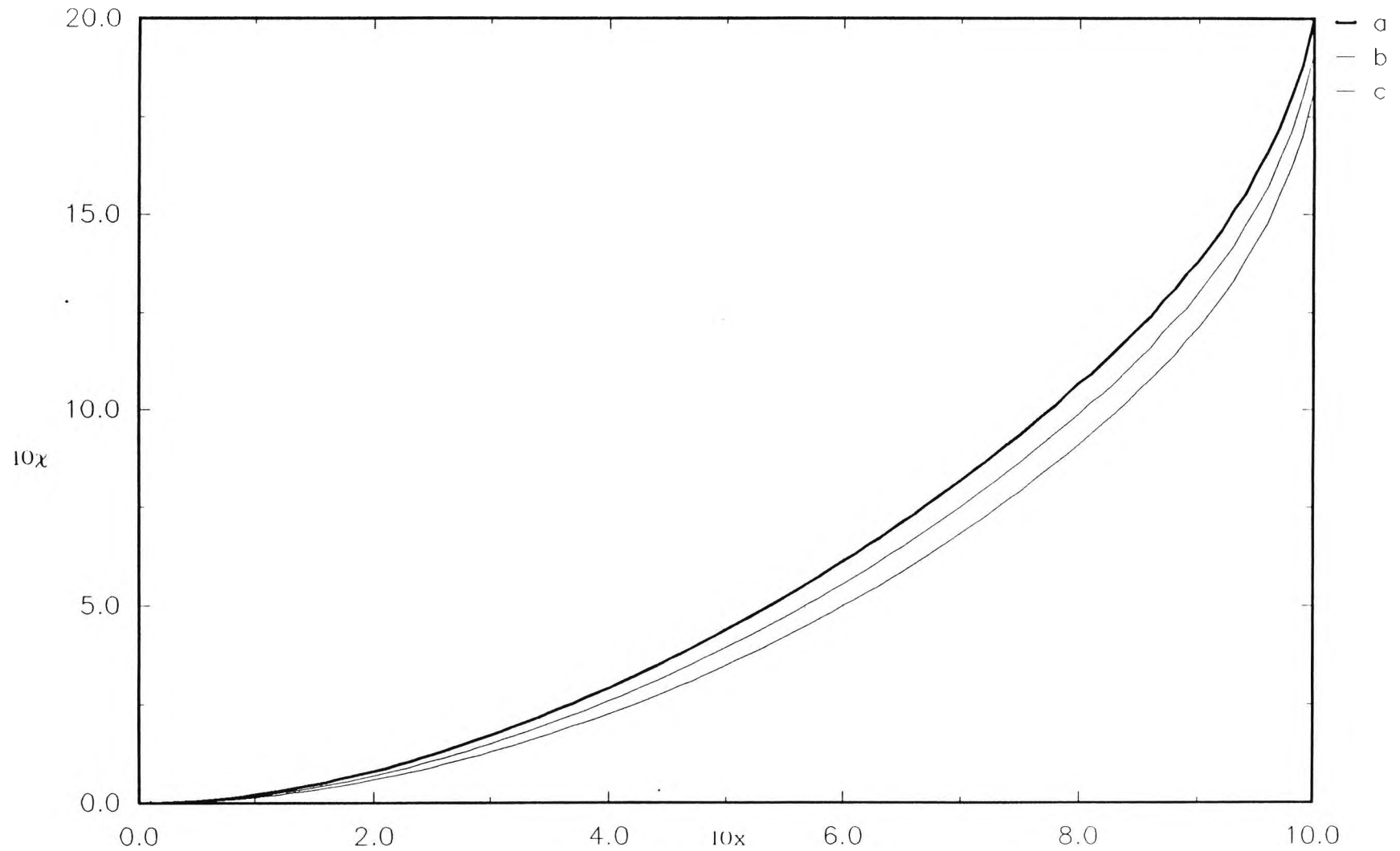


Figure 4.7 : The graph of $\chi = \int_0^x U(x') dx'$ for a) $K=2$,
 b) $K=1.5$, c) $K=1$.

5.1 Introduction

In this chapter the equations and boundary conditions governing the end-zone flow are solved numerically for finite values of the Darcy-Rayleigh number in the range $0 < A < \infty$. Artificial time derivatives are introduced in the governing equations to yield a parabolic system which is then solved using a simple explicit finite difference scheme. The computations proceed until a steady-state solution is obtained to within a specified tolerance. The numerical method is outlined in Section 5.2 and the main results are described in Section 5.3, where a comparison is made with the analytical predictions for small and large values of A . The heat transfer across the cavity is discussed in Section 5.4 and the numerical results are used to obtain predictions of the Nusselt number of the flow in the range $0 < A < \infty$.

5.2 Numerical method

Numerical solutions of (2.4.2-7) were computed by inserting artificial time derivatives, $\frac{\partial \psi}{\partial \tau}$, and $\frac{\partial T}{\partial \tau}$ on the right-hand side of (2.4.2) and (2.4.3) respectively, giving the parabolic system

$$\frac{\partial \psi}{\partial \tau} = \nabla^2 \psi + A \frac{\partial T}{\partial x}, \quad (5.2.1)$$

$$\frac{\partial T}{\partial \tau} = \nabla^2 T - \frac{\partial (T, \psi)}{\partial (x, z)}. \quad (5.2.2)$$

The steady-state solution is then allowed to evolve as

$t \rightarrow \infty$ from an initial state usually taken to be

$$\psi = Ax(1-x)(1-e^{-z})/2, \quad T = x. \quad (5.2.3)$$

The equations were put into discrete form using centred differences for the spatial variation and forward differences for the time variation, leading to explicit expressions for the values of ψ and T at interior mesh points at each new time step, $\psi_{i,j}^{(N)}$ and $T_{i,j}^{(N)}$, in terms of values at the previous time step, $\psi_{i,j}^{(0)}$, $T_{i,j}^{(0)}$:

$$\begin{aligned} \psi_{i,j}^{(N)} = & \psi_{i,j}^{(0)} + \Delta t \{ (\psi_{i+1,j}^{(0)} - 2\psi_{i,j}^{(0)} + \psi_{i-1,j}^{(0)}) / (\Delta x)^2 + (\psi_{i,j+1}^{(0)} \\ & - 2\psi_{i,j}^{(0)} + \psi_{i,j-1}^{(0)}) / (\Delta z)^2 + A(T_{i+1,j}^{(0)} - T_{i-1,j}^{(0)}) / 2\Delta x \}, \end{aligned} \quad (5.2.4)$$

$$\begin{aligned} T_{i,j}^{(N)} = & T_{i,j}^{(0)} + \Delta t \{ (T_{i+1,j}^{(0)} - 2T_{i,j}^{(0)} + T_{i-1,j}^{(0)}) / (\Delta x)^2 + (T_{i,j+1}^{(0)} \\ & - 2T_{i,j}^{(0)} + T_{i,j-1}^{(0)}) / (\Delta z)^2 + [(\psi_{i+1,j}^{(0)} - \psi_{i-1,j}^{(0)}) (T_{i,j+1}^{(0)} - T_{i,j-1}^{(0)}) \\ & - (\psi_{i,j+1}^{(0)} - \psi_{i,j-1}^{(0)}) (T_{i+1,j}^{(0)} - T_{i-1,j}^{(0)})] / 4\Delta x \Delta z \}. \end{aligned} \quad (5.2.5)$$

Here Δx and Δz are the step lengths in the x and z directions respectively, and Δt is the time step. The computational mesh is defined by $x=(i-1)\Delta x$, ($i=1,2, \dots, M$) and $z=(j-1)\Delta z$, ($j=1,2, \dots, N$), with $(M-1)\Delta x=1$ and the outer boundary in the z direction taken at $z_{\infty}=(N-1)\Delta z$.

On the boundaries of the computational domain the new values of ψ and T are given either directly from the boundary conditions or, where $\frac{\partial T}{\partial z}$ is involved, by using an extrapolation based on the new values of T at two interior mesh points. Thus to find the temperature at the bottom of the cavity, where $\frac{\partial T}{\partial z} = 0$, it is assumed that T has the quadratic form

$$T = a + bz + cz^2 \quad (5.2.6)$$

Equating this to values of T at $z=0$, Δz , $2\Delta z$ and using the fact that $b = \left. \frac{\partial T}{\partial z} \right|_{z=0} = 0$, it is found that on the lower boundary

$$T_{i,1}^{(N)} = (4T_{i,2}^{(N)} - T_{i,3}^{(N)})/3 \quad (5.2.7)$$

Time steps for the computation were generally chosen to conform to the criterion for stability associated with a diffusion equation, namely:

$$\Delta t \leq \frac{(\Delta x \Delta z)^2}{2\{(\Delta x)^2 + (\Delta z)^2\}} \quad (5.2.8)$$

This result is an extension of the more familiar criterion for the explicit scheme for a diffusion equation in one spatial dimension and can be established from the results given, for example, by Mitchell (1969, p.49). The scheme was allowed to run for the number of time steps, n_0 , needed to ensure that differences between successive values of ψ and T throughout the flow field, as measured by

$$\Delta\psi = \text{Max}(|\psi_{i,j}^{(N)} - \psi_{i,j}^{(0)}|), \quad \Delta T = \text{Max}(|T_{i,j}^{(N)} - T_{i,j}^{(0)}|), \quad (5.2.9)$$

were as small as desired.

5.3 Numerical results

Results were obtained for values of the Darcy-Rayleigh number in the range $A=1$ to $A=200$ and for a selection of values of the computational parameters Δt , Δx , Δz , z_∞ and n_0 , as indicated in Table 5.1. As part of the

numerical calculation , heat-transfer properties of the solution were determined. In order to determine the heat transfer through the cold wall of the cavity , a cubic polynomial form is assumed for T , with

$$T = a + bx + cx^2 + dx^3 \quad (5.3.1)$$

near $x=0$. Equating this to the values of T at $x=0$, Δx , $2\Delta x$, $3\Delta x$, it is found that

$$\frac{\partial T}{\partial X}(0, z) = b = \{3T_{2,j} - \frac{3}{2} T_{3,j} + \frac{1}{3} T_{4,j}\} / \Delta x , \quad (5.3.2)$$

where $T(x, z)$ is the steady-state temperature field. The corresponding formula for the heat transfer through the hot wall is

$$\frac{\partial T}{\partial X}(1, z) = -\{3T_{M-1,j} - \frac{3}{2} T_{M-2,j} + \frac{1}{3} T_{M-3,j} - \frac{11}{6}\} / \Delta x. \quad (5.3.3)$$

These formulae are used to calculate the two integrals

$$\alpha = \int_0^{\infty} \left(\frac{\partial T}{\partial X}(0, z) - 1 \right) dz , \quad (5.3.4)$$

$$\beta = \int_0^{\infty} \left(\frac{\partial T}{\partial X}(1, z) - 1 \right) dz , \quad (5.3.5)$$

taken along the cold and hot walls of the end-zone, respectively. These provide a measure of the total heat-transfer through each wall relative to that of the conductive solution $T=x$ and can be used as a useful check on the accuracy of the numerical scheme, as follows. From the steady heat equation (2.4.3)

$$\begin{aligned}
\left[\frac{\partial T}{\partial x}\right]_{x=0}^{x=1} + \int_{x=0}^{x=1} \frac{\partial^2 T}{\partial z^2} dx &= \int_0^1 \frac{\partial}{\partial z} \left(\psi \frac{\partial T}{\partial x}\right) dx - \int_0^1 \frac{\partial}{\partial x} \left(\psi \frac{\partial T}{\partial z}\right) dx \\
&= \int_0^1 \frac{\partial}{\partial z} \left(\psi \frac{\partial T}{\partial x}\right) dx
\end{aligned}
\tag{5.3.6}$$

and now integration from $z=0$ to $z=\infty$, using the fact that $\psi = \partial T / \partial z = 0$ on $z=0$, gives

$$\beta - \alpha = \frac{A}{2} \int_0^1 x(1-x) dx = \frac{A}{12} .
\tag{5.3.7}$$

Table 5.2 shows a comparison of the numerical value of $\beta - \alpha$ computed for each steady-state solution with the corresponding value of $A/12$. This indicates reasonable agreement and the increasing discrepancy at large values of A is not unexpected in view of the difficulty in adequately resolving the boundary-layer structure of the solution.

Figures 5.1-5 show computed streamlines and isotherms for Darcy-Rayleigh numbers $A=1, 20, 50, 100$ and 200 . For $A=1$ (Figure 5.1), the time step was $\Delta t=0.001$ with $\Delta x=0.05$ and $\Delta z=0.1$. The number of time steps needed for convergence of ψ and T to within a degree of accuracy of 10^{-10} was $n_0=2000$. The outer boundary of the flow domain was taken as $z_\infty=5$. The isotherms remain parallel to the vertical walls to a high level of approximation and the streamlines are virtually symmetric about the centre-line $x=1/2$, consistent with the conductive solution for small A outlined in Chapter 3.

The same step sizes were used for $A=20$ (Figure 5.2), again with an outer boundary at $z_\infty=5$, and 2000 time

steps led to convergence of ψ and T to within an accuracy of 10^{-7} . At this Darcy-Rayleigh number there is a significant shift of isotherms towards the hot wall at the bottom of the cavity and a small asymmetry in the flow field is also evident. These trends are even more pronounced in the results for $A=50$ which are shown in Figure 5.3 and were obtained with the same step sizes. Here however, the outer boundary of the computation was taken as $z_{\infty}=7$ to allow for the spreading of the end-zone upwards as A increases. At high values of A smaller steps in x , and therefore in t also, were used to resolve the increasingly narrow region near the bottom of the hot wall. In Figure 5.4, where $A=100$, the time step was taken as $\Delta t=0.00025$, with $\Delta x=0.025$ and $\Delta z=0.01$. The number of time steps needed for ψ and T to converge to within an accuracy of 10^{-9} and 10^{-10} (respectively) was 6000 and here the outer boundary was taken at $z_{\infty}=10$. The isotherm pattern is consistent with the development of the vertical boundary layer near the base of the hot wall of the cavity and the streamlines indicate how fluid is drawn across the cavity and entrained into the boundary layer. Results for $A=200$ (Figure 5.5) further confirm the development of the asymptotic structure although it becomes increasingly difficult to accurately resolve the behaviour of the solution near the lower hot corner.

The numerical results were used to make a prediction of the value of the constant K which arises in the asymptotic solution of Chapter 4. In the square zone at the base of the end region and right up to the cold wall, the convective dominance implied by the asymptotic

structure suggests that to leading order as $A \rightarrow \infty$, the ratio AT/ψ should approximate the constant value of K . The shape of the isotherm $T=0.1$ in Figures 5.4 and 5.5, in comparison with the streamlines at the same location, gives some evidence that this is the case, and quantitative results for AT/ψ taken across the base of the cavity, and particularly near the cold wall, suggest a value of K of about 1.3 (see Tables 5.3 and 5.4).

A second method of testing this prediction is to compare the temperature profile along the base of the cavity, as given by the numerical computation, with that predicted by the asymptotic analysis of Section 4.4. The asymptotic prediction given by (4.4.27) involves the value of K , with

$$A^{3/4}T(x,0) \sim 2K\chi^{1/2}/\pi^{1/2} \quad (A \gg 1), \quad (5.3.8)$$

where χ is defined by (4.4.9). A comparison of this result with the numerical computation of $A^{3/4}T(x,0)$ is made in Figure 5.6 for a range of values K between $K=1$ and $K=2$. The trend of the computation for large A seems to confirm a value of K consistent with that predicted earlier.

5.4 Heat transfer

Numerical results for the heat transfer through the vertical walls of the end-zone are shown in Figures 5.7 and 5.8 for Darcy-Rayleigh numbers in the range $A=1$ to $A=200$. As A increases the main transfer of heat, relative to that of pure conduction, is into the end zone through

the hot wall. Although some of this heat escapes through the cold wall, most is converted into the vertical transfer $\frac{A}{12}$, implied by (5.3.7) and is conveyed, via the core, to the end zone at the top of the cavity, where it leaves through the cold wall.

A representative Nusselt number for the overall cavity flow is defined by the heat transfer out of the cold wall,

$$Nu = \int_0^h \left. \frac{\partial \bar{T}}{\partial X} \right|_{x=0} dz . \quad (5.4.1)$$

This integral, taken down the entire cold wall, must be subdivided into three parts, corresponding to contributions arising from the core region and from the two end zones at the top and bottom of the cavity. Thus

$$Nu \sim \int_0^h 1 dz + \int_0^{\infty} \left\{ \frac{\partial \bar{T}}{\partial X}(0, z) - 1 \right\} dz + \int_{h-\infty}^h \left\{ \frac{\partial \bar{T}}{\partial X}(0, z) - 1 \right\} dz \quad (h \rightarrow \infty) . \quad (5.4.2)$$

In the upper end-zone the temperature field can be found in terms of the solution in the lower end-zone by use of the centro-symmetry relation

$$\bar{T}(x, z) = 1 - \bar{T}(1-x, h-z) , \quad (5.4.3)$$

which implies that

$$\int_{h-\infty}^h \left\{ \frac{\partial \bar{T}}{\partial X}(0, z) - 1 \right\} dz = \int_0^{\infty} \left\{ \frac{\partial \bar{T}}{\partial X}(1, z) - 1 \right\} dz . \quad (5.4.4)$$

Thus (5.4.2) becomes

$$Nu \sim h + \{ \alpha + \beta \} \quad (h \rightarrow \infty) , \quad (5.4.5)$$

where α and β are the two integrals defined by (5.3.4,5) and given as functions of A in Table 5.2. Since α and β are of order A as $A \rightarrow \infty$, with

$$\alpha \sim A\alpha_0, \quad \beta \sim A\beta_0 \quad (A \rightarrow \infty), \quad (5.4.6)$$

where $\alpha_0 \approx -0.012$, $\beta_0 \approx 0.076$, the Nusselt number formula (5.4.5) is a valid approximation for Darcy-Rayleigh numbers $A \ll h$.

A	Δt	Δx	z_∞	n_0	$\Delta\psi$ $t=n_0\Delta t$	$\Delta\psi$ $t=0$	ΔT $t=n_0\Delta t$	ΔT $t=0$
1	.001	.05	5	2000	$.42 \cdot 10^{-10}$	$.36 \cdot 10^{-3}$	$.69 \cdot 10^{-10}$	$.11 \cdot 10^{-3}$
1	.002	.1	5	1000	$.23 \cdot 10^{-12}$	$.36 \cdot 10^{-3}$	$.46 \cdot 10^{-12}$	$.11 \cdot 10^{-3}$
20	.001	.05	5	2000	$.84 \cdot 10^{-7}$	$.18 \cdot 10^{-1}$	$.38 \cdot 10^{-7}$	$.18 \cdot 10^{-2}$
20	.002	.1	5	1000				
50	.001	.05	7	2000	$.47 \cdot 10^{-10}$	$.47 \cdot 10^{-1}$	$.62 \cdot 10^{-11}$	$.46 \cdot 10^{-2}$
50	.002	.1	5	1000				
100	.00025	.025	10	6000	$.40 \cdot 10^{-9}$	$.18 \cdot 10^{-1}$	$.26 \cdot 10^{-10}$	$.34 \cdot 10^{-2}$
100	.001	.05	10	2000	$.72 \cdot 10^{-10}$	$.96 \cdot 10^{-1}$	$.62 \cdot 10^{-11}$	$.39 \cdot 10^{-2}$
200	.001	.05	20	6000	$.32 \cdot 10^{-13}$.154851	$.18 \cdot 10^{-14}$	$.12 \cdot 10^{-1}$
200	.00025	.025	20	4000	$.30 \cdot 10^{-6}$	$.44 \cdot 10^{-1}$	$.10 \cdot 10^{-7}$	$.74 \cdot 10^{-2}$

Table 5.1 : Computational parameters and convergence properties.
The vertical step length is $\Delta z=0.1$.

A	$\frac{A}{12}$	α	β	$\beta-\alpha$	$\beta+\alpha$	$\frac{\alpha}{A}$	$\frac{\beta}{A}$
1	0.083	-0.040	0.042	0.082	0.002	-0.040	0.042
20	1.66	-0.516	1.145	1.661	0.629	-0.083	0.057
50	4.16	-0.864	3.47	4.33	2.60	-0.017	0.069
100	8.33	-1.33	7.11	8.45	5.78	-0.013	0.071
200	16.66	-2.3	15.23	17.53	12.93	-0.012	0.076

Table 5.2 : Computations of α and β for different values of A .

$z \setminus x$	0.05	0.1	0.15	0.2	0.25	0.3	0.35	0.4	0.45	0.5
0.1	2.11	2.20	2.29	2.38	2.47	2.56	2.65	2.74	2.84	2.93
0.2	1.53	1.58	1.64	1.69	1.74	1.80	1.85	1.91	1.98	2.05
0.3	1.47	1.52	1.57	1.61	1.66	1.71	1.76	1.81	1.88	1.95
0.4	1.50	1.55	1.60	1.65	1.70	1.75	1.80	1.86	1.93	2.02
0.5	1.56	1.60	1.66	1.74	1.76	1.82	1.88	1.95	2.03	2.12
0.6	1.60	1.66	1.72	1.77	1.83	2.19	2.26	2.34	2.43	2.55
0.7	1.65	1.71	1.77	1.83	1.90	1.97	2.00	2.13	2.23	2.36
0.8	1.69	1.76	1.82	1.89	1.96	2.00	2.12	2.22	2.33	2.47
0.9	1.73	1.80	1.87	1.94	2.02	2.10	2.19	2.30	2.43	2.58
1	1.89	1.97	1.91	1.99	2.07	2.16	2.26	2.38	2.52	2.69

Table 5.3 : The numerical results for AT/ψ with $A=100$,

$$\Delta x = 0.025 , \Delta z = 0.1 .$$

$z \backslash x$.05	.1	.15	.2	.25	.3	.35	.4	.45	.5
.1	1.75	1.82	1.88	1.94	2.00	2.05	2.11	2.16	2.21	2.25
.2	1.36	1.4	1.44	1.47	1.51	1.54	1.57	1.61	1.63	1.67
.3	1.35	1.39	1.42	1.46	1.49	1.52	1.55	1.57	1.63	1.64
.4	1.40	1.44	1.47	1.51	1.54	1.57	1.60	1.63	1.66	1.70
.5	1.44	1.49	1.53	1.56	1.60	1.63	1.66	1.70	1.74	1.78
.6	1.49	1.53	1.57	1.80	1.77	1.69	1.73	1.65	1.81	1.87
.7	1.53	1.58	1.62	1.66	1.71	1.75	1.79	1.84	1.89	1.95
.8	1.50	1.61	1.66	1.71	1.75	1.80	1.85	1.90	1.96	2.03
.9	1.60	1.67	1.70	1.75	1.80	1.85	1.90	1.96	2.03	2.17
1	1.03	1.68	1.74	1.79	1.84	1.90	1.96	2.02	2.02	2.00

Table 5.4 : The numerical results for AT/ψ with $A=200$, $\Delta x=0.025$
 $\Delta z=0.1$.

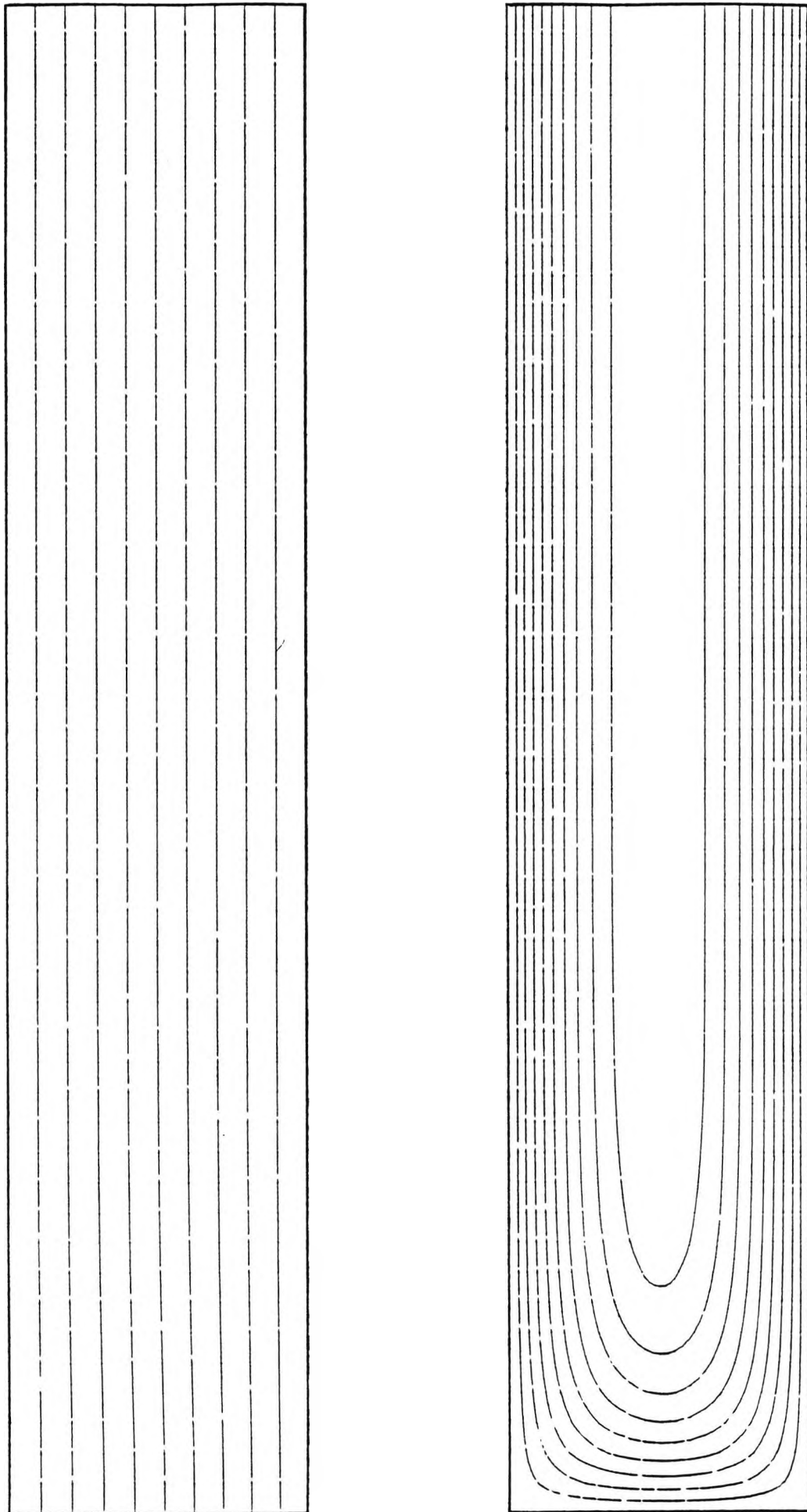


Figure 5.1 : Isotherms and streamlines for $A=1$.

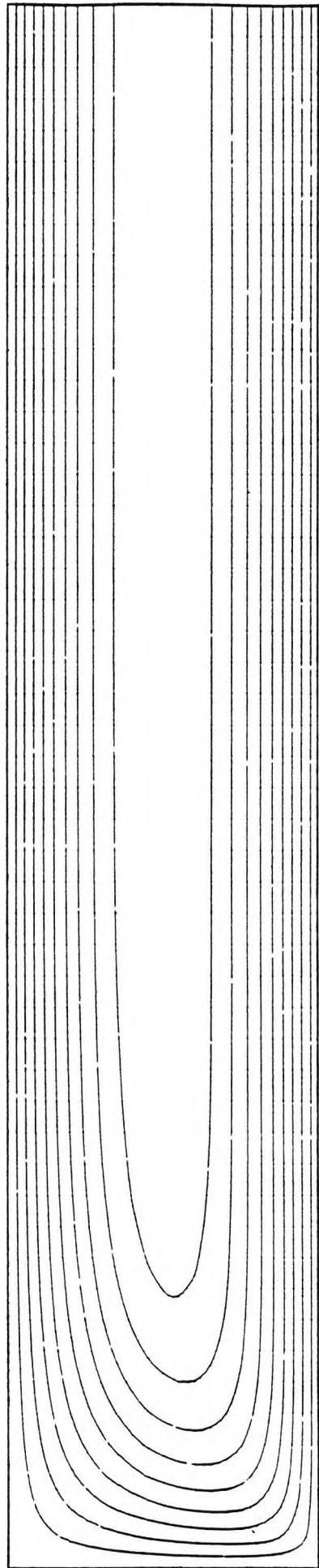
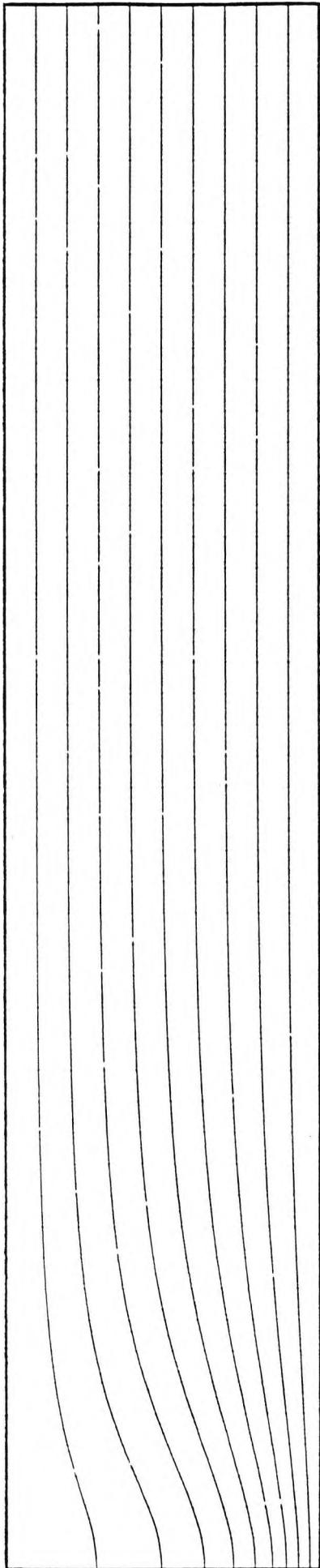


Figure 5.2 : Isotherms and streamlines for $A=20$.

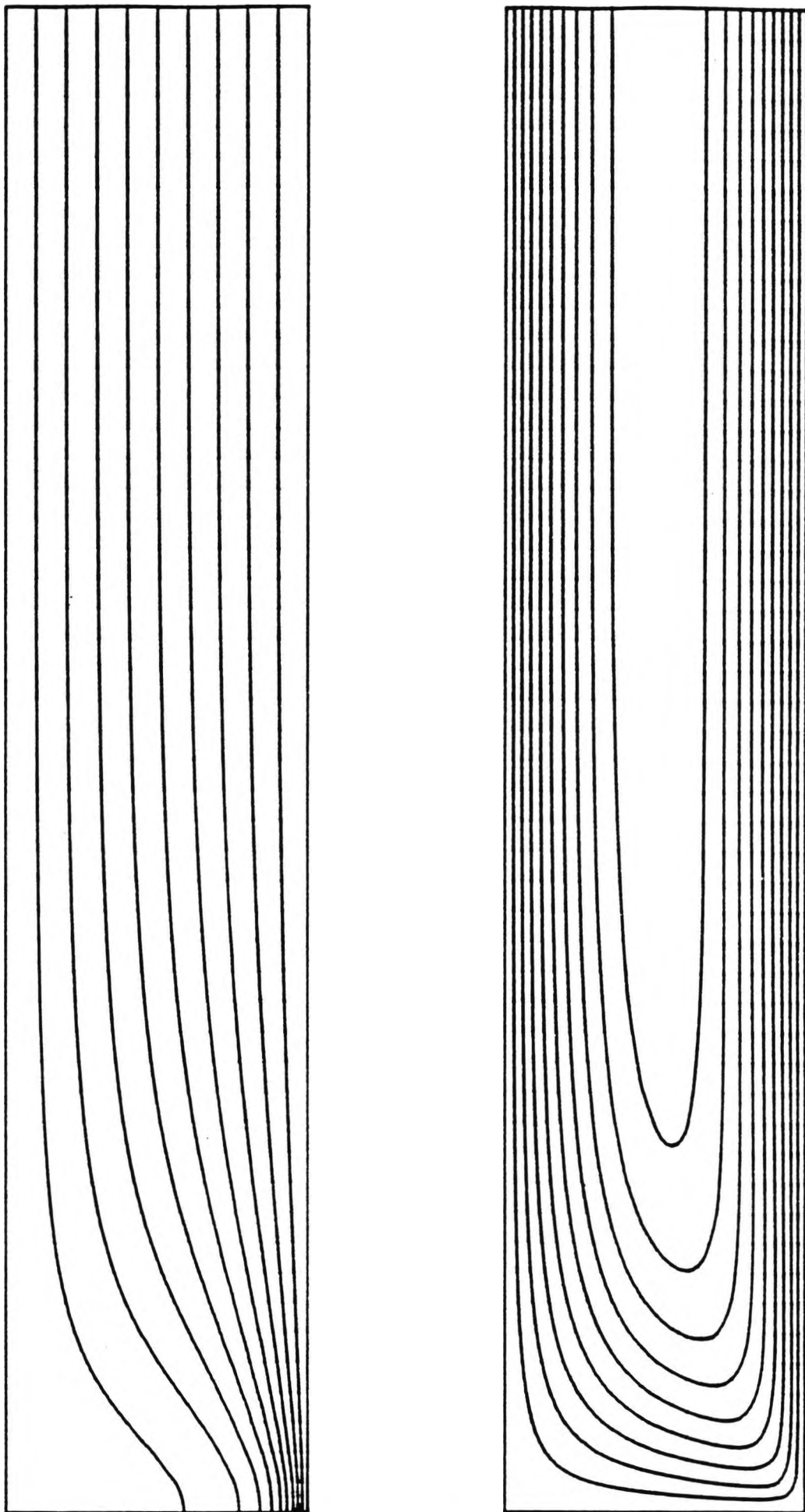


Figure 5.3 : Isotherms and streamlines for $A=50$.

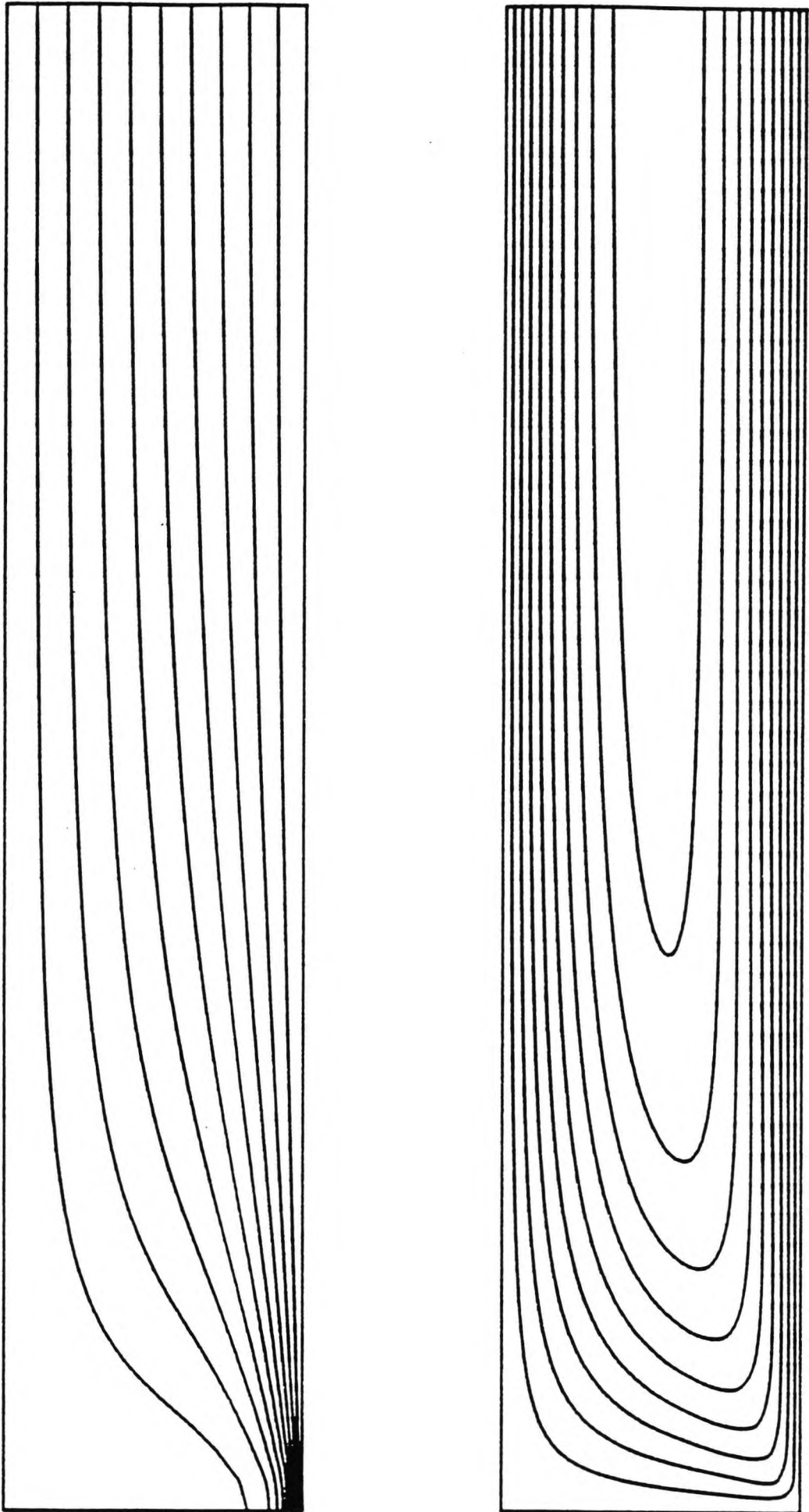


Figure 5.4 : Isotherms and streamlines for $A=100$,

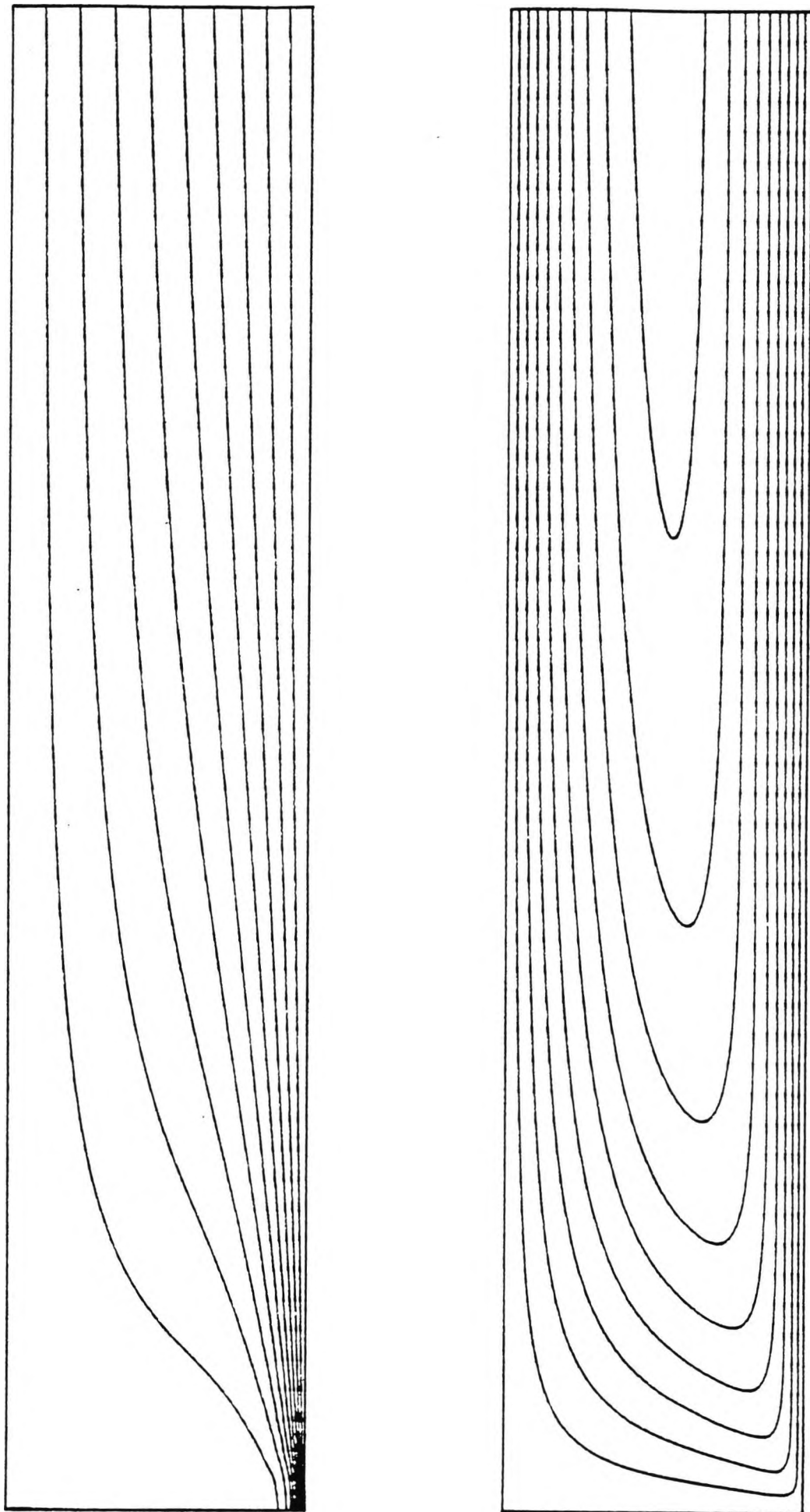


Figure 5.5 : Isotherms and streamlines for $A=200$.

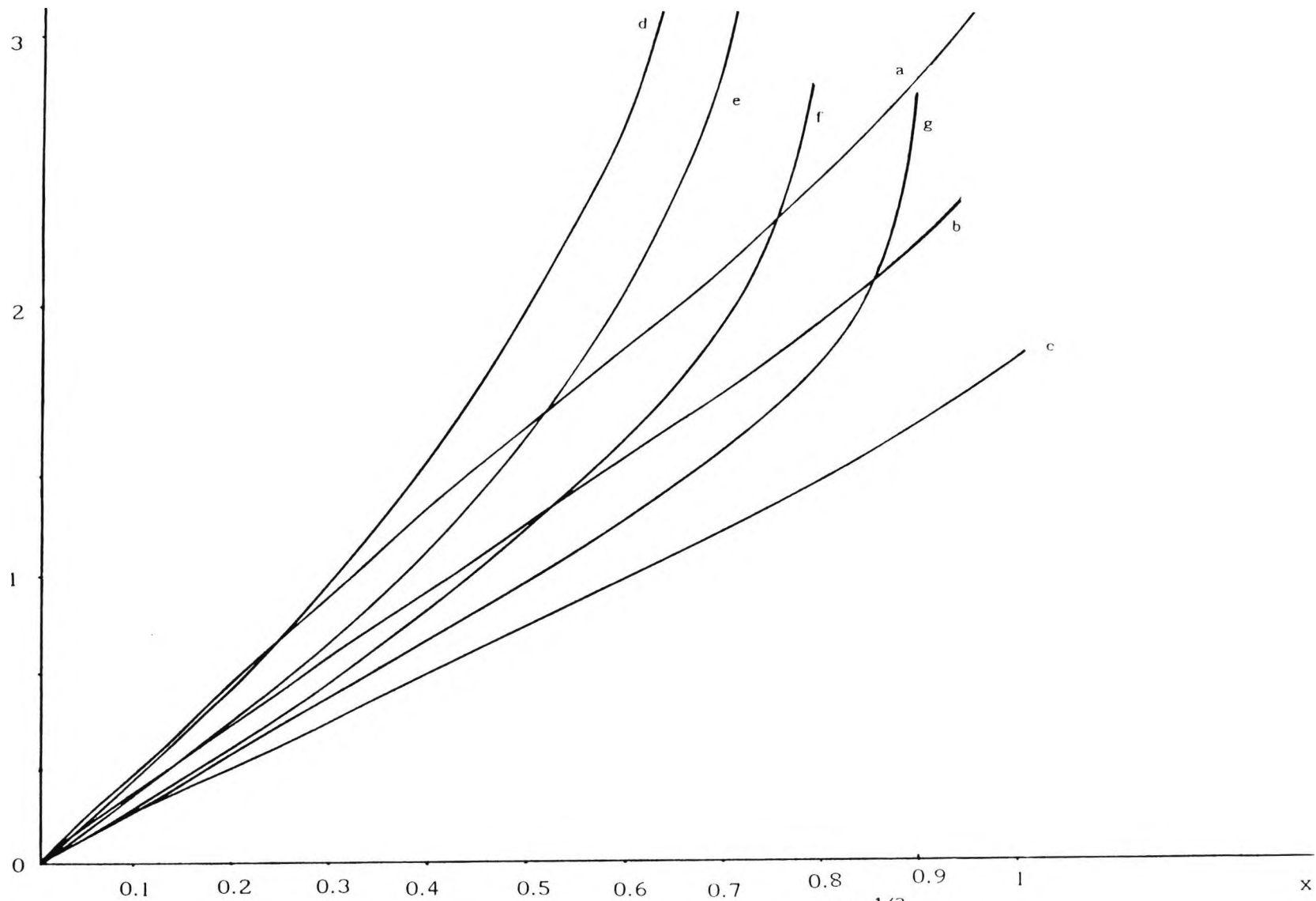


Figure 5.6 : The comparison of $\frac{2K\chi^{1/2}}{\pi^{1/2}}$ for a) $K=2$,
 b) $K=1.5$, c) $K=1$ and the numerical values of $A^{3/4}T$
 at $z=0$ for d) $A=20$, e) $A=50$, f) $A=100$, g) $A=200$.

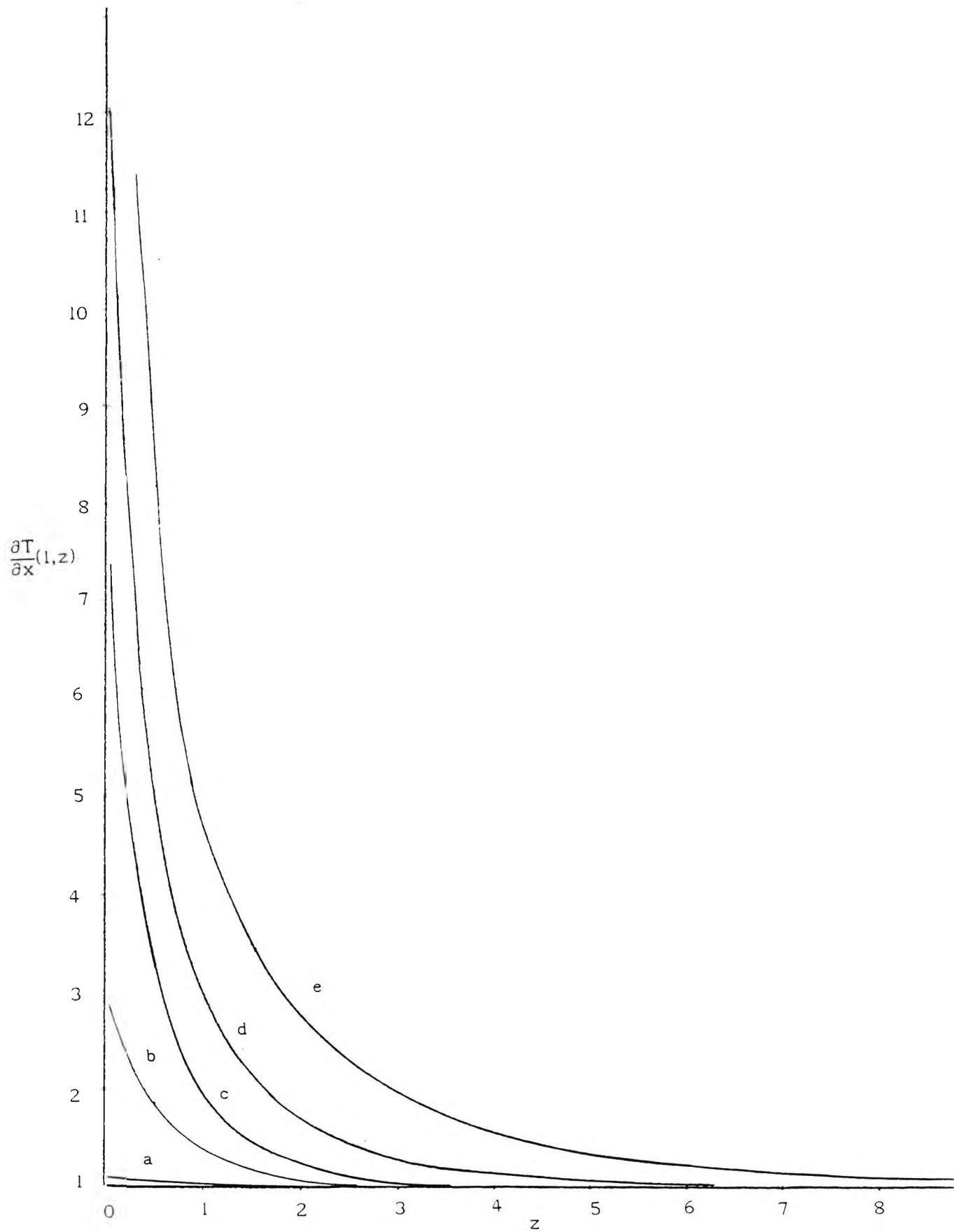


Figure 5.7 : The numerical values of the heat transfer at the hot wall for a)A=1, b)A=20, c)A=50, d)A=100, e)A=200

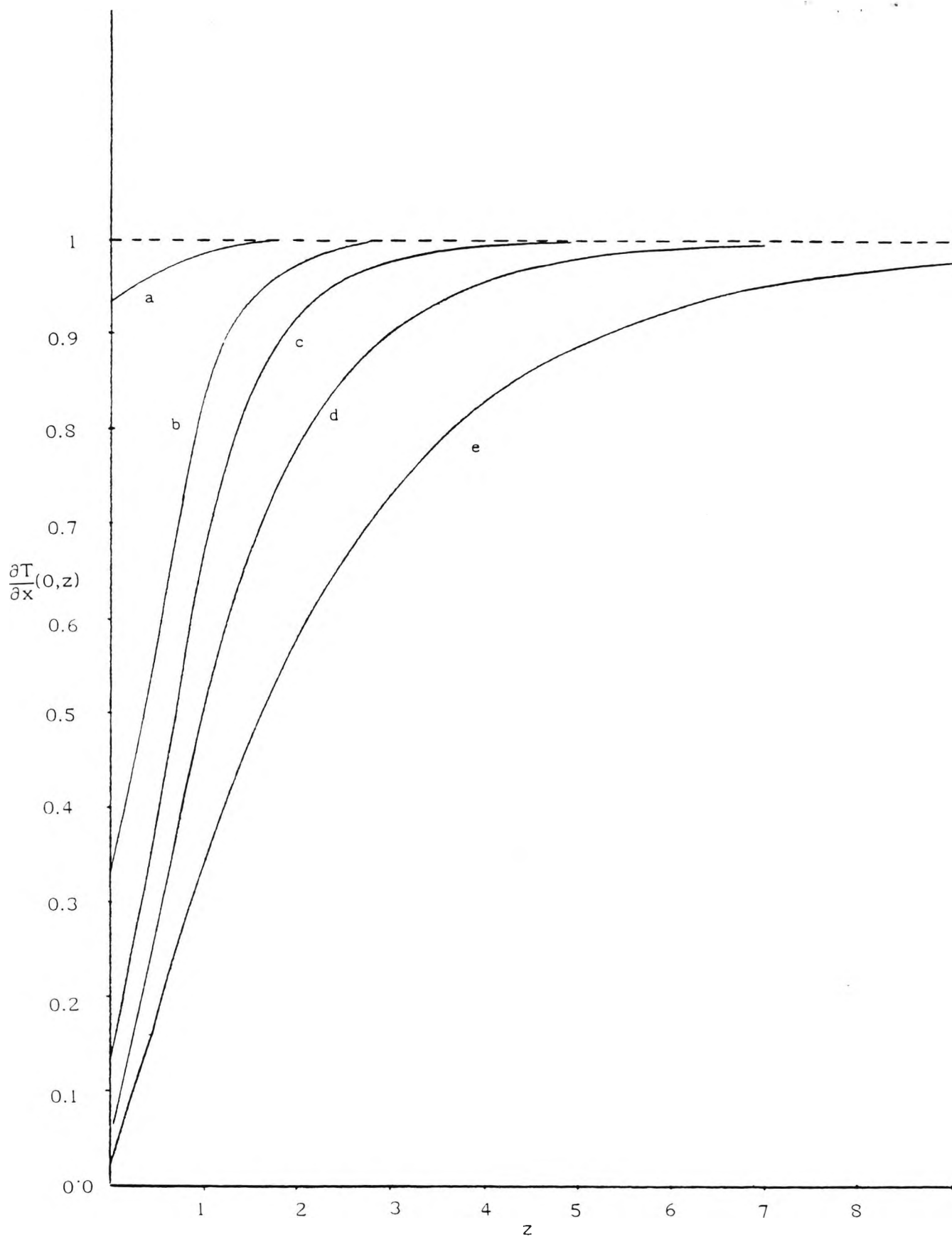


Figure 5.8 : The numerical values of the heat transfer at the cold wall for a) $A=1$, b) $A=20$, c) $A=50$, d) $A=100$, e) $A=200$.

Chapter 6 Convection in a vertical slot filled with
a porous medium for Darcy-Rayleigh numbers

$$\underline{A=O(h)}$$

6.1 Introduction

In this chapter the cavity flow is studied for large Darcy-Rayleigh numbers, A , comparable with the aspect ratio, h , of the slot. The key difference from the asymptotic structure studied in Chapters 2-5 is that the core flow is governed by the vertical boundary layer equations and is no longer parallel to the sidewalls of the cavity. The temperature field is no longer dominated by conduction and as convective effects spread throughout the cavity there is a significant change in the heat transfer characteristics of the system. The Nusselt number must be found by solving the core problem and this is the main objective of the present chapter.

The core problem is formulated in Section 6.2 and is shown to require the solution of a vertical boundary-layer form of the governing equations in the rectangular domain, subject to appropriate boundary conditions on each side of the rectangle. A similar boundary-layer problem has been formulated and solved for a Newtonian fluid by Daniels(1987), and here the same method of solution is used. This consists of using a Fourier decomposition in the z direction to reduce the system to an infinite coupled set of nonlinear ordinary differential equations in x , a truncated form of which is then solved by a finite difference method. Details of the numerical method are given

in Section 6.4 and the results are described in Section 6.5. As $A/h \rightarrow 0$ the conduction-dominated solution of Chapters 2-5 is recovered, while as $A/h \rightarrow \infty$ the solution approaches that of the high Darcy-Rayleigh number structure in a cavity of finite aspect ratio, previously considered by Weber (1975), Walker and Homsy (1978), Blythe, Daniels and Simpkins (1982) and Daniels (1983). Comparisons with this work are included in Section 6.5. Finally, in Section 6.6 the main heat transfer results are presented. Of particular importance is the prediction of a position of minimum heat transfer at a finite value of A/h .

6.2 Formulation

When A is of order h the end-zones studied in Chapters 2-5 have expanded to such a degree that they are comparable in vertical extent to the height of the cavity itself. The core solution $\bar{T} = T_c(x)$, $\bar{\psi} = A\psi_c(x)$ is therefore no longer valid and must be replaced by more general forms

$$\bar{T} = \tilde{T}(x, \tilde{z}) + \dots, \quad \bar{\psi} = A\tilde{\psi}(x, \tilde{z}) + \dots \quad (A \rightarrow \infty), \quad (6.2.1)$$

where

$$z = A\tilde{z} \quad (0 < \tilde{z} < h/A). \quad (6.2.2)$$

Substitution of (6.2.1) into (2.2.1,2) gives

$$\frac{\partial^2 \tilde{\psi}}{\partial x^2} = - \frac{\partial \tilde{T}}{\partial x}, \quad (6.2.3)$$

$$\frac{\partial^2 \tilde{T}}{\partial x^2} = \frac{\partial(\tilde{T}, \tilde{\psi})}{\partial(x, \tilde{z})}, \quad (6.2.4)$$

and these must be solved subject to the boundary

conditions

$$\tilde{\psi} = \tilde{T} = 0 \quad (x=0) \quad , \quad \tilde{\psi} = 0 \quad , \quad \tilde{T} = 1 \quad (x=1) \quad , \quad (6.2.5)$$

$$\tilde{\psi}=0 \quad (\tilde{z} =0 \text{ and } \tilde{z}=h/A) \quad . \quad (6.2.6)$$

Here the conditions at $\tilde{z} = 0$ and $\tilde{z} = h/A$ are necessary for consistency with solutions in end regions adjacent to the upper and lower boundaries , to be discussed in Chapter 7 below .

It is convenient to recast the system into a form in which the vertical coordinate varies on the unit interval, which may be achieved by writing

$$\tilde{T} = \Theta(X,Z) \quad , \quad \tilde{\psi} = \ell^{-1}\Psi(X,Z) \quad , \quad x = \ell^{-1}X \quad , \quad \tilde{z} = \ell^{-2}Z \quad , \quad (6.2.7)$$

where

$$\ell = (A/h)^{1/2} \quad . \quad (6.2.8)$$

Then it is required to solve

$$\frac{\partial^2 \Psi}{\partial X^2} = - \frac{\partial \Theta}{\partial X} \quad , \quad (6.2.9)$$

$$\frac{\partial^2 \Theta}{\partial X^2} = \frac{\partial (\Theta, \Psi)}{\partial (X, Z)} \quad , \quad (6.2.10)$$

subject to

$$\Psi = \Theta = 0 \quad (X = 0) \quad , \quad \Psi = 0 \quad , \quad \Theta = 1 \quad (X = \ell) \quad , \quad (6.2.11)$$

$$\Psi = 0 \quad (Z = 0, Z = 1) \quad . \quad (6.2.12)$$

Solutions are sought for values of the parameter ℓ in the range $0 < \ell < \infty$.

6.3 Core solution

The solution of (6.2.9-12) is expressed in the form

$$\Theta(X, Z) = Z + \sum_{n=1}^{\infty} a_n(X) \sin n\pi Z, \quad (6.3.1)$$

$$\Psi(X, Z) = \sum_{n=1}^{\infty} b_n(X) \sin n\pi Z, \quad (6.3.2)$$

where $a_n(X), b_n(X)$ ($n=1, 2, \dots$) are functions of X to be determined. This solution is consistent with the end conditions (6.2.12). Substitution of (6.3.1,2) into (6.2.9,10) gives

$$\sum_{n=1}^{\infty} b_n'' \sin n\pi Z = - \sum_{n=1}^{\infty} a_n' \sin n\pi Z, \quad (6.3.3)$$

$$\begin{aligned} \sum_{n=1}^{\infty} a_n'' \sin n\pi Z &= \sum_{n=1}^{\infty} a_n' \sin n\pi Z \sum_{n=1}^{\infty} n\pi b_n \cos n\pi Z \\ &\quad - (1 + \sum_{n=1}^{\infty} n\pi a_n \cos n\pi Z) \sum_{n=1}^{\infty} b_n' \sin n\pi Z. \end{aligned} \quad (6.3.4)$$

Equating the coefficients of $\sin n\pi Z$ in (6.3.3) gives

$$b_n'' + a_n' = 0. \quad (6.3.5)$$

From (6.3.4),

$$\begin{aligned} \sum_{n=1}^{\infty} \{a_n'' + b_n'\} \sin n\pi Z &= \sum_{n=1}^{\infty} a_n' \sin n\pi Z \sum_{n=1}^{\infty} n\pi b_n \cos n\pi Z \\ &\quad - \sum_{n=1}^{\infty} b_n' \sin n\pi Z \sum_{n=1}^{\infty} n\pi a_n \cos n\pi Z. \end{aligned} \quad (6.3.6)$$

Each of the two terms on the right-hand side of (6.3.6) can be expressed in the form

$$\sum_{n=1}^{\infty} r_n \sin n\pi Z \sum_{n=1}^{\infty} s_n \cos n\pi Z = \sum_{m=1}^{\infty} t_m, \quad (6.3.7)$$

where

$$\begin{aligned}
t_m &= \sum_{k=1}^m r_k s_{m-k+1} \sin k\pi Z \cos(m-k+1)\pi Z \\
&= \frac{1}{2} \sum_{k=1}^m r_k s_{m-k+1} \{\sin(m+1)\pi Z + \sin(2k-m-1)\pi Z\}. \quad (6.3.8)
\end{aligned}$$

In order to equate coefficients of $\sin n\pi Z$ in (6.3.8) it is therefore necessary to isolate the coefficient of $\sin n\pi Z$ in the expression

$$\frac{1}{2} \sum_{m=1}^{\infty} \sum_{k=1}^m r_k s_{m-k+1} \{\sin(m+1)\pi Z + \sin(2k-m-1)\pi Z\}. \quad (6.3.9)$$

The coefficient of $\sin n\pi Z$ in the expression

$$\frac{1}{2} \sum_{m=1}^{\infty} \sum_{k=1}^m r_k s_{m-k+1} \sin(m+1)\pi Z \quad (6.3.10)$$

is simply found by letting $m+1=n$, to give

$$\frac{1}{2} \sum_{k=1}^{n-1} r_k s_{n-k}, \quad (6.3.11)$$

while the coefficient of $\sin n\pi Z$ in the expression

$$\frac{1}{2} \sum_{m=1}^{\infty} \sum_{k=1}^m r_k s_{m-k+1} \sin(2k-m-1)\pi Z \quad (6.3.12)$$

is found by letting $2k-m-1 = \pm n$ so that either

$$k = \frac{m+n+1}{2} \longrightarrow m-k+1 = \frac{m-n+1}{2}, \quad (6.3.13)$$

or

$$k = \frac{m-n+1}{2} \longrightarrow m-k+1 = \frac{m+n+1}{2}. \quad (6.3.14)$$

For (6.3.13) the restriction $k \leq m$ implies that $k = (m+n+1)/2 \leq m$ while for (6.3.14) the restriction $k \geq 1$ implies that $k = (m-n+1)/2 \geq 1$ so that m ranges over the

values $m=n+1, n+3, \dots$. The coefficient of $\sin n\pi Z$ in (6.3.12) is therefore

$$\frac{1}{2} \sum_{m=n+1, n+3, \dots}^{\infty} \left[r \frac{m+n+1}{2} s \frac{m+1-n}{2} - r \frac{m+1-n}{2} s \frac{m+n+1}{2} \right]. \quad (6.3.15)$$

From (6.3.11) and (6.3.15), the coefficient of $\sin n\pi Z$ in the first summation on the right-hand side of (6.3.6) is

$$\phi_{n1} = \frac{1}{2} \left\{ \sum_{k=1}^{n-1} r_k s_{n-k} + \sum_{m=n+1, n+3, \dots}^{\infty} \left[r \frac{m+n+1}{2} s \frac{m+1-n}{2} - r \frac{m+1-n}{2} s \frac{m+n+1}{2} \right] \right\}, \quad (6.3.16)$$

where

$$r_n = a_n \quad \text{and} \quad s_n = n\pi b_n, \quad (6.3.17)$$

while in the second summation on the right-hand side of (6.3.6) the coefficient of $\sin n\pi Z$ is

$$\phi_{n2} = \frac{1}{2} \left\{ \sum_{k=1}^{n-1} r_k^* s_{n-k}^* + \sum_{m=n+1, n+3, \dots}^{\infty} \left[r \frac{m+n+1}{2} s \frac{m+1-n}{2} - r \frac{m+1-n}{2} s \frac{m+n+1}{2} \right] \right\}, \quad (6.3.18)$$

where

$$r_n^* = b_n \quad \text{and} \quad s_n^* = n\pi a_n. \quad (6.3.19)$$

Substitution of (6.3.16,18) into (6.3.6) now gives

$$a_n'' + b_n' = \phi_n, \quad (6.3.20)$$

where

$$\phi_n = \phi_{n1} - \phi_{n2}. \quad (6.3.21)$$

In practice the Fourier series (6.3.1,2) are truncated at N modes and then (6.3.16,18) become

$$\phi_{n1}^N = \frac{1}{2} \left\{ \sum_{k=1}^{n-1} r_k s_{n-k} + \sum_{m=n+1, n+3, \dots}^{2N-1-n} \left[r \frac{m+n+1}{2} s \frac{m-n+1}{2} - r \frac{m-n+1}{2} s \frac{m+n+1}{2} \right] \right\} \quad (n=1, 2, \dots, N), \quad (6.3.22)$$

$$\phi_{n2}^N = \frac{1}{2} \left\{ \sum_{k=1}^{n-1} r_k^* s_{n-k}^* + \sum_{m=n+1, n+3, \dots}^{2N-1-n} \left[r^* \frac{m+n+1}{2} s^* \frac{m-n+1}{2} - r^* \frac{m-n+1}{2} s^* \frac{m+n+1}{2} \right] \right\} \quad (n=1, 2, \dots, N). \quad (6.3.23)$$

Here it is understood that the summations do not contribute when the lower limit exceeds the upper limit and the final formula for the coefficient of $\sin n\pi Z$ on the right-hand side of (6.3.6) is

$$\phi_n^N = \frac{\pi}{2} \left[\sum_{k=1}^{n-1} (n-k) (a_k' b_{n-k}' - b_k' a_{n-k}') + \sum_{m=n+1, n+3, \dots}^{2N-1-n} \left\{ \left(\frac{m-n+1}{2} \right) (a' \frac{m+n+1}{2} b \frac{m-n+1}{2} - b' \frac{m+n+1}{2} a \frac{m-n+1}{2}) - \left(\frac{m+n+1}{2} \right) (a' \frac{m-n+1}{2} b \frac{m+n+1}{2} - b' \frac{m-n+1}{2} a \frac{m+n+1}{2}) \right\} \right], \quad (n=1, 2, 3, \dots, N). \quad (6.3.24)$$

The truncated problem is now to solve the equations

$$b_n'' + a_n' = 0 \quad (n=1, 2, \dots, N), \quad (6.3.25)$$

$$a_n'' + b_n' = \phi_n^N \quad (n=1, 2, \dots, N), \quad (6.3.26)$$

where ϕ_n^N is given by (6.3.24).

Boundary conditions for a_n and b_n are determined from (6.2.11). The stream function vanishes at the cold wall, giving

$$b_n = 0 \quad (X=0) \quad (6.3.27)$$

and the temperature also vanishes there , implying that

$$Z + \sum_{n=1}^{\infty} a_n(0) \sin n\pi Z = 0 . \quad (6.3.28)$$

Thus

$$a_n(0) = -2 \int_0^1 Z \sin n\pi Z \, dZ = 2(-1)^n/n\pi . \quad (6.3.29)$$

The computation of a_n and b_n can be limited to the colder half of the cavity by making use of the centro-symmetry conditions

$$\Psi(X,Z) = \Psi(\ell-X,1-Z), \quad \Theta(X,Z) = 1-\Theta(\ell-X,1-Z), \quad (6.3.30)$$

which imply that in particular

$$\Psi(\ell/2,Z) = \Psi(\ell/2,1-Z). \quad (6.3.31)$$

Thus

$$\begin{aligned} \sum_{n=1}^{\infty} b_n(\ell/2) \sin n\pi Z &= \sum_{n=1}^{\infty} b_n(\ell/2) \sin n\pi(1-Z) \\ &= - \sum_{n=1}^{\infty} (-1)^n b_n(\ell/2) \sin n\pi Z \end{aligned} \quad (6.3.32)$$

and so for even values of n ,

$$b_n = 0 \quad \text{at} \quad X = \ell/2 . \quad (6.3.33)$$

Similarly, for Θ

$$Z + \sum_{n=1}^{\infty} a_n(\ell/2) \sin n\pi Z = 1-(1-Z) + \sum_{n=1}^{\infty} (-1)^n a_n(\ell/2) \sin n\pi Z \quad (6.3.34)$$

and so for odd values of n ,

$$a_n = 0 \quad \text{at } X = \ell/2 \quad . \quad (6.3.35)$$

Also, from (6.3.30)

$$\frac{\partial \Psi}{\partial X}(\ell/2, Z) = - \frac{\partial \Psi}{\partial X}(\ell/2, 1-Z) \quad , \quad (6.3.36)$$

giving

$$\begin{aligned} \sum_{n=1}^{\infty} b_n(\ell/2) \sin n\pi Z &= - \sum_{n=1}^{\infty} b_n(\ell/2) \sin n\pi(1-Z) \\ &= \sum_{n=1}^{\infty} (-1)^n b_n(\ell/2) \sin n\pi Z, \end{aligned} \quad (6.3.37)$$

so that for odd values of n ,

$$b_n = 0 \quad \text{at } X=\ell/2 \quad . \quad (6.3.38)$$

Similarly, from $\partial\theta/\partial X$ it follows that for even values of n

$$a_n = 0 \quad \text{at } X=\ell/2 \quad . \quad (6.3.39)$$

In summary, the boundary conditions for (6.3.25,26) are

$$b_n = 0 \quad , \quad a_n = 2(-1)^n/n\pi \quad \text{at } X = 0 \quad (n=1,2,\dots,N), \quad (6.3.40)$$

$$a_n = b_n = 0 \quad \text{at } X=\ell/2 \quad (n \text{ odd}) \quad , \quad (6.3.41)$$

$$a_n = b_n = 0 \quad \text{at } X=\ell/2 \quad (n \text{ even}). \quad (6.3.42)$$

6.4 Numerical method

If ϕ_n^N is viewed as a given function of X , the system of equations (6.3.25,26), has a general solution

$$a_n = a_{np}(X) + c_1 \cosh X + c_2 \sinh X + c_3, \quad (6.4.1)$$

$$b_n = b_{np}(X) - c_1 \sinh X - c_2 \cosh X + c_4, \quad (6.4.2)$$

where c_1, c_2, c_3, c_4 are constants and a_{np} and b_{np} are particular solutions generated by ϕ_n^N . Assuming without loss of generality that

$$a_{np} = b_{np} = a'_{np} = b'_{np} = 0 \quad \text{at } X=0, \quad (6.4.3)$$

it follows from (6.3.40-42) that for odd values of n

$$\left. \begin{aligned} \frac{-2}{n\pi} &= c_1 + c_3, \\ c_2 &= c_4, \\ a_{np}\left(\frac{\ell}{2}\right) + c_1 \cosh \frac{\ell}{2} + c_2 \sinh \frac{\ell}{2} + c_3 &= 0, \\ b'_{np}\left(\frac{\ell}{2}\right) - c_1 \cosh \frac{\ell}{2} - c_2 \sinh \frac{\ell}{2} &= 0, \end{aligned} \right\} \quad (6.4.4)$$

giving

$$\left. \begin{aligned} c_1 &= a_{np}\left(\frac{\ell}{2}\right) + b'_{np}\left(\frac{\ell}{2}\right) - \frac{2}{n\pi}, \\ c_3 &= -a_{np}\left(\frac{\ell}{2}\right) - b'_{np}\left(\frac{\ell}{2}\right), \\ c_2 = c_4 &= b'_{np}\left(\frac{\ell}{2}\right) \operatorname{cosech} \frac{\ell}{2} - \left\{ a_{np}\left(\frac{\ell}{2}\right) + b'_{np}\left(\frac{\ell}{2}\right) - \frac{2}{n\pi} \right\} \coth \frac{\ell}{2} \end{aligned} \right\} \quad \begin{array}{l} (n \text{ odd}) \\ (6.4.5) \end{array}$$

and for even values of n

$$\left. \begin{aligned} c_1 + c_3 &= \frac{2}{n\pi}, \\ -c_2 + c_4 &= 0, \\ b_{np}\left(\frac{\ell}{2}\right) - c_1 \sinh \frac{\ell}{2} - c_2 \cosh \frac{\ell}{2} + c_4 &= 0, \\ a'_{np}\left(\frac{\ell}{2}\right) + c_1 \sinh \frac{\ell}{2} + c_2 \cosh \frac{\ell}{2} &= 0, \end{aligned} \right\} \quad (6.4.6)$$

giving

$$\left. \begin{aligned}
 c_1 &= -a'_{np} \left(\frac{\ell}{2}\right) \operatorname{cosech} \frac{\ell}{2} + \{a_{np} \left(\frac{\ell}{2}\right) + b_{np} \left(\frac{\ell}{2}\right)\} \coth \frac{\ell}{2} \\
 c_3 &= \frac{2}{n\pi} + a'_{np} \left(\frac{\ell}{2}\right) \operatorname{cosech} \frac{\ell}{2} - \{a_{np} \left(\frac{\ell}{2}\right) + b_{np} \left(\frac{\ell}{2}\right)\} \coth \frac{\ell}{2} \\
 c_2 = c_4 &= -\{b_{np} \left(\frac{\ell}{2}\right) + a'_{np} \left(\frac{\ell}{2}\right)\}
 \end{aligned} \right\} \begin{array}{l} (6.4.7) \\ (n \text{ even}) \end{array}$$

The particular solutions a_{np} and b_{np} are found by a numerical approach using a central difference approximation. The half-width of the cavity $0 \leq X \leq \ell/2$ is divided into equal intervals of length ΔX and values of a_n , b_n , $u_n = b'_n$ and $v_n = a'_n$ are approximated by

$$\left. \begin{aligned}
 a'_n &= \frac{a_n^{i+1} - a_n^i}{\Delta X} & , & & b'_n &= \frac{b_n^{i+1} - b_n^i}{\Delta X} \\
 a_n &= \frac{a_n^{i+1} + a_n^i}{2} & , & & b_n &= \frac{b_n^{i+1} + b_n^i}{2} \\
 u'_n &= \frac{u_n^{i+1} - u_n^i}{\Delta X} & , & & v'_n &= \frac{v_n^{i+1} - v_n^i}{\Delta X} \\
 u_n &= \frac{u_n^{i+1} + u_n^i}{2} & , & & v_n &= \frac{v_n^{i+1} + v_n^i}{2}
 \end{aligned} \right\} (6.4.8)$$

at location $X = (i + \frac{1}{2})\Delta X$, where a_n^i denotes $a_n(i\Delta X)$ etc. Hence the system of equations (6.3.25,26) becomes

$$\left. \begin{aligned}
 \frac{u_n^{i+1} - u_n^i}{\Delta X} &= -\left(\frac{v_n^{i+1} + v_n^i}{2}\right) \\
 \frac{v_n^{i+1} - v_n^i}{\Delta X} &= -\left(\frac{u_n^{i+1} + u_n^i}{2}\right) + \frac{f_n^{i+1} + f_n^i}{2} \\
 \frac{b_n^{i+1} - b_n^i}{\Delta X} &= \frac{u_n^{i+1} + u_n^i}{2} \\
 \frac{a_n^{i+1} - a_n^i}{\Delta X} &= \frac{v_n^{i+1} + v_n^i}{2}
 \end{aligned} \right\} (6.4.9)$$

where $f_n(X) = \phi_n^N(X)$. Solving (6.4.9) for the unknown

values at step $i+1$ in terms of known values at step i gives

$$\left. \begin{aligned} u_n^{i+1} &= \{4\Delta X v_n^i - ((\Delta X)^2 + 4)u_n^i + (\Delta X)^2(f_n^{i+1} + f_n^i)\} / \{(\Delta X)^2 - 4\}, \\ v_n^{i+1} &= -2 \left(\frac{u_n^{i+1} - u_n^i}{\Delta X} \right) - v_n^i, \\ b_n^{i+1} &= \frac{\Delta X}{2} (u_n^{i+1} + u_n^i) + b_n^i, \\ a_n^{i+1} &= \frac{\Delta X}{2} (v_n^{i+1} + v_n^i) + a_n^i, \end{aligned} \right\} (6.4.10)$$

and these formulae allow the solution to be computed from $X=0$ to $X=\ell/2$ starting from the initial configuration given by (6.4.3):

$$a_n^0 = b_n^0 = u_n^0 = v_n^0 = 0. \quad (6.4.11)$$

For a 1-mode truncation, $N=1$, $\phi_1^1 = 0$, and the system (6.3.25,26) is

$$\left. \begin{aligned} a_1' + b_1' &= 0, \\ b_1' + a_1' &= 0, \end{aligned} \right\} (6.4.12)$$

allowing the solution to be obtained analytically as

$$\left. \begin{aligned} a_1 &= \frac{2}{\pi} (\coth \frac{\ell}{2} \sinh X - \cosh X), \\ b_1 &= \frac{2}{\pi} (\sinh X - \coth \frac{\ell}{2} \cosh X + \coth \frac{\ell}{2}). \end{aligned} \right\} (6.4.13)$$

For a 2-mode truncation, $N=2$, the functions ϕ_1^2 and ϕ_2^2 are

$$\left. \begin{aligned} \phi_1^2 &= \frac{\pi}{2} [a_2' b_1' - b_2' a_1' - 2(a_1' b_2' - b_1' a_2')] = f_1, \\ \phi_2^2 &= \frac{\pi}{2} (a_1' b_1' - b_1' a_1') = f_2, \end{aligned} \right\} (6.4.14)$$

and the system (6.3.25,26) is

$$\left. \begin{aligned} b_1'' + a_1' &= 0 \\ a_1'' + b_1' &= f_1 \end{aligned} \right\} \quad (6.4.15)$$

$$\left. \begin{aligned} b_2'' + a_2' &= 0 \\ a_2'' + b_2' &= f_2 \end{aligned} \right\} \quad (6.4.16)$$

Here , and for all truncations $N \geq 2$, the system is nonlinear and the solution (6.4.1,2) is used in an iterative scheme in which the right-hand sides f_n are updated until convergence is achieved at a given truncation level , N . The solution for the previous truncation level is used as initial guess , together with

$$a_N = b_N = u_N = v_N = 0 . \quad (6.4.17)$$

A relaxation of the form

$$\left. \begin{aligned} a_n &= r a_n^{(new)} + (1-r) a_n^{(old)} \\ b_n &= r b_n^{(new)} + (1-r) b_n^{(old)} \end{aligned} \right\} \quad (6.4.18)$$

is incorporated and was found to be necessary to achieve convergence, particularly at high values of ℓ and high truncation levels, as in computations of the corresponding Newtonian problem (Daniels 1987). The values $a_n^{(old)}$ and $a_n^{(new)}$ in (6.4.18) are those pertaining to the previous and new values of a_n and r is introduced as a relaxation factor. For a given value of ℓ the scheme starts with $N=2$ and solutions are found for truncation levels up to a maximum value N_{max} . Most

computations were performed with a step length $\ell/200$ and at each truncation level convergence is achieved to within a specified tolerance, ϵ :

$$\max |a_n^{(new)} - a_n^{(old)}| < \epsilon, \quad \max |b_n^{(new)} - b_n^{(old)}| < \epsilon. \quad (6.4.19)$$

Numerical results were obtained for values of ℓ in the range $2 \leq \ell \leq 10$. At high truncation levels, a relaxation factor of the form $r = r_0 / N_{max}$ was used, with the maximum truncation level, N_{max} , usually taken as 25. Generally it was found necessary to decrease the value of the constant r_0 for increasing values of ℓ , with values varying from $r_0 = 4$ at $\ell = 2$ to $r_0 = 1/6$ at $\ell = 10$, representing a severe under-relaxation of the system.

6.5 Numerical results

Numerical results for Θ and Ψ with $\ell = 2$, $N_{max} = 25$ and $r = 0.16$ are shown in Figure 6.1 and at the highest truncation level 1155 iterations were needed to achieve convergence to within a tolerance of 10^{-5} . At this level of ℓ the isotherms are parallel throughout most of the cavity although near the ends they converge to the lower, hot and upper, cold corners. The streamlines are also parallel except near the top and bottom of the cavity where the flow is turned. For $\ell \rightarrow 0$ the solution of (6.2.9-12) throughout most of the cavity is the conduction-dominated, parallel-flow solution

$$\Psi = \frac{\ell}{2} \left(\frac{X}{\ell} \right) \left(1 - \frac{X}{\ell} \right), \quad (6.5.1)$$

$$\Theta = \frac{X}{\ell}, \quad (6.5.2)$$

so that in particular at the centre of the slot

$$\Psi(\ell/2, 1/2) \sim \ell/8 \quad (\ell \rightarrow 0). \quad (6.5.3)$$

The convergence of the isotherms to the two corners of the cavity is more pronounced in the result of Figure 6.2 for $\ell=4$, obtained with $N_{\max}=25$ and $r=0.01333$. Here convergence of Ψ and Θ at the highest truncation level is achieved to within a tolerance of 10^{-5} after 1073 iterations. Also the isotherms and streamlines are no longer parallel to the cold and hot walls, with the influence of the horizontal walls now extending throughout the cavity. In Figure 6.3, where $\ell=6$, $N_{\max}=25$ and $r=0.01$, the results for Ψ and Θ are obtained to within a tolerance of 10^{-4} after 564 iterations at the highest truncation level. The slope of the isotherms is more evident than in Figure 6.2 and the streamlines are more compressed to the cold and hot walls. The initial formation of vertical boundary-layer structures in the upper, cold and lower, hot corners of the cavity is also observed. These trends are even more evident in the results of Figure 6.4 for $\ell=8$ with $N_{\max}=25$ and $r=0.0066$, and where the results are obtained to within a tolerance of 10^{-4} after 946 iterations at the highest truncation level. The vertical boundary-layer structures spread further along the hot and cold walls and there are significant regions near the ends of the cavity where the isotherms and streamlines are near-horizontal. In Figure 6.5 where $\ell=10$ with $N_{\max}=25$ and $r=0.0066$, the results are obtained to within a tolerance of 10^{-4} after 2946 iterations at the highest truncation level. Here

the solution in the core of the cavity is seen to be increasingly independent of X , with a region of horizontal flow and vertical stratification sandwiched between vertical boundary layers on the hot and cold walls.

The structure which emerges for large values of ℓ is that which pertains in a cavity of finite aspect ratio, previously considered by Weber(1975), Walker and Homsy(1978), Blythe Daniels and Simpkins (1982) and Daniels(1983). This consists of a core region $X=O(\ell)$ sandwiched between boundary layers of thickness $O(1)$ on each vertical wall. Near the cold wall $X=0$,

$$\Psi \sim \tilde{\Psi}(X,Z), \quad \Theta \sim \tilde{\Theta}(X,Z) \quad (\ell \rightarrow \infty) \quad (6.5.4)$$

and substitution into (6.2.9,10) gives the full vertical boundary-layer system

$$\frac{\partial^2 \tilde{\Theta}}{\partial X^2} = \frac{\partial \tilde{\Psi}}{\partial Z} \frac{\partial \tilde{\Theta}}{\partial X} - \frac{\partial \tilde{\Psi}}{\partial X} \frac{\partial \tilde{\Theta}}{\partial Z}, \quad (6.5.5)$$

$$\frac{\partial^2 \tilde{\Psi}}{\partial X^2} = - \frac{\partial \tilde{\Theta}}{\partial X}. \quad (6.5.6)$$

At the wall the boundary conditions are

$$\tilde{\Psi} = \tilde{\Theta} = 0 \quad (X = 0). \quad (6.5.7)$$

In the core region where $X=O(\ell)$ the governing equations (6.2.9,10) reduce, at leading order, to

$$\frac{\partial \Theta}{\partial X} = \frac{\partial \Psi}{\partial X} = 0 \quad (6.5.8)$$

and so there is a vertically stratified, horizontal flow, with

$$\Psi \sim \Psi_c(Z), \quad \Theta \sim \Theta_c(Z) \quad (\ell \rightarrow \infty), \quad (6.5.9)$$

where Ψ_c and Θ_c are functions of Z to be determined. These must satisfy the centro-symmetry relations

$$\Psi_c(Z) = \Psi_c(1-Z), \quad \Theta_c(Z) = 1 - \Theta_c(1-Z). \quad (6.5.10)$$

The vertical boundary-layer problem is now completed by the requirement that at the edge of the layer the solution must match with the core solution, that is

$$\tilde{\Psi} \rightarrow \Psi_c(Z), \quad \tilde{\Theta} \rightarrow \Theta_c(Z) \quad (X \rightarrow \infty) \quad (6.5.11)$$

and also by the assumption of the zero mass-flux condition (6.2.12) at the ends of the layer

$$\tilde{\Psi}(X, 0) = \tilde{\Psi}(X, 1) = 0. \quad (6.5.12)$$

The vertical boundary-layer problem (6.5.5-7) and (6.5.10-12) has been solved by both Oseen and integral techniques (Weber 1975, Blythe and Simpkins 1977, 1980) and numerical techniques (Walker and Homsy 1978, Daniels 1983) and asymptotic properties of the solution for $Z \rightarrow 0$ and $Z \rightarrow 1$ have been discussed in detail by Blythe, Daniels and Simpkins (1982). The solution determines the core functions $\Psi_c(Z)$ and $\Theta_c(Z)$ and in particular gives the results

$$\Psi_c(1/2) = 0.734, \quad (6.5.13)$$

$$\frac{d\Theta_c}{dZ}(1/2) = 0.726. \quad (6.5.14)$$

These results compare favourably with the trend of the present numerical calculations at large values of ℓ , as shown in Figure 6.6 where the stream function and

vertical temperature gradient at the centre of the cavity are displayed as functions of ℓ . These are given by the formulae

$$\Psi(\ell/2, 1/2) = \sum_{m=0}^{\infty} (-1)^m b_{2m+1}(\ell/2), \quad (6.5.15)$$

$$\frac{d\Theta}{dZ}(\ell/2, 1/2) = 1 + \sum_{m=1}^{\infty} (-1)^m 2m\pi a_{2m}(\ell/2) \quad (6.5.16)$$

and values are incorporated in Table 6.1. The overshoot in the value of $\partial\Theta/\partial Z(\ell/2, 1/2)$ is also a feature of the corresponding problem for a Newtonian fluid (Daniels 1987). The behaviour of the solution at small values of ℓ is consistent with the behaviour predicted by (6.5.3) and the vertical temperature gradient is exponentially small in this limit.

6.6 Heat transfer

The Nusselt number for the cavity flow is defined by

$$Nu = \int_{z=0}^h \frac{\partial \bar{T}}{\partial X}(0, z) dz \quad (6.6.1)$$

and since $z=hZ$ and $X=\ell x$ the contribution from the core region is

$$Nu \sim h\ell \int_{Z=0}^1 \frac{\partial \Theta}{\partial X}(0, Z) dZ = h\ell \bar{Nu}(\ell), \quad (6.6.2)$$

where

$$\bar{Nu} = \int_{Z=0}^1 \frac{\partial \Theta}{\partial X}(0, Z) dZ. \quad (6.6.3)$$

From (6.3.1)

$$\frac{\partial \Theta}{\partial X} = \sum_{n=1}^{\infty} a_n' (X) \sin n\pi Z \quad (6.6.4)$$

and so

$$\overline{Nu} = \int_0^1 \frac{\partial \Theta}{\partial X}(0, Z) dZ = \frac{2}{\pi} \sum_{m=0}^{\infty} \frac{v_{2m+1}(0)}{2m+1} \quad (6.6.5)$$

The numerical results for \overline{Nu} are shown in Table 6.1 and Figure 6.7 for different values of ℓ . The most interesting result is the prediction of a position of minimum heat transfer $\overline{Nu} = 0.48$ when $\ell \approx 4.25$, similar to that which occurs for a Newtonian fluid (Daniels 1990). This is of obvious importance in the context of cavity-wall insulation in buildings and in other applications.

The results may also be compared with the asymptotic predictions, for small and large values of ℓ , where conduction and convection, respectively, are the main mechanisms of heat transfer. For small values of ℓ the relevant results may be obtained from the formulae described in Chapter 5, where it was shown that for finite Darcy-Rayleigh numbers A

$$Nu \sim h + \{\alpha + \beta\} \quad (h \rightarrow \infty) \quad (6.6.6)$$

where α and β are functions of A which, in the limit as $A \rightarrow \infty$, have the behaviours

$$\alpha \sim A\alpha_0, \quad \beta \sim A\beta_0 \quad (A \rightarrow \infty), \quad (6.6.7)$$

where

$$\alpha_0 + \beta_0 \approx 0.06. \quad (6.6.8)$$

This implies that for the present regime

$$\overline{Nu} \sim \ell^{-1} + (\alpha_0 + \beta_0)\ell, \quad \ell \rightarrow 0 \quad (6.6.9)$$

and this result compares well with the computed values of \overline{Nu} for $\ell \leq 4$, as shown in Figure 6.7.

For large values of ℓ , the boundary layer theory for a finite cavity (Daniels 1983, Walker and Homsy 1978) predicts that

$$Nu = \int_0^h \frac{\partial \overline{T}}{\partial x}(0, z) dz \sim 0.515(Ah)^{1/2}, \quad (Ah \gg 1) \quad (6.6.10)$$

which, for the present regime, infers that

$$\overline{Nu} = \frac{Nu}{\ell h} \rightarrow 0.515. \quad (\ell \rightarrow \infty) \quad (6.6.11)$$

This result is also shown in Figure 6.7.

Values of the Nusselt number obtained by other authors (Lauriat and Prasad 1987, Shiralkar, Haadjizadeh and Tien 1983, Prasad and Kulacki 1984) by full numerical simulations of the cavity flow at various aspect ratios and Darcy-Rayleigh numbers are shown in Table 6.2 and these results are also included in Figure 6.7. The results are in good agreement with those of the present calculation shown in Table 6.3, confirm the existence of the universal Nusselt number curve $\overline{Nu}(\ell)$ predicted here and are also consistent with the prediction of the minimum of the Nusselt number at

$$\ell \approx 4.25, \quad \text{where } \overline{Nu} \approx 0.48. \quad (6.6.12)$$

ℓ	r	ϵ	It	\overline{Nu}	$\Psi(\ell/2, 1/2)$	$\partial\theta/\partial Z(\ell/2, 1/2)$
2	.013	.00001	1155	0.599	.25	-.2
3	.013	.0001	415	.498	.37	.06
3.5	.007	.0001	830	.482	.43	.19
4	.013	.00001	1073	.477	.47	.32
4.25	.007	.0001	830	.476	.50	.39
4.5	.007	.0001	830	.476	.52	.46
4.75	.007	.0001	830	.477	.53	.51
5	.007	.0001	830	.478	.55	.58
6	.01	.0001	564	.483	.61	.76
8	.007	.0001	946	.490	.67	.85
10	.007	.0001	2946	.495	.70	.72

Table 6.1 : Computational parameters and the numerical results for \overline{Nu} , $\Psi(\ell/2, 1/2)$, $\partial\theta/\partial Z(\ell/2, 1/2)$ for different values of ℓ with $N_{\max} = 25$.

A	$\ell = (A/h)^{1/2}$	\overline{Nu}		
		(1)	(2)	(3)
10	1.414	0.735		0.735
20	2	0.56	0.565	0.565
30	2.449	0.506		
50	3.1622	0.4680		
100	4.472	0.4651	0.4673	0.4606
200	6.3245	0.4790	0.4806	0.4759
350	8.366	0.4876		0.4888
500	10	0.492	0.491	0.496
750	12.247	0.4956		
1000	14.142	0.4963		0.5126

Table 6.2 : Values of the Nusselt number obtained by other authors for $h=5$ and various Darcy-Rayleigh numbers : (1) Lauriat & Prasad 1987, (2) Shiralkar, Haadjizadeh and Tien 1983, (3) Prasad & Kulacki 1984 .

ℓ	\overline{Nu}
2	0.5997
3	0.4984
3.5	0.4827
4	0.4771
4.25	0.4765
4.5	0.4767
4.75	0.4775
5	0.4786
6	0.4837
8	0.4905
10	0.4956

Table 6.3 : Computed Nusselt number \overline{Nu}
for various values of ℓ

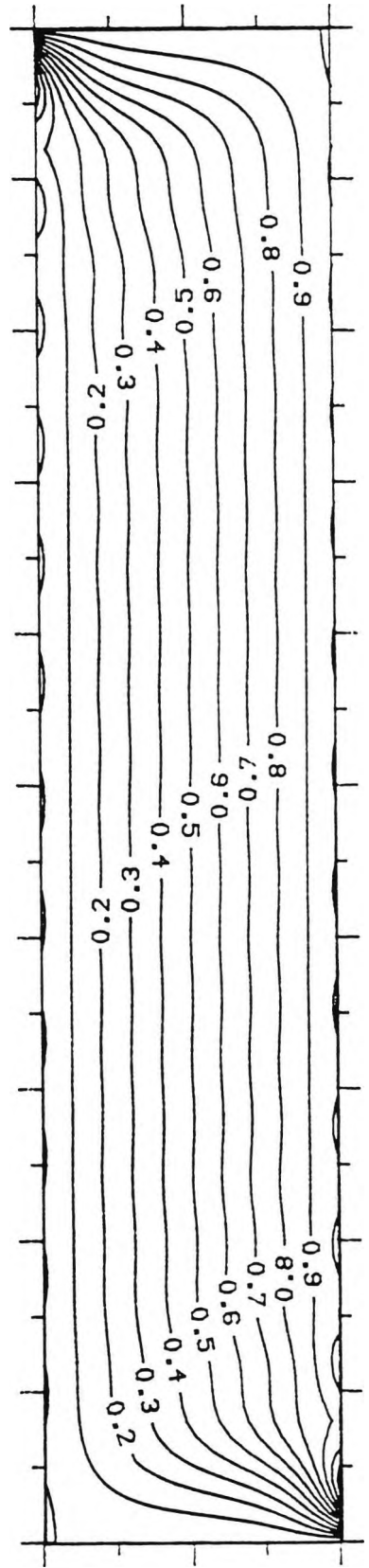
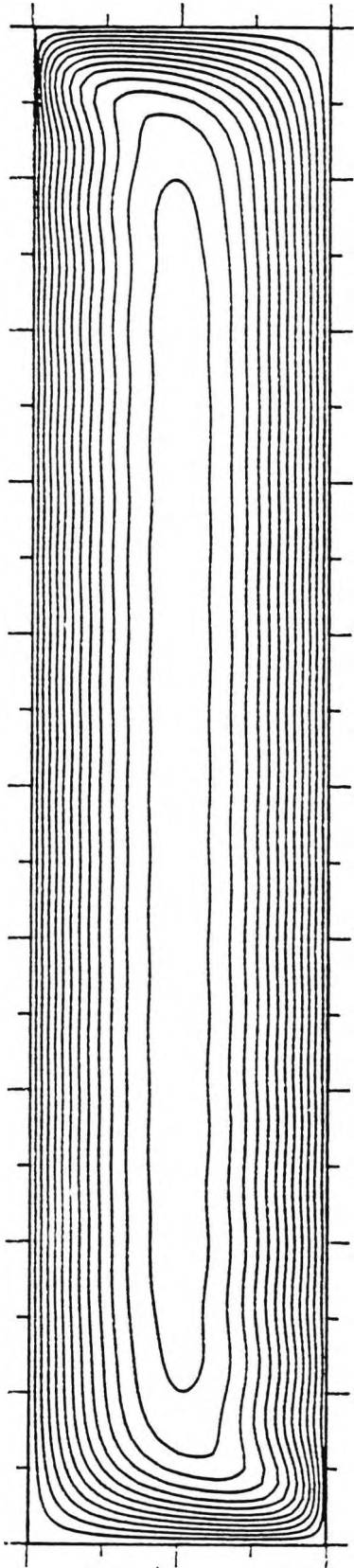


Figure 6.1 : Computed streamlines and isotherms for $\ell=2$.

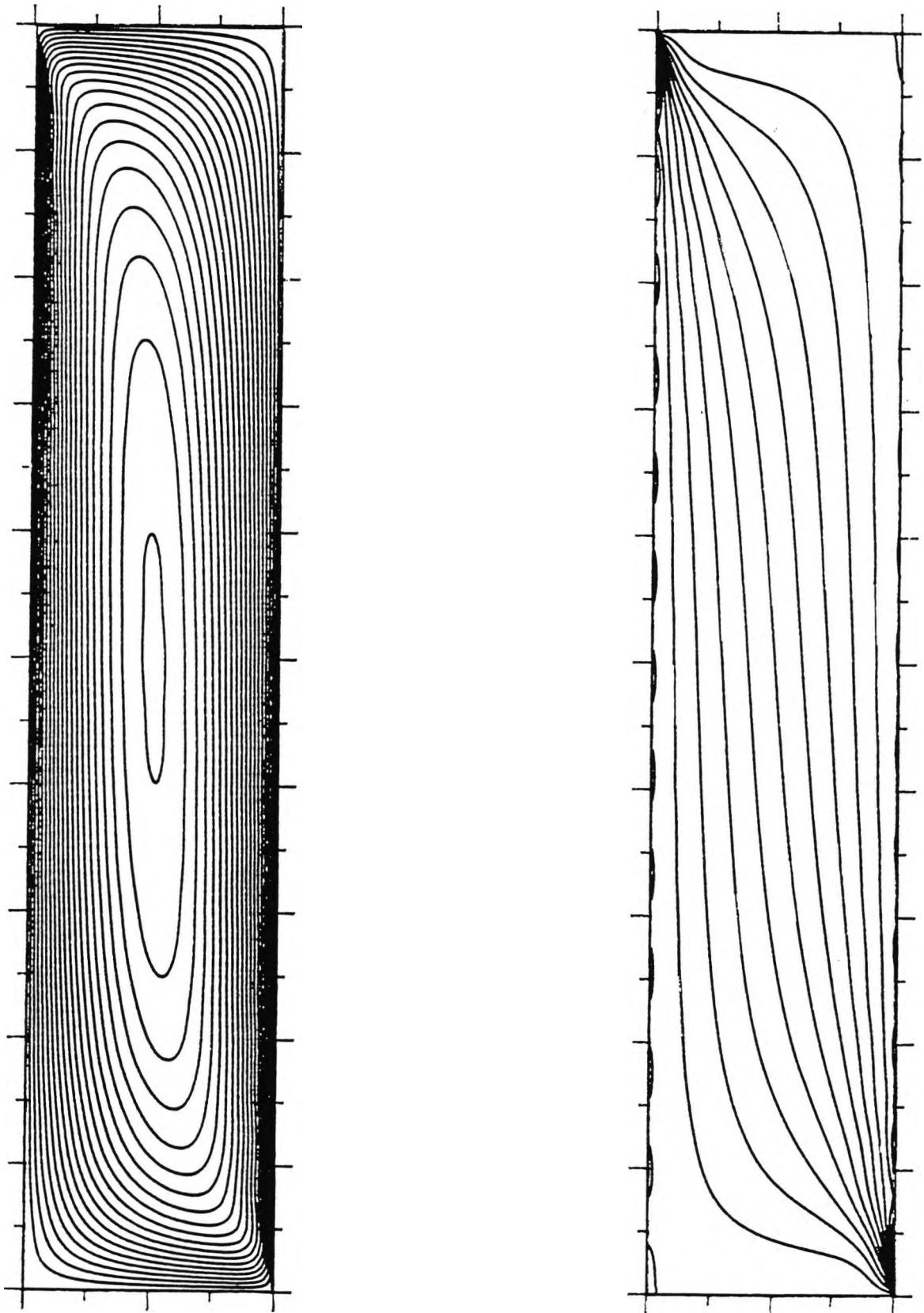


Figure 6.2 : Computed streamlines and isotherms for $l=4$.

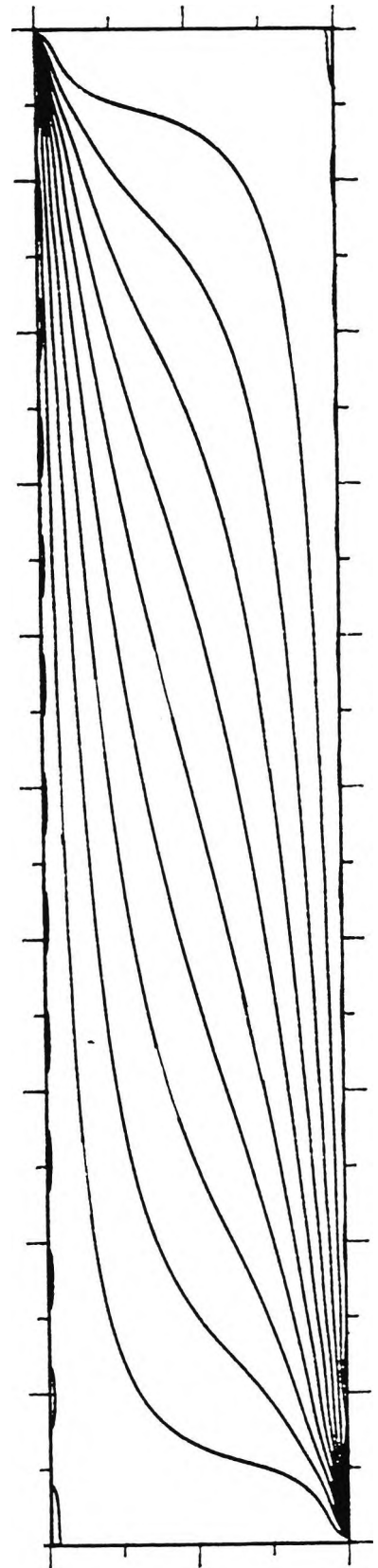
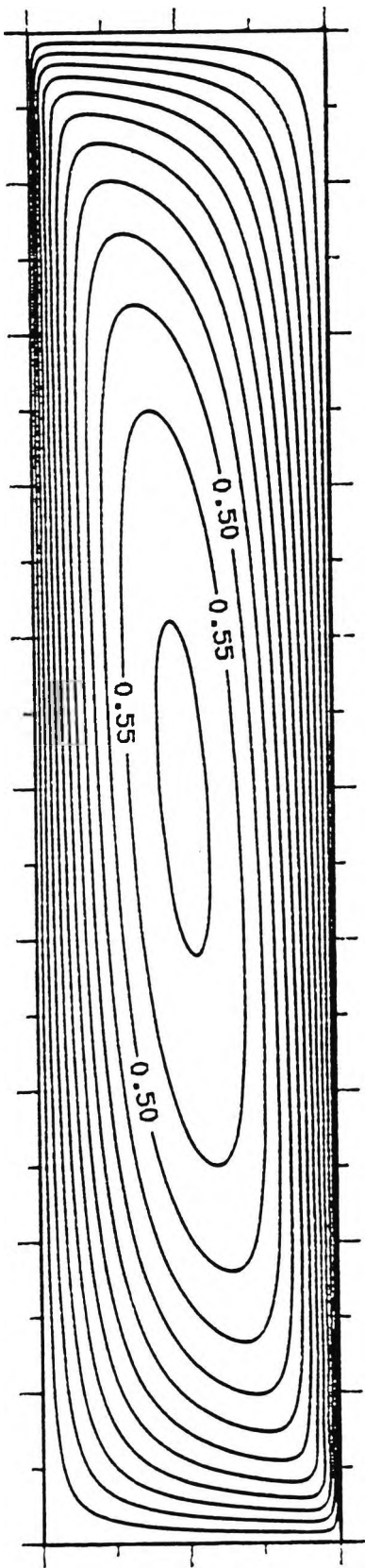


Figure 6.3 : Computed streamlines and isotherms for $l=6$,

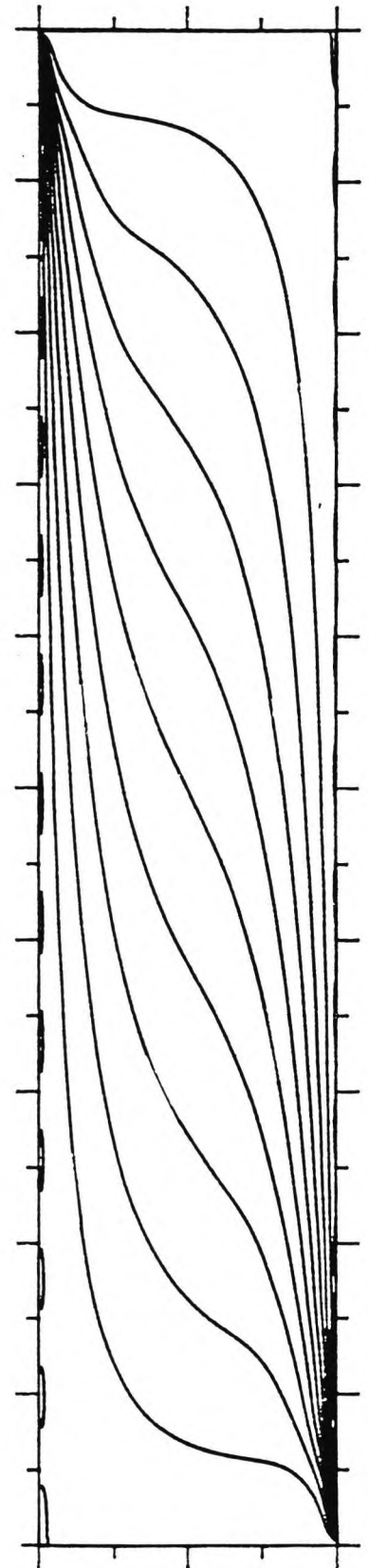
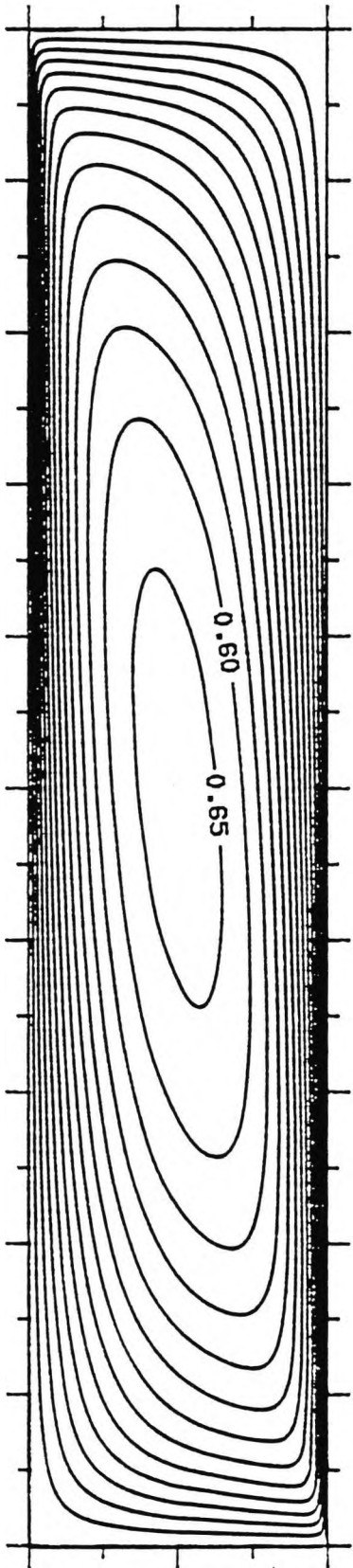


Figure 6.4 : Computed streamlines and isotherms for $l=8$,

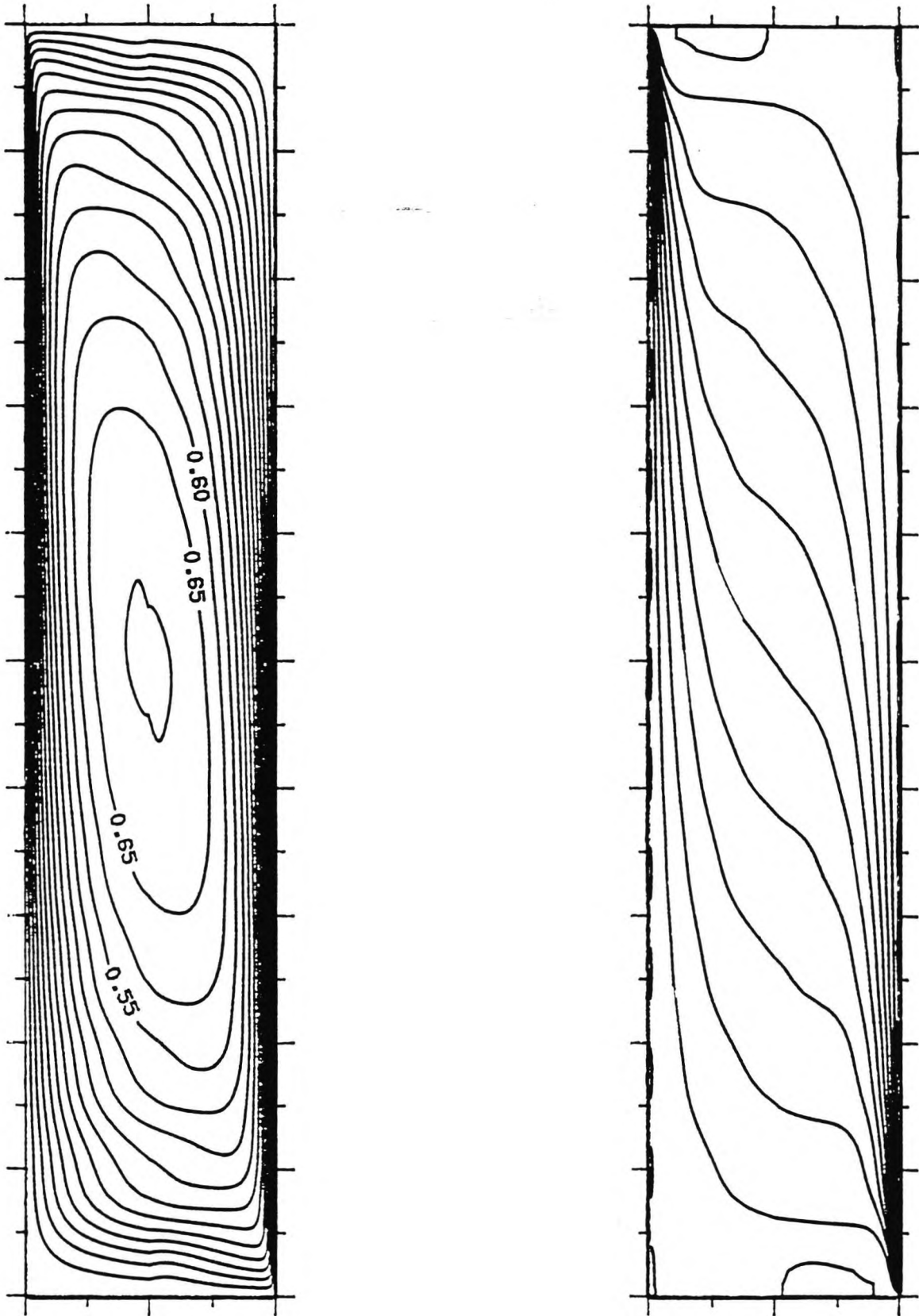


Figure 6.5 : Computed streamlines and isotherms for $l=10$.

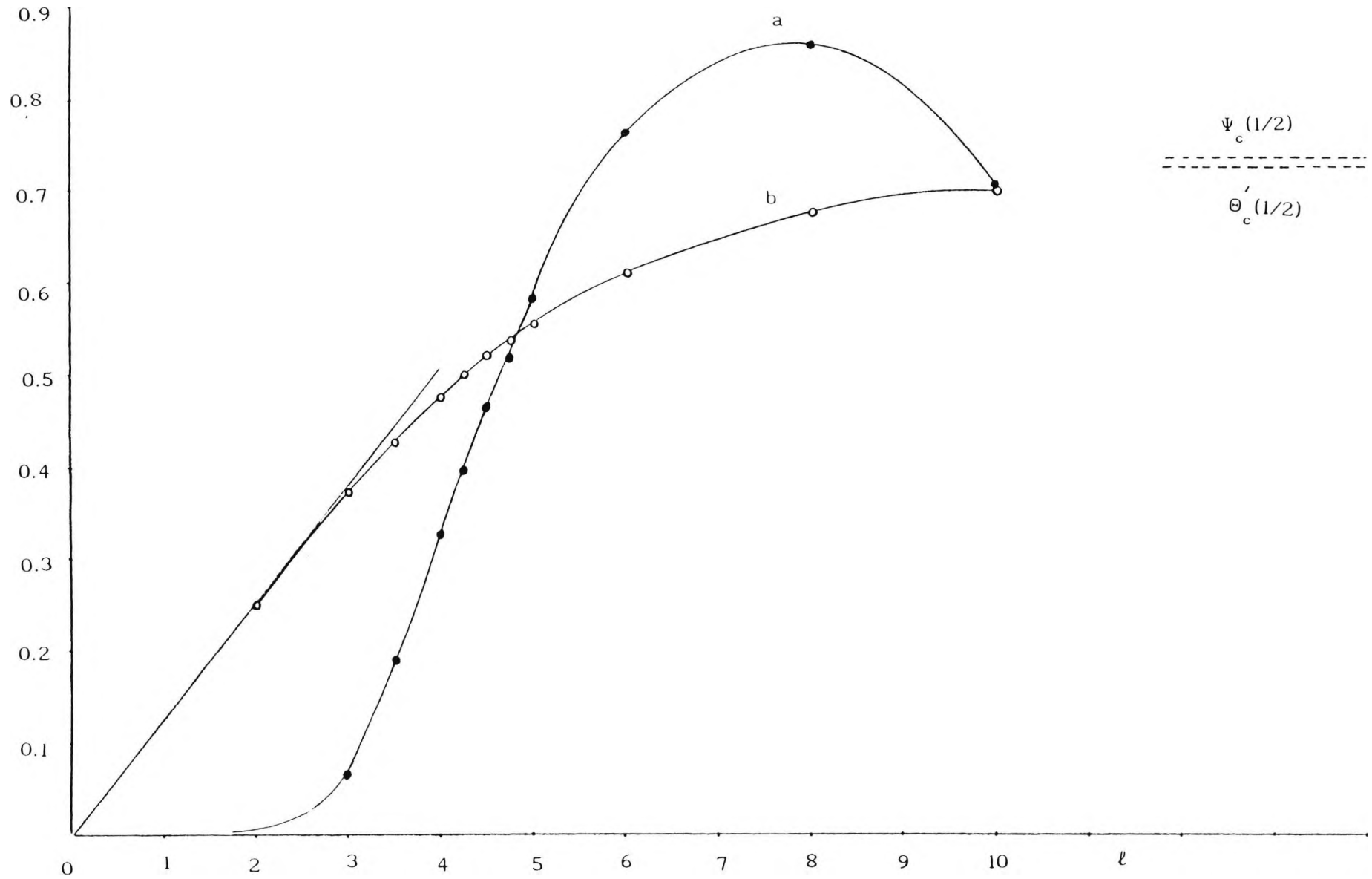


Figure 6.6 : The numerical results for a) $\partial\theta/\partial Z(l/2, 1/2)$, b) $\Psi(l/2, 1/2)$ shown by dots. The asymptotes (6.5.3), (6.5.13, 14) are also indicated.

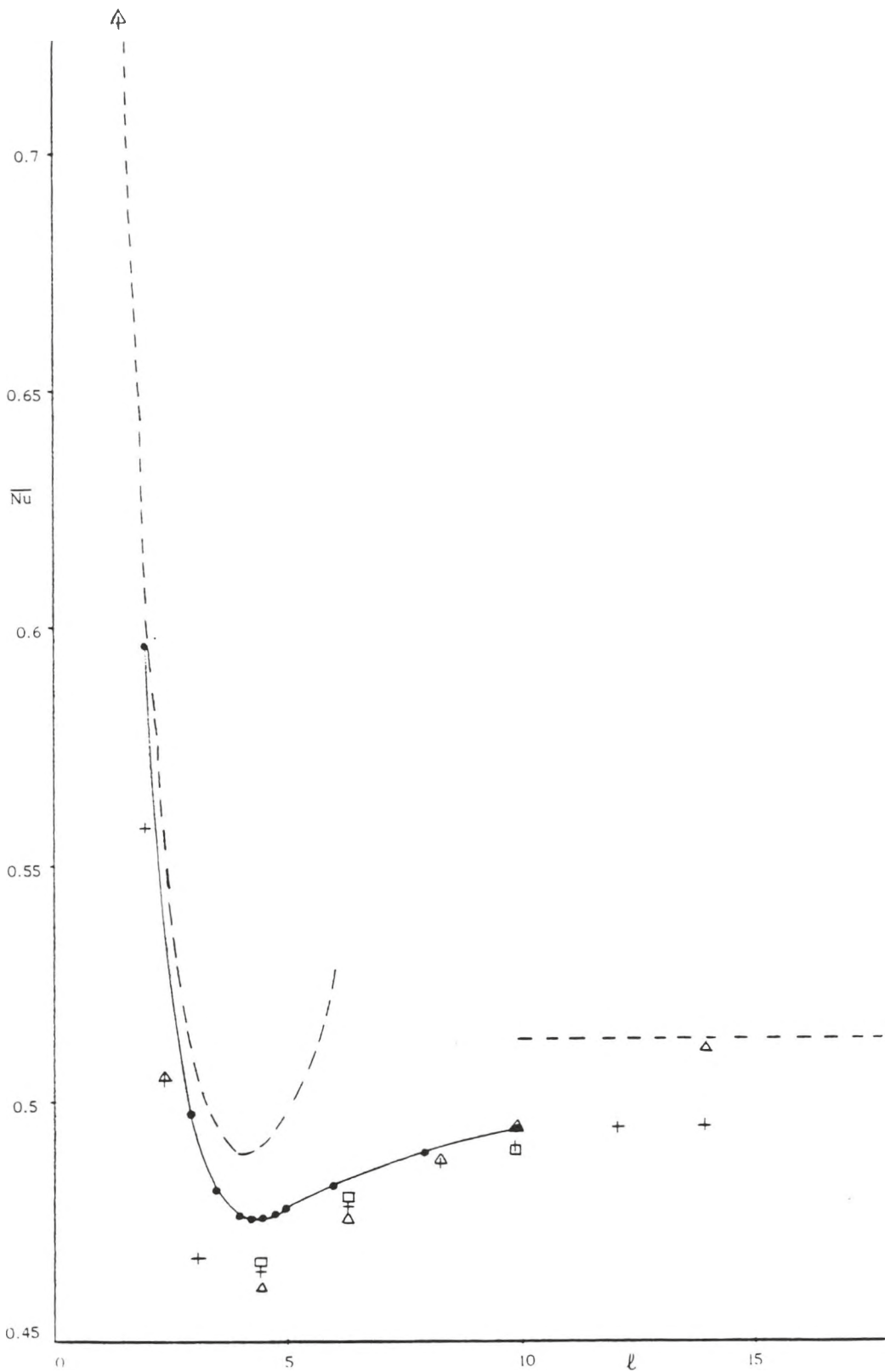


Figure 6.7 : The comparison of theoretical and numerical values of the Nusselt number with the results of Lauriat and Prasad 1987, +, Shiralkar, Haadjizadeh and Tien 1983, \square , Prasad and Kulacki 1984, \triangle . The results computed here are shown by dots and the asymptotes (6.6.9) and (6.6.11) are also indicated.

Chapter 7 Solution of the end-zone problems for
Darcy-Rayleigh numbers $A=O(h)$

7.1 Introduction

In this chapter the remainder of the solution structure for Darcy-Rayleigh numbers A of order h is considered. The core solution considered in Chapter 6 must be consistent with structures near the two ends of the cavity which allow the full boundary conditions to be satisfied at $z=0$ and $z=h$. It will be shown that the end structure is essentially of the form already identified in Chapter 4 except that the constant K now becomes a function of the core parameter $\ell = (A/h)^{1/2}$. The centro-symmetry of the flow means that only the end region near $z = 0$ need be considered. In Section 7.2 The form of the core solution as $Z \rightarrow 0$ is described and this leads to a description of the main end-zone structure in Section 7.3. This is dominated by convection, except near the hot wall, and an inner horizontal layer, where conduction is significant, provides the final adjustment to the thermal boundary condition on the bottom wall of the cavity. The inner horizontal layer is considered in Section 7.4.

Section 7.5 considers the manner in which the overall core and end-zone structure develops as $\ell \rightarrow \infty$, equivalent to Darcy-Rayleigh numbers $A \gg h$. This allows the present work to be related to previous studies of the high Darcy-Rayleigh number limit in rectangular cavities of finite aspect ratio, $h=O(1)$ (Daniels, Blythe and

Simpkins 1982) and completes the description of high Darcy-Rayleigh number flows in porous media for the entire range of aspect ratios ; shallow cavity flows have been considered in a series of papers by Daniels , Blythe and Simpkins(1982 , 1986 , 1989). A final discussion of the present work is given in Section 7.6 .

7.2 Core structure , $Z \rightarrow 0$

The solution of the core region governed by the boundary layer equations

$$\frac{\partial^2 \Theta}{\partial X^2} = \frac{\partial \Theta}{\partial X} \frac{\partial \Psi}{\partial Z} - \frac{\partial \Theta}{\partial Z} \frac{\partial \Psi}{\partial X} \quad (7.2.1)$$

$$\frac{\partial^2 \Psi}{\partial X^2} = - \frac{\partial \Theta}{\partial X} \quad (7.2.2)$$

is first considered as $Z \rightarrow 0$. The structure is similar to that described in Section 4.2 and so only the main results will be summarised here . Near the hot wall , there is a region where $\eta = (l-X)/Z^{1/2} = O(1)$ and

$$\Psi = Z^{1/2} F_0(\eta) + \dots , \quad \Theta = G_0(\eta) + \dots \quad (Z \rightarrow \infty) . \quad (7.2.3)$$

Substitution into (7.2.1,2) gives

$$G_0'' + \frac{1}{2} G_0' F_0 = 0 , \quad F_0'' = G_0' \quad (7.2.4)$$

and the boundary conditions are

$$F_0 = 0 , \quad G_0 = 1 \quad (\eta = 0) , \quad (7.2.5)$$

$$F_0' \rightarrow 0 , \quad G_0 \rightarrow 0 \quad (\eta \rightarrow \infty) . \quad (7.2.6)$$

The system (7.2.4-6) is the same as that of (4.2.10-12).

Elimination of G_0 gives

$$F_0'''' + \frac{1}{2}F_0'' F_0' = 0 ; F_0 = 0, \quad F_0' = 1 \quad (\eta = 0), \quad F_0' \longrightarrow 0 \quad (\eta \longrightarrow \infty) \quad (7.2.7)$$

and the solution has the property

$$\lim_{\eta \longrightarrow \infty} F_0 = a_0 = 1.616. \quad (7.2.8)$$

Across the main part of the core region ($0 < X < \ell$)

$$\Psi = Z^{1/2} \Psi_0(X) + \dots, \quad \Theta = Z^{1/2} \Theta_0(X) + \dots \quad (Z \longrightarrow 0) \quad (7.2.9)$$

and substitution into (7.2.1,2) gives

$$\Theta_0' \Psi_0 - \Theta_0 \Psi_0' = 0, \quad \Psi_0'' = -\Theta_0'. \quad (7.2.10)$$

The relevant boundary conditions are

$$\Psi_0 = 0 \quad (X=0), \quad \Psi_0 = a_0 \quad (X=\ell). \quad (7.2.11)$$

This system of equations has solution

$$\Theta_0 = K_0(\ell) \Psi_0, \quad (7.2.12)$$

with

$$\Psi_0(X) = \frac{a_0(1-e^{-K_0 X})}{1-e^{-K_0 \ell}}, \quad \Theta_0(X) = \frac{K_0 a_0(1-e^{-K_0 X})}{1-e^{-K_0 \ell}} \quad (7.2.13)$$

Here K_0 can in principle be determined as a function of ℓ from the numerical solution of the core region.

Near the cold wall, there is a region where $\zeta = X/Z^{1/4} = O(1)$ and

$$\Psi = Z^{3/4} f_0(\zeta) + \dots, \quad \Theta = Z^{3/4} g_0(\zeta) + \dots \quad (Z \longrightarrow 0). \quad (7.2.14)$$

Substitution into (7.2.1,2) gives

$$g_0'' = \frac{3}{4} g_0' f_0 - \frac{3}{4} g_0 f_0', \quad f_0'' = 0 \quad (7.2.15)$$

and the relevant solution subject to the boundary conditions

$$f_0 = g_0 = 0 \quad (\zeta = 0), \quad g_0 \sim K_0 f_0 \sim \frac{a_0 K_0^2 \zeta}{1 - e^{-K_0 \ell}} \quad (\zeta \rightarrow \infty) \quad (7.2.16)$$

is

$$f_0 = \frac{a_0 K_0 \zeta}{1 - e^{-K_0 \ell}}, \quad g_0 = \frac{a_0 K_0^2 \zeta}{1 - e^{-K_0 \ell}}. \quad (7.2.17)$$

7.3 End-zone solution

The main end-zone structure is shown in Figure 7.1 and consists of three regions on the vertical scale $z=O(1)$ which match, as $z \rightarrow \infty$, with the core structure described in the previous section. In region I (vertical boundary layer) the solution is

$$\bar{\psi} = A^{1/2} \psi_1(x_1, z) + \dots, \quad \bar{T} = T_1(x_1, z) + \dots \quad (A \rightarrow \infty), \quad (7.3.1)$$

where $1-x = A^{-1/2} x_1$, and

$$\psi_1 = z^{1/2} F_0(\eta), \quad T_1 = G_0(\eta), \quad (7.3.2)$$

where $\eta = x_1 / z^{1/2}$.

In region II, the solution is given by

$$\bar{\psi} = A^{1/2} \psi_2(x, z) + \dots, \quad \bar{T} = A^{-1/2} T_2(x, z) + \dots \quad (A \rightarrow \infty) \quad (7.3.3)$$

and substitution into (2.2.1,2) gives

$$\nabla^2 \psi_2 = - \frac{\partial T_2}{\partial x}, \quad (7.3.4)$$

$$\frac{\partial(T_2, \psi_2)}{\partial(x, z)} = 0. \quad (7.3.5)$$

The solution of (7.3.5) is

$$T_2 = F_2(\psi_2) \quad (7.3.6)$$

and in order to find F_2 it is necessary to match the solution as $z \rightarrow \infty$ with that in the core region. From (7.2.9) this requires that

$$\psi_2 \sim z^{1/2} \Psi_0(\ell x), \quad T_2 \sim z^{1/2} \ell \Theta_0(\ell x) \quad (z \rightarrow \infty) \quad (7.3.7)$$

where Ψ_0 and Θ_0 are given by (7.2.13). Thus

$$\psi_2 \sim \frac{a_0 z^{1/2} (1 - e^{-K_0 \ell x})}{1 - e^{-K_0 \ell}}, \quad T_2 \sim \frac{a_0 z^{1/2} K_0 \ell (1 - e^{-K_0 \ell x})}{1 - e^{-K_0 \ell}} \quad (z \rightarrow \infty) \quad (7.3.8)$$

and it follows that $T_2 \sim K_0 \ell \psi_2$ ($z \rightarrow \infty$), giving

$$T_2 = F_2(\psi_2) = K_2(\ell) \psi_2 \quad (7.3.9)$$

throughout region II, where

$$K_2(\ell) = \ell K_0(\ell) \quad (7.3.10)$$

is a function of ℓ . From (7.3.4) it follows that throughout region II, the governing equation for ψ_2 is

$$\nabla^2 \psi_2 = -K_2 \frac{\partial \psi_2}{\partial x} \quad (7.3.11)$$

This equation must be solved subject to the boundary conditions

$$\psi_2 = 0 \quad (x=0), \quad \psi_2 = a_0 z^{1/2} \quad (x=1) \quad (7.3.12)$$

$$\psi_2 = 0 \quad (z=0), \quad \psi_2 \sim \frac{a_0 z^{1/2} (1 - e^{-K_2 x})}{1 - e^{-K_2}} \quad (z \rightarrow \infty). \quad (7.3.13)$$

The system (7.3.11-13) is precisely that considered in Section 4.3 except that the constant K is replaced by K_2 .

The solution is therefore

$$\psi_2 = \frac{a_0}{(2\pi)^{1/2}} e^{K_2(1-x)/2} \int_0^\infty \omega^{-3/2} \frac{\sinh\{(K_2^2+4\omega^2)^{1/2}x/2\}}{\sinh\{(K_2^2+4\omega^2)^{1/2}/2\}} \sin(\omega z) d\omega. \quad (7.3.14)$$

As $x \rightarrow 0$

$$\psi_2 \sim x B_2(z; \ell) \quad , \quad T_2 \sim K_2 x B_2(z; \ell) \quad (7.3.15)$$

where $B_2(z; \ell)$ is a function of z and ℓ . Thus in region III, where $x = O(A^{-1/4})$ the solution is

$$\bar{\psi} = A^{1/4} \psi_3(x_3, z) + \dots, \quad \bar{T} = A^{-3/4} T_3(x_3, z) + \dots \quad (A \rightarrow \infty) \quad (7.3.16)$$

and it is readily shown that the solution which satisfies $T_3 = \psi_3 = 0$ on $x_3 = 0$ and which matches with the solution in region II as $x_3 \rightarrow \infty$ is simply

$$\psi_3 = x_3 B_2(z; \ell) \quad , \quad T_3 = K_2 x_3 B_2(z; \ell). \quad (7.3.17)$$

At the base of the central zone ψ_2 and T_2 have the forms

$$\psi_2 = z U_2(x; \ell) + \dots, \quad T_2 = z K_2 U_2(x; \ell) + \dots \quad (z \rightarrow 0) \quad (7.3.18)$$

where $U_2(x; \ell)$ is a function of x and ℓ . Since $\partial T_2 / \partial z$ is non-zero as $z \rightarrow 0$ an inner horizontal layer is needed to allow the solution to adjust to the thermal boundary condition at the bottom wall.

7.4 Inner horizontal layer

In the inner thermal boundary layer on the

bottom surface of the cavity

$$\bar{T} = A^{-3/4} T_4(x, z_4) + \dots, \quad \bar{\psi} = A^{1/4} \psi_4(x, z_4) + \dots \quad (A \rightarrow \infty), \quad (7.4.1)$$

where $z = A^{-1/4} z_4$. Substitution into (2.2.1,2) gives

$$\frac{\partial^2 \psi_4}{\partial z_4^2} = 0, \quad \frac{\partial^2 T_4}{\partial z_4^2} = \frac{\partial(T_4, \psi_4)}{\partial(x, z_4)}, \quad (7.4.2)$$

and the boundary conditions are

$$\psi_4 = \frac{\partial T_4}{\partial z_4} = 0 \quad \text{at} \quad z_4 = 0, \quad (7.4.3)$$

$$\psi_4 \sim U_2(x; \ell) z_4, \quad T_4 \sim K_2 U_2(x; \ell) z_4 \quad (z_4 \rightarrow \infty), \quad (7.4.4)$$

$$T_4 = 0 \quad \text{at} \quad x = 0. \quad (7.4.5)$$

This system is the same system as that solved in Section 4.4 and so the required solution is

$$T_4 = K_2 \left\{ \frac{2\chi^{1/2}}{\pi^{1/2}} \exp(-\psi_4^2/4\chi) + \psi_4 \operatorname{erf}(\psi_4/2\chi^{1/2}) \right\}, \quad (7.4.6)$$

where

$$\psi_4 = U_2(x; \ell) z_4 \quad \text{and} \quad \chi = \int_0^x U_2(x'; \ell) dx'. \quad (7.4.7)$$

The results of this and the preceding sections determine that the high Darcy-Rayleigh number structure for $z=O(1)$ outlined in Chapter 4 remains qualitatively unchanged throughout the regime for which $A=O(h)$. The one difference is that the constant K is now replaced by $K_2(\ell)$, a function of the parameter $\ell=(A/h)^{1/2}$. This leads to a range of different solutions (7.3.14) of the central zone problem in region II and thus, in particular, a

range of functions $U_2(x;\ell)$ which determine the solution in the inner horizontal layer .

The parameter $K_2(\ell)$ is determined by the solution of the core problem and cannot easily be determined from the Fourier series solution developed in Chapter 6. However, as $\ell \rightarrow 0$, the conductive core solution is recovered and near $z = 0$ the adjustment to the boundary condition $\Psi = 0$ at $Z = 0$ occurs on a vertical length scale $Z \sim \ell^2$ where $X = O(\ell)$, $\Theta = O(1)$ and $\Psi = O(\ell)$. It follows that the linear relation which develops at the base of this region is of the form $\Theta = K(\Psi\ell^{-1})$ where K is the pure constant estimated in Section 5.3 to have the value 1.3. It follows that

$$K_0(\ell) \sim K\ell^{-1} \quad (\ell \rightarrow 0) \quad (7.4.8)$$

and hence, from (7.3.10), that

$$K_2(\ell) \rightarrow K \quad (\ell \rightarrow 0) . \quad (7.4.9)$$

The end-zone structure described in this chapter therefore merges precisely, as $\ell \rightarrow 0$, with that described in Chapter 4.

Of further interest is the form taken by the end-zone structure in the opposite limit as $\ell \rightarrow \infty$ and this is considered in the next section.

7.4 The limiting structure for $A/h \rightarrow \infty$

It has been argued that in the limit as $\ell \rightarrow \infty$ the core solution adopts the structure first identified by Weber(1975), with vertical boundary layers where $X=O(1)$ and $(-X=O(1))$ separated by a vertically-stratified core

region $0 < X < \ell$ in which the flow is parallel to the horizontal walls of the cavity. The properties of the vertical boundary-layers now determine the value of $K_0(\ell)$, as shown by Blythe, Daniels and Simpkins(1982). Since Θ , Ψ , X and Z are all of order one within the vertical boundary layer on the cold wall, it follows that, as $\ell \rightarrow \infty$, $K_0(\ell)$ approaches a pure constant value

$$K_0(\ell) \rightarrow \hat{K} \quad (\ell \rightarrow \infty) . \quad (7.5.1)$$

Thus

$$K_2(\ell) \sim \hat{K} \ell \quad (\ell \rightarrow \infty) . \quad (7.5.2)$$

The value of \hat{K} is estimated by Daniels (1983) to be 0.167.

The implications for the end-zone structure as $\ell \rightarrow \infty$ can now be considered. Since K_2 is large as $\ell \rightarrow \infty$ the governing equation (7.3.11) in the central zone reduces formally to $\partial\psi_2/\partial x = 0$, implying that the solution is $\psi_2 = a_0 z^{1/2}$ nearly everywhere. However, an adjustment to the boundary condition $\psi_2 = 0$ at $x=0$ now occurs in a boundary layer near the cold wall where $x = O(K_2^{-1}) = O(\ell^{-1})$, and it is readily shown from (7.3.11) that the relevant solution is

$$\psi_2 \sim a_0 z^{1/2} (1 - e^{-\hat{K}x}) \quad , \quad x = \ell^{-1} \hat{x} \quad , \quad (7.5.3)$$

giving

$$B_2(z; \ell) = \frac{\partial\psi_2}{\partial x}(0, z) \sim \ell \hat{K} a_0 z^{1/2} \quad (\ell \rightarrow \infty) . \quad (7.5.4)$$

Adjustment to the boundary condition $\psi_2 = 0$ at $z = 0$ occurs in a layer near the base where $z = O(K_2^{-1/2}) = O(\ell^{-1/2})$ and $\psi_2 = O(\ell^{-1/4})$. This implies that $U_2(x; \ell) = O(\ell^{1/4})$ as

$\ell \rightarrow \infty$ and therefore that the inner horizontal layer assumes a vertical scale $z=O(A^{-1/4}\ell^{1/3})$ as $\ell \rightarrow \infty$. The precise form of $U_2(x;\ell)$ as $\ell \rightarrow \infty$ can be found by solving the boundary-layer problem at the base of the central zone, where

$$\psi_2 = \ell^{-1/4} \hat{\psi}_2(x, \hat{z}) + \dots, \quad z = \ell^{-1/2} \hat{z} \quad (7.5.5)$$

and from (7.3.11,13)

$$\frac{\partial^2 \hat{\psi}_2}{\partial \hat{z}^2} = -K \frac{\partial \hat{\psi}_2}{\partial x}, \quad (7.5.6)$$

with

$$\hat{\psi}_2 = 0 \quad (\hat{z} = 0), \quad \hat{\psi}_2 \sim a_0 \hat{z}^{1/2} \quad (\hat{z} \rightarrow \infty), \quad (7.5.7)$$

$$\hat{\psi}_2 = a_0 \hat{z}^{1/2} \quad (x = 1). \quad (7.5.8)$$

This problem has the similarity solution

$$\hat{\psi}_2 = a_0 \left(\frac{\pi \hat{z}}{2\hat{\zeta}} \right)^{1/2} \exp(-\hat{\zeta}^2/4) \left\{ V(1, \hat{\zeta}) - \frac{U(1, \hat{\zeta})}{2\pi^{1/2}} \right\} \\ \hat{\zeta} = \frac{K^{1/2} \hat{z}}{\sqrt{2}(1-x)^{1/2}}, \quad (7.5.9)$$

where U and V are the parabolic cylinder functions defined by Abramowitz and Stegun(1965,p.686), and so

$$U_2 = \frac{\partial \psi_2}{\partial z}(x, 0) \sim \ell^{1/4} \frac{a_0}{2\Gamma(3/4)} (\pi^2 K)^{1/4} (1-x)^{-1/4} \quad (\ell \rightarrow \infty). \quad (7.5.10)$$

The main features of the end-zone structure for a cavity of finite aspect ratio have now emerged. Recalling that $\ell = (A/h)^{1/2}$ the high Darcy-Rayleigh number structure for finite aspect ratios $h=O(1)$ corresponds to

the limit $A \rightarrow \infty$, with ℓ of order $A^{1/2}$. The main part of the central zone now merges with the core and the region (7.5.5) becomes an outer horizontal layer on the bottom boundary of thickness

$$z=O(A^{-1/4}), \quad (7.5.11)$$

where the solution is given by (7.5.9). The layer is dominated by convection and is parabolic in the negative x direction. Below this, there is a conductive sublayer, or inner horizontal layer, of thickness

$$z=O(A^{-5/16}), \quad (7.5.12)$$

which is parabolic in the positive x direction and where the solution is given by (7.4.6,7) with U_2 as determined by (7.5.10). This double horizontal structure is precisely that identified by Daniels, Blythe and Simpkins (1982).

7.6 Discussion

In this chapter the main properties of the end-zone structure for the regime in which A is of order h have been considered. By taking the further limit $\ell=(A/h)^{1/2} \rightarrow \infty$ it has been shown that this structure develops into a double horizontal layer applicable to the high Darcy-Rayleigh number flow in a cavity of finite aspect ratio, as previously identified by Daniels, Blythe and Simpkins(1982). There are a series of flow regimes which describe the transition from high Darcy-Rayleigh number flows in finite cavities to conduction-dominated flows in shallow cavities (Daniels, Blythe and Simpkins 1982, 1986, 1989). The work described in the present thesis now

completes the picture for the transition to the tall cavity limit and in particular provides the formula for heat transfer across the cavity in the high Darcy-Rayleigh number limit. This shows that there is a position of minimum heat transfer when the Darcy-Rayleigh number and aspect ratio are such that

$$\ell = (A/h)^{1/2} \approx 4.25. \quad (7.6.1)$$

For general values of ℓ , the Nusselt number takes the form given by (6.6.2),

$$Nu \sim (Ah)^{1/2} \overline{Nu}(\ell) \quad (Ah \gg 1), \quad (7.6.2)$$

where $\overline{Nu}(\ell)$ is shown in Figure 6.7. For a Darcy-Rayleigh number R based on the cavity height, h^* ,

$$R = \alpha g \Delta T^* k h^* / \kappa \nu = Ah, \quad (7.6.3)$$

so that (7.6.2) can be re-interpreted as

$$Nu \sim R^{1/2} \overline{Nu}(\ell) \quad (R \gg 1), \quad (7.6.4)$$

where

$$\ell^* = R^{-1/2} h^* \ell. \quad (7.6.5)$$

For a vertical slot of given height h^* and across which there is a specified temperature difference ΔT^* , the Darcy-Rayleigh number R given by (7.6.3) is fixed and thus Nu is a minimum as a function of the cavity width ℓ^* when \overline{Nu} is a minimum as a function of ℓ . Thus the position of minimum heat transfer is attained for a cavity width ℓ^* given by

$$\ell^* \approx 4.25 R^{-1/2} h^* \quad (R \gg 1) \quad (7.6.6)$$

and at this point

$$\text{Nu} \approx 0.48 R^{1/2} \quad (R \gg 1). \quad (7.6.7)$$

These formulae provide practical results of direct interest to engineers involved in heat-loss minimization.

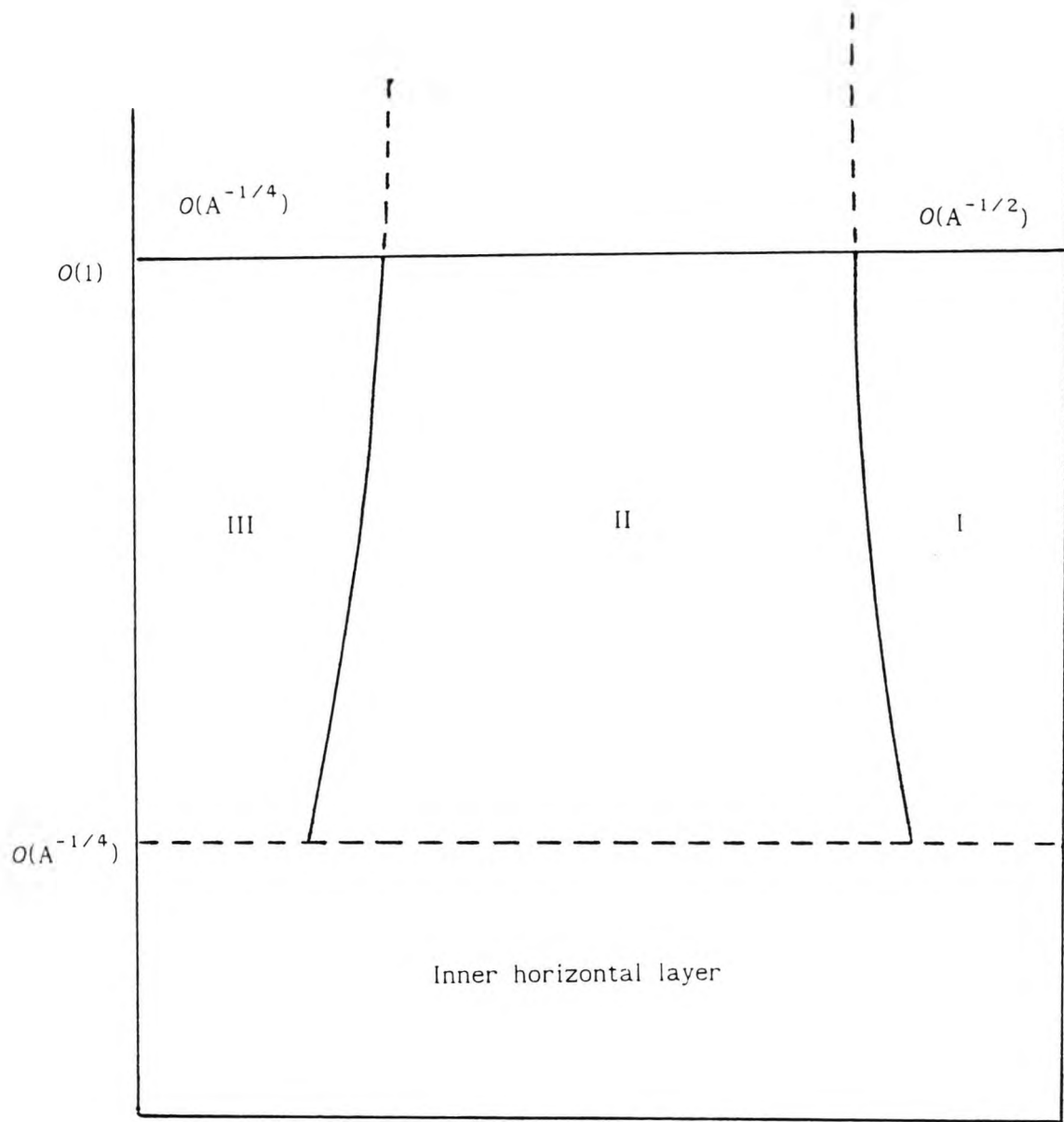


Figure 7.1 : The main end-zone structure

References

1. Abramowitz , M.& Stegun, I. A. 1965 Handbook of mathematical functions. New York: Dover publications.
2. Bankvall, C.G. 1974 Natural convection in a vertical permeable space, *Warme-und Stoffubertragung*, vol.7, pp. 22-30.
3. Bear,J., 1968 Dynamics of fluids in porous media. New York : Dover publications.
4. Bejan,A. & Tien,C.L. 1978 Natural convection in a horizontal porous medium subject to an end-to-end temperature difference. *A.S.M.E. Journal of Heat Transfer*, vol. 100, pp. 191-198.
5. Blythe,P.A., Daniels,P.G. & Simpkins,P.G. 1982 Thermally driven cavity flows in porous media. Part I. The vertical boundary layer structure. *Proc.Roy.Soc. Lond.*, vol.A380, pp.119-136.
6. Blythe,P.A. & Simpkins,P.G. 1977 Thermal convection in a rectangular cavity. *Physicochemical Hydrodynamics*, vol.2 (ed. D.B Spalding), pp. 511-524. New York: Advance publications.

7. Blythe, P.A. & Simpkins, P.G. 1981 Convection in a porous layer for a temperature dependent viscosity. Int. Journal of Heat and Mass Transfer, vol. 24, pp.497-506.
8. Blythe, P.A., Simpkins, P.G. & Daniels, P.G. 1983 Thermal convection in a cavity filled with a porous medium: a classification of limiting behaviours. Int. Journal of Heat and Mass Transfer, vol.26, pp.701-708.
9. Burns, P.J., Chow, L.C. & Tien, C.L. 1977 Convection in a vertical slot filled with porous insulation. Int. Journal of Heat and Mass Transfer, vol.20, pp.919-926.
10. Chan, B. K. C., Ivey, C. M. & Barry, J.M. 1970 Natural convection in enclosed porous media with rectangular boundaries. Journal of Heat Transfer, vol.2, pp. 21-26.
11. Cormack, D.E., Leal, L.G. & Imberger, J. 1974 Natural convection in a shallow cavity with differentially heated end walls. I Asymptotic theory. J. Fluid Mech., vol.65, pp.209-229.
12. Daniels, P.G. 1983 A numerical solution of the vertical boundary-layer equations in a horizontally heated porous cavity. Journal of Engineering Mathematics, vol.17, pp.285-300.

13. Daniels, P.G. 1987 Convection in a vertical slot. J. Fluid Mech., vol.176, pp.419-441.
14. Daniels, P.G. 1990, Minimum heat transfer by laminar natural convection across a laterally heated vertical slot. Int. J. Heat and Fluid Flow, vol.11, pp.371-375.
15. Daniels, P.G., Blythe, P.A. & Simpkins, P.G. 1982 Thermally driven cavity flows in porous media. Part II, The horizontal boundary layer structure. Proc. Roy. Soc. Lond., vol. A382, pp. 135-154.
16. Daniels, P.G. , Blythe, P. A. & Simpkins, P.G. 1986 Thermally driven shallow cavity flows in porous media : the intermediate regime. Proc. Roy. Soc. Lond., vol.A406, pp. 263-285.
17. Daniels, P.G., Blythe, P.A, & Simpkins, P.G. 1987 Onset of multicellular convection in a shallow laterally heated cavity . Proc. Roy. Soc. Lond., vol. A411, pp.327-350.
18. Daniels, P.G., Simpkins, P.G. & Blythe, P.A. 1989 Thermally driven shallow cavity flows in porous media : the merged-layer regime. Proc. Roy. Soc. Lond. vol. A426, pp.107-124.
19. Ditkin, V.A. & Prudnikov, A.P. 1965 Integral transforms and operational calculus. Pergamon, Oxford.

20. Gill, A.E. 1966 The boundary layer regime for convection in a rectangular cavity. J. Fluid Mech., vol.26, pp. 515-536.
21. Gill,A.E. 1969 A proof that convection in a porous vertical slab is stable, J. Fluid Mech. vol.35, pp.545-547.
22. Haadjizadeh,M.& Tien,C.L.1983 Natural convection in a rectangular porous cavity with one permeable end wall. Journal of Heat Transfer,vol.105,pp.803-808.
23. Hickox,C.E. & Gartling,D.K. 1981 A numerical study of natural convection in a horizontal porous layer subjected to an end-to-end temperature difference. A.S.M.E. Journal of Heat Transfer, vol. 103, pp.797-802.
24. Holst,P.H. & Aziz, K.1972 A theoretical and experimental study of natural convection in a confined porous medium. Canadian Journal of Chemical Engineering, vol.50, pp.232-241.
25. Howarth,L. 1959 Appendix to paper by G.I. Taylor. The dynamics of thin sheets of fluid I. Proc. Roy.Soc. Lond., vol.A253, pp.289-295.

26. Klarsfeld, S. 1970 Champs de temperature associes aux movement de convection naturelle dans un milieu poreux limite. Rev. Gen. Thermique, vol.9, pp.1403-1424.
27. Lapwood, E.R. 1948 Convection of fluid in a porous medium. Proc. Camb. Phil.Soc., vol.44, pp. 508-521.
28. Lauriat, G. & Prasad, V. 1987 Natural convection in a vertical porous cavity: a numerical study for Brinkman-extended Darcy formulation. Int.Journal of Heat and Mass Transfer, vol. 109, pp. 688-696.
29. Mitchell, A.R. 1969 Computational methods in partial differential equations. Wiley, London.
30. Prasad, V. & Kulacki, F.A. 1984a Natural convection in a rectangular porous cavity with constant heat flux on one vertical wall. A.S.M.E. Journal of Heat Transfer, vol.106, pp. 152-157.
31. Prasad, V. & Kulacki, F.A. 1984b Convective heat transfer in a rectangular porous cavity-effect of aspect ratio on flow structure and heat transfer. A.S.M.E. Journal of Heat Transfer, vol. 106, pp.158-165.

32. Prasad, V. & Kulacki, F. A. 1984 Natural convection in a vertical porous annulus. Int. J. of Heat and Mass Transfer, vol. 27, pp. 207-219.
33. Riley, D.S. 1988 Steady two-dimensional thermal convection in a vertical porous slot with spatially periodic boundary imperfections. Int. Journal of Heat and Mass Transfer, vol.31, pp. 2365-2380.
34. Sakiadis, B.C. 1961 Boundary layer behaviour on continuous surfaces II : the boundary layer on a continuous flat surface. A.I.Ch.E. Journal, vol.17, pp. 221-225.
35. Seki, N., Fukusako, S. & Inaba, H. 1978 Heat transfer in a confined rectangular cavity packed with porous media. Int. Journal of Heat and Mass Transfer, vol. 21, pp. 985-989.
36. Shiralkar, G.S. , Haadjizadeh, M. & Tien, C.L. 1983 Numerical study of high Rayleigh number convection in a vertical porous enclosure. Numerical Heat Transfer, vol.6, pp.223-234.
37. Simpkins, P.G. & Blythe, P.A. 1980 Convection in a porous layer. Int. Journal of Heat and Mass Transfer, vol.23, pp.881-887.

38. Singh, K.R. & Cowling, T.G. 1963 Thermal convection in magneto-hydrodynamics II. Flow in a rectangular box. Quart. Journal of Mech. Appl. Math., vol. 16, pp. 17-31.
39. Walker, K.L. & Homsy, G.M. 1978 Convection in a porous cavity. J. Fluid Mech., vol. 87, pp. 449-474.
40. Weber, J.E. 1975 The boundary-layer regime for convection in a vertical porous layer, Int. Journal of Heat and Mass Transfer, vol. 18, pp. 569-573.